

A catalogue of integrated $H\alpha$ fluxes for 1,258 Galactic planetary nebulae

David J. Frew^{1,2*}, Ivan S. Bojčić^{1,2,3} and Q.A. Parker^{1,2,3}

¹*Department of Physics and Astronomy, Macquarie University, NSW 2109, Australia*

²*Research Centre in Astronomy, Astrophysics and Astrophotonics, Macquarie University, NSW 2109, Australia*

³*Australian Astronomical Observatory, PO Box 915, North Ryde, NSW 1670, Australia*

Accepted ; Received ; in original form

ABSTRACT

We present a catalogue of new integrated $H\alpha$ fluxes for 1258 Galactic planetary nebulae (PNe), with the majority, totalling 1234, measured from the Southern $H\alpha$ Sky Survey Atlas (SHASSA) and/or the Virginia Tech Spectral-line Survey (VTSS). Aperture photometry on the continuum-subtracted digital images was performed to extract $H\alpha + [N\text{II}]$ fluxes in the case of SHASSA, and $H\alpha$ fluxes from VTSS. The $[N\text{II}]$ contribution was then deconvolved from the SHASSA flux using spectrophotometric data taken from the literature or derived by us. Comparison with previous work shows that the flux scale presented here has no significant zero-point error. Our catalogue is the largest compilation of homogeneously derived PN fluxes in any waveband yet measured, and will be an important legacy and fresh benchmark for the community. Amongst its many applications, it can be used to determine statistical distances for these PNe, determine new absolute magnitudes for delineating the faint end of the PN luminosity function, provide baseline data for photoionization and hydrodynamical modelling, and allow better estimates of Zanstra temperatures for PN central stars with accurate optical photometry. We also provide total $H\alpha$ fluxes for another 76 objects which were formerly classified as PNe, as well as independent reddening determinations for ~ 270 PNe, derived from a comparison of our $H\alpha$ data with the best literature $H\beta$ fluxes. In an appendix, we list corrected $H\alpha$ fluxes for 49 PNe taken from the literature, including 24 PNe not detected on SHASSA or VTSS, re-calibrated to a common zero-point.

Key words: planetary nebulae: general – HII regions – catalogues – techniques: photometric – techniques: spectroscopic

1 INTRODUCTION

Planetary nebulae (PNe) are a key end-point in the evolution of mid-mass stars which range from ~ 1 to 8 times the mass of the Sun. While the number of known Galactic PNe has essentially doubled over the last decade (Parker et al. 2012a), many hundreds of PNe have very little observational data such as an integrated Balmer-line flux. The integrated flux is analogous to the apparent magnitude of a star, and is one of the most fundamental observable parameters that needs to be determined for any PN. Calculations involving the distance, the ionized mass and electron density, the temperature and luminosity of the central star, and the PN luminosity function (PNLF; Ciardullo 2010) are all critically dependent on accurate integrated line fluxes. In-

deed, the majority of distance estimates for Galactic PNe are determined from a statistical method, which depend on having an accurate integrated flux either in the radio continuum (e.g. Milne & Aller 1975; Daub 1982; Cahn, Kaler & Stanghellini 1992; van de Steene & Zijlstra 1994; Zhang 1995; Bensby & Lundström 2001; Phillips 2004; Stanghellini, Shaw & Villaver 2008), or in an optical Balmer line (O’Dell 1962; Frew & Parker 2006, 2007; Frew 2008).

Traditionally, the $H\beta$ flux has been determined, based on the historical precedence of blue-sensitive photoelectric photometers that were widely used from the 1950s to the 1980s. Integrated $H\beta$ and $[O\text{III}]$ fluxes for PNe were measured either with an objective prism (Liller & Aller 1954), with scanning spectrographs (Capriotti & Daub 1960; Collins, Daub & O’Dell 1961; Liller & Aller 1963; Aller & Faulkner 1964; O’Dell & Terzian 1970; Peimbert & Torres-Peimbert 1971; Barker & Cudworth 1984) or using con-

* E-mail: david.frew@mq.edu.au

ventional aperture photometry with interference filters (e.g. Liller 1955; Osterbrock & Stockhausen 1961; Collins, Daub & O’Dell 1961; O’Dell 1962, 1963; Webster 1969; Perek 1971; Kaler 1976, 1978; Carrasco, Serrano & Costero 1983, 1984; Shaw & Kaler 1985). Consequently, most of the brighter Galactic PNe now have integrated $H\beta$ fluxes available, as compiled by Acker et al. (1991, hereafter ASTR91) and Cahn, Kaler & Stanghellini (1992, hereafter CKS92), based on the efforts of many observers over several decades (see references therein). A few studies (e.g. Webster 1969, 1983; Kohoutek & Martin 1981a, hereafter KM81) have also measured the integrated $H\gamma$ flux, but this line is intrinsically fainter than $H\beta$ by more than a factor of two, and is more susceptible to interstellar extinction.

Nowadays, global fluxes in the red $H\alpha$ line are becoming the preferred benchmark, especially since the majority of PNe discovered over the last decade are mostly faint and reddened, and often undetected at $H\beta$. The bulk of these discoveries came from the MASH catalogues (Parker et al. 2006; Miszalski et al. 2008), which utilized the SuperCOSMOS $H\alpha$ Survey (SHS; Parker et al. 2005). We also note the new objects uncovered from the INT Photometric H-Alpha Survey (IPHAS; Drew et al. 2005), totalling 950 objects (Vironen et al. 2009a,b; Sabin et al. 2010, 2012; L. Sabin, 2012, pers. comm.).

To date, there have been considerably fewer $H\alpha$ fluxes published in the literature. Some notable early efforts included Peimbert & Torres-Peimbert (1971), Peimbert (1973) and Torres-Peimbert & Peimbert (1977, 1979), while about 200 integrated $H\alpha$ fluxes for PNe were contributed by the Illinois group (e.g. Kaler 1981, 1983a,b; Kaler & Lutz 1985; Shaw & Kaler 1989, hereafter SK89), excluding fluxes derived from earlier photographic estimates (see Cahn & Kaler 1971). Thirty compact southern PNe have accurate integrated $H\alpha$, $H\beta$, $H\gamma$, [O III], [N II] and He II $\lambda 4686$ fluxes determined by KM81, and 39 more PNe have accurate fluxes in several lines measured by Dopita & Hua (1997, hereafter DH97). Recent works include Ruffle et al. (2004) who determined diameters, $H\alpha$ fluxes and extinctions for 70 PNe, and the accurate multi-wavelength data for six northern PNe published by Wright, Corradi & Perinotto (2005, hereafter WCP05). Other $H\alpha$ flux measurements for smaller numbers of PNe are widely scattered through the literature.

1.1 Motivation for the Catalogue

Given the significant numbers of Galactic PNe that are currently being unearthed from recent narrow-band optical and infrared (IR) wide-field surveys, the time is right to address the lack of systematic fluxes in the literature. This can now be done properly for the first time thanks to the availability of accurately calibrated emission-line surveys. Tellingly, some of the brightest PNe in the sky have very few flux determinations. The integrated $H\alpha$ flux for the Helix nebula (NGC 7293) given here is only the second published in the literature, after Reynolds et al. (2005), while the $H\beta$ flux has been determined only twice (O’Dell 1962, 1998). The Dumbbell nebula (M 27, NGC 6853) has been similarly neglected, with only two measurements of its integrated $H\beta$ flux (Osterbrock & Stockhausen 1961; O’Dell 1998), and a single observation of its integrated $H\alpha$ flux, an old one by Gebel (1968). Furthermore, the solar neighbourhood (Frew

& Parker 2006) is dominated by the demographically common low-surface brightness (LSB) PNe, typified by the discoveries of Abell (1966). For these faint nebulae, the $H\beta$ or $H\alpha$ fluxes are often poorly determined, if known at all. The data published to date have been measured from a variety of techniques and are often inconsistent (cf. Kaler 1983b; Ishida & Weinberger 1987; Kaler, Shaw & Kwitter 1990; Pottasch 1996; Xilouris et al. 1996, hereafter XPPT), so it is obvious that more work needs to be done.

Here we directly address these issues by presenting a homogenous catalogue of integrated $H\alpha$ fluxes for 1258 Galactic PNe. We incorporate some $H\alpha$ fluxes derived from SHASSA and VTSS that were previously published by our group. These are for PFP 1 (Pierce et al. 2004), RCW 24, RCW 69 and CVMP 1 (Frew, Parker & Russeil 2006), K 1-6 (Frew et al. 2011), M 2-29 (Miszalski et al. 2011), Abell 23, Abell 51, and Hf 2-2 (Bojičić et al. 2011b), and for the H II region around PHL 932 (Frew et al. 2010).

This paper is organised as follows: In §2, we outline the SHASSA and VTSS surveys used to provide the $H\alpha$ fluxes, in §3 we describe the photometry pipeline and provide a discussion of the flux uncertainties, before describing our results, and the catalogue of fluxes, in §4. We provide new independent reddening determinations for ~ 270 PNe in §5 and we outline our suggestions for future work in §6. We summarise our conclusions in §7. In addition, in Appendix A, we provide corrected $H\alpha$ fluxes for 49 objects, many little studied, from Abell (1966), Giesekeing, Hippelein & Weinberger (1986, hereafter GHW), Hippelein & Weinberger (1990, hereafter HW90), Xilouris et al. (1994), XPPT, and Ali et al. (1997), re-calibrated to our common zero-point; 24 of these are not included in either Table 3 or Table 4. Finally, as a resource for the wider community, we provide total $H\alpha$ fluxes for 76 misclassified objects from the literature in Appendix B.

2 THE $H\alpha$ SURVEY MATERIAL

The increasing online availability of wide-field digital imaging surveys in the $H\alpha$ line is changing our ability to undertake large-scale projects such as this (for a review of earlier $H\alpha$ surveys, see Parker et al. 2005). Here we use two narrow-band CCD surveys: the Southern $H\alpha$ Sky Survey Atlas¹ (SHASSA; Gaustad et al. 2001, hereafter GMR01) and the Virginia Tech Spectral-line Survey² (VTSS; Dennison, Simonetti & Topasna 1998), to provide the base data for our new PN flux determinations. Other surveys such as the Mt Stromlo Wide Field $H\alpha$ Survey (Buxton, Bessell & Watson 1998) and the Manchester Wide Field Survey (e.g. Boumis et al. 2001) were unavailable in digital form so were not utilized in this study.

2.1 SHASSA

SHASSA is a robotic wide-angle digital imaging survey covering 21 000 sq. degrees of the southern and equatorial sky undertaken with the aim of detecting $H\alpha$ emission from the

¹ <http://amundsen.swarthmore.edu/>

² <http://www.phys.vt.edu/halpha>

warm ionized interstellar medium (WIM). The survey consists of 2168 images covering 542 fields south of $+16^\circ$ declination, between Galactic longitudes of 195° and 45° at the mid-plane (GMR01). SHASSA used a 52-mm focal length Canon lens operated at $f/1.6$, placed in front of a 1024×1024 pixel Texas Instruments chip with $12\mu\text{m}$ pixels. This produced images with a field of view of $13^\circ \times 13^\circ$ (1014×998 pixels) and a scale of $47.64''$ per pixel. The H α interference filter ($\lambda_{\text{eff}} = 6563\text{\AA}$, FWHM = 32\AA) and a dual-band notch filter (that transmits two bands at $\lambda_{\text{eff}} = 6440\text{\AA}$ and 6770\AA , both with FWHM = 61\AA) are mounted in a filter wheel in front of the camera lens (GMR01).

There are four images available for each field: H α , red continuum, continuum-corrected H α (generated by subtracting each continuum image from the corresponding H α image), and a smoothed H α image. The continuum-subtracted H α images have a limiting sensitivity³ of better than 2 R pixel^{-1} , corresponding to an emission measure of $\sim 4\text{ cm}^{-6}\text{ pc}$. The continuum-subtracted SHASSA data are available as either the original $48''$ resolution data, or smoothed data median-filtered to 5 pixels ($4.0'$), which allows the detection of large-scale features as faint as 0.5 R (or an emission measure of $\approx 1\text{ pc cm}^{-6}$). GMR01 repeated all fields with offsets of 5° in both coordinates, which helped confirm objects of very low surface brightness. Thus, the number of individual measurements for a PN can be up to five in some favourable cases.

The full-resolution, continuum-subtracted SHASSA data often show pixels with unphysical, negative values which are residuals from poorly subtracted stellar images. These are largely removed in the smoothed images. However these were not utilised for determining flux measurements, as smoothing mingles the flux from the PN with the ambient sky background, and can lead to an overestimate of the true flux when this background is significant.

Despite the relatively coarse resolution of the SHASSA data, a large fraction of Galactic PNe are either large enough or bright enough to be readily detected by the survey, which allows for an accurate H α flux determination. The CCD camera had a linear response up to the full-well capacity ($\approx 60\,000\text{ ADU}$), but the variance (σ^2) increased non-linearly above $20\,000\text{ ADU}$. Note that almost all of the observed PNe give values below this limit. Further details on the camera and the data processing pipeline are given by GMR01.

The SHASSA intensity calibration was derived using the PN spectrophotometric standards of DH97, after the continuum images had been scaled and subtracted from the H α frames. However, a difficulty in applying PN line fluxes to H α narrow-band imaging is the proximity of the two [N II] $\lambda\lambda 6548, 6584$ lines which are included in the flanks of the SHASSA H α filter bandpass. These vary in strength relative to H α between PNe and may significantly affect the flux determination if not taken into account, especially for the so-called Type I nebulae (Peimbert 1978; Peimbert & Serrano 1980; Peimbert & Torres-Peimbert 1983; Kingsburgh & Barlow 1994), which have elevated [N II]/H α ratios. The

DH97 standards were all compact so the [N II]/H α ratios are reliable. However, this ratio can vary quite significantly across well resolved PN and will be affected if the slit just happens to be oriented to intersect low-ionisation structures such as ansae and FLIERS (Balick et al. 1994; Gonçalves, Corradi & Mampaso 2001). We further discuss this point in §3.2, below.

Calculating the transmission properties of the interference filter to these lines is also complicated by the blue-shifting of the bandpass with incident angle of the converging beam (e.g. Parker & Bland-Hawthorn 1998). These effects are considered in §4 of GMR01 and are carefully accounted for in their calibration. An additional uncertainty in the SHASSA zero-point derives from the contribution of geocoronal H α emission. GMR01 estimated this by comparing the SHASSA intensities with overlapping 1° field-of-view data points from the Wisconsin H-Alpha Mapper (WHAM; Haffner et al. 2003), and interpolating if there is no available WHAM data. WHAM provides a stable intensity zero-point over 70% of the sky at 1° resolution, and is now being extended to the southern sky by the WHAM-South Survey (Haffner et al. 2010). Finkbeiner (2003, hereafter F03) showed there is no significant offset between WHAM and SHASSA data (cf. VTSS, see below), which indicates that the geocoronal contribution to the SHASSA H α images has been appropriately corrected for.

In order to further ascertain the reliability of the SHASSA intensity calibration, a first-step analysis was conducted by Pierce et al. (2004; see also Parker et al. 2005) which showed that the aperture photometry from the full-resolution data returns the best measurement of the integrated H α flux. Available spectroscopic data were used to deconvolve the contribution from the [N II] lines passed by the SHASSA filter (see §3.2 and 3.3 below) for these calibration PNe.

2.2 VTSS

A complementary survey to SHASSA, the VTSS (Dennison et al. 1998) covers a wide strip around the northern Galactic plane ($15^\circ < l < 230^\circ$, $|b| \leq 30^\circ$), north of $\delta > -15^\circ$. Like SHASSA, the combination of fast optics, narrowband interference filters, and a CCD detector gives this survey very deep sensitivity to diffuse H α emission. The VTSS used the Spectral Line Imaging Camera which utilised a Noct-Nikkor lens ($f/1.2$) of 58mm focal length placed in front of a Tektronix 512×512 pixel chip with $27\mu\text{m}$ pixels. This produced images with a circular field of view with a diameter of 10° , with a resolution of $96''$ pixels. A filter wheel in front of the lens holds a narrow bandpass H α interference filter ($\lambda_{\text{eff}} = 6570\text{\AA}$, FWHM = 17.5\AA), various wider continuum filters, and an [S II] filter centred at $\lambda 6725\text{\AA}$. Further details are given by Topasna (1999).

Each VTSS survey field was planned to have four images available: H α , continuum-corrected H α , [S II] and continuum-corrected [S II]. The continuum-corrected H α and [S II] images are produced by subtracting an aligned and scaled continuum image from the H-alpha or [S II] image. Continuum images are taken with a wide-bandpass filter, or a double-bandpass filter astride the H α line or [S II] doublet (Dennison et al. 1998). Each field name consists of the standard 3-letter IAU constellation abbreviation, plus a 2-

³ The sensitivity limits of the various H α surveys are generally quoted in Rayleighs, where $1\text{ R} = 10^6/4\pi\text{ photons cm}^{-2}\text{ s}^{-1}\text{ sr}^{-1} = 2.41 \times 10^{-7}\text{ erg cm}^{-2}\text{ s}^{-1}\text{ sr}^{-1} = 5.66 \times 10^{-18}\text{ erg cm}^{-2}\text{ s}^{-1}\text{ arcsec}^{-2}$ at H α .

digit running number (e.g. Cyg10). However, VTSS remains incomplete and is likely to remain so. The original survey footprint was planned to cover >1000 sq. degrees (Dennison et al. 1998), but at the time of writing, continuum-corrected H α images are available for only 106 of 227 fields (an additional six fields have uncorrected H α images), and no [S II] images are available. The narrow bandpass of the VTSS H α filter, with essentially no transmission of the flanking [N II] lines, makes the H α flux determination straightforward in principle. The sensitivity limit of VTSS is ~ 1 R, comparable to SHASSA for diffuse emission, but since the resolution is only half that of SHASSA, the VTSS has a factor-of-four brighter detection limit for PNe (and other compact H α emitters) due to confusion noise.

3 METHODOLOGY

The following sections describe our flux measurement process, including the derivation of the input catalogue, the source references for the [N II] fluxes which need to be deconvolved from the SHASSA fluxes, and detailed descriptions of the photometry pipeline and our error budget.

3.1 Input Catalogue

The fluxes presented here are based on the contents of a ‘living’ relational database we have designed (Bojičić et al. 2013, in preparation) containing all bona fide, possible, and misclassified PNe from the major catalogues that have been published previously. The PNe have been taken from Perek & Kohoutek (1967), Acker et al. (1992, 1996), Kimeswenger (2001), Kohoutek (2001), the MASH catalogues (Parker et al. 2006; Miszalski et al. 2008), and the preliminary IPHAS discovery lists (Mampaso et al. 2006; Sabin 2008; Viironen et al. 2009a,b, 2011; Sabin et al. 2010; Corradi et al. 2011).

To supplement these catalogues, we also added a sample of ~ 320 true and candidate PNe from the recent literature, primarily discovered (or confirmed) optically. These were taken from Zanin et al. (1997), Weinberger et al. (1999), Beer & Vaughan (1999), Kerber et al. (2000), Cappellaro et al. (2001), Eracleous et al. (2002), Whiting, Hau & Irwin (2002), Bond, Pollacco & Webbink (2003), Boumis et al. (2003, 2006), Lanning & Meakes (2004), Jacoby & Van de Steene (2004), Suárez et al. (2006), Frew, Madsen & Parker (2006), Whiting et al. (2007), Miszalski et al. (2009), Fesen & Milisavljevic (2010), Jacoby et al. (2010), Miranda et al. (2010), Acker et al. (2012), Parker et al. (2012b), Parthasarathy et al. (2012), and Kronberger et al. (2012).

We also included over 100 unpublished candidates found by the Macquarie group,⁴ plus sundry other objects, e.g. Mu 1 (A. Murrell, pers. comm. 2004) and Ju 1 (Jurasevich 2009). All objects were cross-checked for duplication and identity, noting that the classifications of many nebulae have been fluid over time. An example is the Type I planetary K 1-9 (PK 219+01.1; Kondratyeva & Denissyuk 2003) as noted in the SIMBAD database.

⁴ So far 30 nebulae have been *discovered* from the SHASSA and VTSS; the nomenclature for those objects listed in this paper continues on from Frew et al. (2006) and Frew (2008).

Additional candidate PNe recently found in near/mid-IR surveys were also added to our database. These are unlikely to be detected in the SHASSA or VTSS surveys, but were included as we wanted to calculate the fraction of PNe found in the survey footprint that were detected by our photometry pipeline. These PNe were taken from Phillips & Ramos-Larios (2008), Kwok et al. (2008), Froebrich et al. (2011), Oliveira et al. (2011), Ramos-Larios et al. (2012) and Parker et al. (2012b), while another 320+ PN candidates found in the mid-IR at 24 μ m were added from Mizuno et al. (2010), Wachter et al. (2010) and Gvaramadze et al. (2010).

Over 6000 individual Galactic objects are currently in our working database, including 3320 bona fide and possible PNe⁵ and 480 post-AGB stars and related objects (Szczerba et al. 2007, 2012; Sahai et al. 2007; Lagadec et al. 2011). There are also ~ 1500 mimics of various kinds (e.g. Kohoutek 2001; Frew & Parker 2010, hereafter FP10; Frew & Parker 2011; Boissay et al. 2012),⁶ with the remaining objects being currently unclassified; these await a more detailed investigation into their nature.

Of the true and possible PNe, 2880 are located in the combined footprint of the two H α surveys, which represent our input catalogue for the photometry pipeline (see §3.3). This is a substantial increase in numbers over the preliminary input list presented by Bojičić, Frew & Parker (2012a). In all, we measured H α fluxes (see § 3.3) for ~ 1120 PNe from SHASSA and 178 PNe from the VTSS, 1234 objects in total because of overlap between the two surveys.⁷ Thus $\sim 43\%$ of the PNe found in the SHASSA or VTSS surveys were bright enough to be detected by the pipeline. For the other 1650 PNe, they were in the main too faint, or were northern PNe which fell outside the VTSS coverage (e.g. NGC 2392). There were also a few moderately bright PNe which were too close to a bright star or artefact to be measurable. We note that $\sim 80\%$ of MASH PNe are too faint to be detected in SHASSA, and almost all of the recent IPHAS discoveries are too faint for VTSS. We have also measured the integrated H α fluxes for 76 mimics and present these in Appendix B. If there is currently no consensus in the literature on the nature of a PN-like object, we included it in the main tables for the time being, and flagged it as a possible or uncertain PN.

3.2 Spectrophotometric Data

The VTSS H α filter is essentially monochromatic, rejecting the flanking [N II] lines (Topasna 1999) which simplifies the data reduction. However, the SHASSA filter, while centred near H α , is broader with a FWHM of 32Å, transmitting both [N II] lines in the filter wings. The transmission factors for the $\lambda 6548$, H α and $\lambda 6584$ lines at rest wavelengths are

⁵ This total includes about 45 transitional objects (e.g. Suárez et al. 2006; Parthasarathy et al. 2012).

⁶ Previous PN catalogues contain many astrophysical sources masquerading as PNe (see Appendix B). We are currently re-investigating the mimics in our database using a suite of multi-wavelength discrimination techniques (FP10; Cohen et al. 2011; Boissay et al. 2012).

⁷ A few shock-excited pre-PNe such as CRL 618 were also detected by the pipeline.

39%, 78% and 26% respectively (GMR01). In order to derive a pure H α flux for each object, the observed nebular $\lambda\lambda 6548, 84/\text{H}\alpha$ ratio (hereafter $R_{[\text{N II}]}$) is required to deconvolve the [N II] contribution to the SHASSA red flux. The spectrophotometric data required to do this is widely scattered in the literature, but we made a concerted effort to recover and evaluate these data.

We gave preference to any integrated values for $R_{[\text{N II}]}$ measured with modern linear detectors, or where we believe the data has been carefully taken and reduced. The primary sources for $R_{[\text{N II}]}$ are as follows: (i) large-aperture narrow-band photoelectric photometry (e.g. KM81; SK89), (ii) narrowband CCD imagery (e.g. Hua, Dopita & Martinis 1998), (iii) wide-slit spectroscopy (e.g. Torres-Peimbert & Peimbert 1977; Gutiérrez-Moreno, Cortes & Moreno 1985; DH97; WCP05; Wang & Liu 2007), (iv) drift-scan long-slit methods (e.g. Liu et al. 2000, 2004; Tsamis et al. 2003; Zhang et al. 2005; Fang & Liu 2011), (v) Integral Field Unit (IFU) spectroscopy (e.g. Tsamis et al. 2008), or (vi), data obtained with large-aperture Fabry-Perot spectrometers such as WHAM (Haffner et al. 2003) or other similar instrumentation (e.g. Lame & Pogge 1996). The WHAM data will be published in detail in a separate paper (G. Madsen et al., in preparation), but some preliminary flux data were presented by Madsen et al. (2006). For these sources, we adopt a conservative uncertainty of 10% in the value of $R_{[\text{N II}]}$.

For PNe without integrated values for $R_{[\text{N II}]}$, we adopted an average of the data presented in the *Catalog of Relative Emission Line Intensities Observed in Planetary Nebulae* (ELCAT)⁸ compiled by Kaler, Shaw & Browning (1997), supplemented with data taken from more recent papers in the literature, including Kraan-Korteweg et al. (1996), Pollacco & Bell (1997), Weinberger, Kerber & Gröbner (1997), Kerber et al. (1997, 1998, 2000), Perinotto & Corradi (1998), Condon, Kaplan & Terzian (1999), Ali (1999), Escudero & Costa (2001), Rodríguez, Corradi & Mampaso (2001), Milingo et al. (2002), Kondratyeva & Denissyuk (2003), Kwitter, Henry & Milingo (2003), Costa, Uchida & Maciel (2004), Emprechtinger et al. (2004), Exter, Barlow & Walton (2004), Costa, Uchida & Maciel (2004), Górny et al. (2004, 2009), Krabbe & Copetti (2006), Henry et al. (2010), Milingo et al. (2010), Miszalski et al. (2012a,b), García-Rojas et al. (2012) and Frew et al. (2012). An average of measurements from several independent sources should be fairly representative of the integrated [N II]/H α ratio for each PN, and we estimate a typical uncertainties in $R_{[\text{N II}]}$ of 10–30%. For the MASH PNe, as well as a significant number of other southern PNe, we utilised our extensive database of >2000 spectra taken as part of the MASH survey. The analysis of these spectra will be published separately. Long slit spectra obtained from the *San Pedro Mártir* (SPM) *Kinematic Catalogue of Galactic Planetary Nebulae*⁹ (López et al. 2012) were also used to estimate $R_{[\text{N II}]}$ for objects with no other published data.

However, it is possible that the value of $R_{[\text{N II}]}$ taken from long-slit spectra is systematically overestimated for some evolved PNe, as spectrograph slits are often placed on bright rims to maximise the S/N ratio for these low-surface

brightness objects. These brighter rims usually result from an interaction of the PN with the interstellar medium, which are expected to have enhanced [N II] emission (Tweedy & Kwitter 1994, 1996; Pierce et al. 2004). If bright ansae or other low-excitation microstructures (Gonçalves et al. 2001) fall within the slit, this also has the potential to upset the [N II]/H α ratio. Alternatively, the slit might only cover the central region of a PN where the excitation is higher, leading to an underestimate of $R_{[\text{N II}]}$. The derived H α flux might therefore be slightly in error in these cases. Fortunately, the integrated H α flux is only weakly sensitive to the exact value of $R_{[\text{N II}]}$, for $R_{[\text{N II}]} < 1$ (see equation 7). In the future, increasing numbers of PNe will be observed with the current and next generation of IFUs (e.g. Roth et al. 2004; Monreal-Ibero et al. 2005; Tsamis et al. 2008; Sandin et al. 2008), which will largely remove these problems.

3.3 Photometry pipeline

To measure the PN fluxes, the IRAF¹⁰ `phot` task was used. A photometry pipeline was scripted in PyRAF, a Python interface to IRAF, by one of us (ISB) to facilitate the semi-automatic flux measurement of the large number of PNe found in the SHASSA and VTSS pixel data. In the case of SHASSA many PNe fall in several (up to 5) separate fields so it is possible to obtain multiple independent flux measurements in these cases. The amount of overlap between VTSS fields is much less, so the majority of PNe have only a flux measurement from a single field.

A PN was assumed to be detected if: (i) at least one pixel within the aperture had a flux of $+5\sigma$ above the adjacent sky background, and (ii), if rule (i) applies in more than 50% of fields containing the PN. For each object, a circular aperture was automatically placed over the catalogued PN position, taken principally from the SIMBAD database (Wenger et al. 2007). Circular apertures were chosen as most PNe are $< 2'$ (or ~ 3 pixels) across, so any asymmetries are largely washed out. We refine the catalogued position using the *centroid* algorithm but with a maximum allowed shift from the original position of one pixel. The PNe with a computed centroid more than one pixel from the catalogued position, and all larger PNe in our catalogue ($\theta_{PN} > 3'$), were carefully examined and, if needed, we applied an appropriate correction to the aperture position. For PNe that were detected on the images, but at less than 5σ above the sky, we individually examined each object and if possible, manually measured an integrated flux. These objects are flagged in the tables accordingly.

The radius in pixels of the aperture (θ_{ap}) to be used was calculated from the estimated FWHM of the point spread function (PSF) and the angular size (major axis) of the nebula (θ_{PN}) in arcsec, using:

$$\theta_{ap} = \begin{cases} \text{PSF} & \text{if } \theta_{PN} < \text{PSF} \\ \text{PSF} + 0.25 (\theta_{PN} - \text{PSF}) / P_S & \text{if } \theta_{PN} \geq \text{PSF} \end{cases} \quad (1)$$

¹⁰ IRAF is distributed by the National Optical Astronomy Observatory, which is operated by the Association of Universities for Research in Astronomy (AURA) under cooperative agreement with the National Science Foundation.

⁸ <http://stdas.stsci.edu/elcat/>

⁹ <http://kincatpn.astrosen.unam.mx>

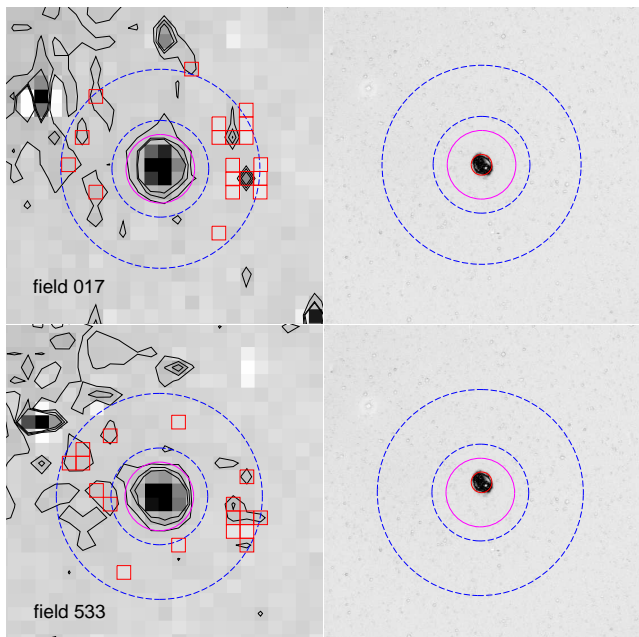


Figure 1. An example showing the image cutouts for the evolved PN NGC 4071 (SHASSA left, SHS right) generated by the photometry pipeline. The top field is extracted from SHASSA field #071 and the bottom is field #533, and all images are 8' on a side with north-east at top left. The left images plot the aperture diameter (magenta circle) and sky annulus (blue dashed circles), plus $H\alpha$ intensity contours at $1\sigma_{\text{sky}}$, $3\sigma_{\text{sky}}$ and $5\sigma_{\text{sky}}$. The right panels also indicate the catalogued PN diameter (small red circle). Note the artefacts from the imperfect off-band continuum subtraction on the two SHASSA panels, which also show the marked-out pixels (red boxes) that are excluded by the photometry routine. A colour version of this figure is available in the online journal.

where P_S is the CCD plate scale (47.64"/pix for SHASSA and 96.4"/pix for VTSS). We chose 2.25 pix and 2.0 pix as the default PSF values, i.e. the minimum aperture radii, for SHASSA and VTSS respectively. We found that an increase in the minimum aperture radius of 20% affects the flux estimate by less than 5%, however it significantly increased the chance of contamination of the measured flux from any nearby objects such as HII regions, or residuals from badly subtracted bright stars. Hence, we adopted a smaller value for VTSS owing to its larger pixel size which increased the chance of contamination by nearby sources on the sky. The uncertainty arising from the choice of the minimum aperture size (σ_{aper}) was estimated by examining curves of growth between 2 and 3 pixels. The applied routine automatically accounts for the differing relative areas of the object aperture and sky-subtraction annulus and it scales the sky subtraction accordingly. The number of pixels in a sky annulus is set to three times the number of pixels in the aperture (Merline & Howell 1995).

For each PN we also created a cutout image from the respective SHASSA or VTSS images, overlaid with circles indicating the catalogued PN diameter, the aperture and annulus sizes, and $H\alpha$ intensity contours at $1\sigma_{\text{sky}}$, $3\sigma_{\text{sky}}$ and $5\sigma_{\text{sky}}$ above the measured sky level, where σ_{sky} is the standard deviation of pixel intensities in the sky annulus. For

PNe imaged by the SHS (Parker et al. 2005) including all of the MASH PNe (Parker et al. 2006; Miszalski et al. 2008), quotient images ($H\alpha$ / broadband R) were also generated for each PN. The fits images were automatically created using the IRAF task `imarith` before being converted to `png` format using the `APLpy` module¹¹). Each image was linearly stretched using the default minimum and maximum pixel values (0.25% and 99.75%) and overlaid with the intensity contours from the corresponding SHASSA/VTSS image.

This procedure allowed for rapid examination of the SHASSA and VTSS images (and SHS images where available) in common image viewing software for quality control. The images were independently examined by all three co-authors and each object was noted as either a definite, possible, or non-detection on the SHASSA or VTSS images. Any PNe that are confused with nearby objects or stellar residuals were flagged accordingly.

Finally, the total pixel counts, the flux after the background correction, and the statistics in the annulus and in the aperture were obtained for each PN. Measurements affected by poor sky estimates, confusion with bright sources, or various stellar residuals or other artefacts contaminating the aperture or sky annulus were carefully examined and re-measured manually. In these cases measurements of the sky background were made through an aperture identical to the PN aperture at a number of representative regions immediately surrounding the nebula, in order to accurately account for the surrounding diffuse $H\alpha$ emission. The dispersion in these is the principal uncertainty in the measurement.

Many compact high surface brightness PNe have surrounding AGB halos (e.g. Corradi et al. 2003; Frew, Bojčić & Parker 2012a) included in the photometry aperture, but as the typical halo surface brightness is a factor of 10^{-3} fainter than the main shell (Corradi et al. 2003; Sandin et al. 2008; Sandin, Roth & Schönberner 2010), we ignore this contribution. For NGC 7293, a structured AGB halo (Malin 1982; O'Dell 1998; Parker et al. 2001; Speck et al. 2002; O'Dell, McCullough & Meixner 2004; Meaburn et al. 2005) is readily visible on SHASSA. For others, such as NGC 3242 (Bond 1981; Phillips et al. 2009) and Abell 21, the surrounding material is more likely to be ionized ISM. These PNe are flagged in the main tables.

Obtaining integrated fluxes from the SHASSA data is quite straightforward. Firstly, a 'red' $H\alpha$ + $[N\text{II}]$ flux in cgs units¹² is given by:

$$F_{\text{red}}^{\text{SHASSA}} = 5.66 \times 10^{-18} \times P_S^2 \times (\text{SUM}/10) \text{ erg cm}^{-2} \text{ s}^{-1} \quad (2)$$

The constant in the expression is the conversion factor from Rayleighs to cgs units (at $H\alpha$ and/or $[N\text{II}]$) and as before, P_S is the plate scale of the SHASSA survey (47.64"/pixel). Note that the native SHASSA units are decirayleighs (1 dR = 0.1 R), hence the SUM of the background-corrected counts obtained from the routine are divided by 10.

As described in § 2.1, the SHASSA filter passes $H\alpha$ and both $[N\text{II}]$ lines. In order to derive a pure $H\alpha$ flux for each

¹¹ The Astronomical Plotting Library in Python, available from <http://aplpy.github.com>

¹² $1 \text{ erg cm}^{-2} \text{ s}^{-1} = 1 \text{ mW m}^{-2}$ in the SI system.

object, we used the observed [N II]/H α ratio (obtained as described in §3.2) to deconvolve the [N II] contribution to the SHASSA red flux. The expression for correcting the [N II] contribution is:

$$F(\text{H}\alpha)_{\text{SHASSA}} = \frac{F_{\text{red}}}{K_{\text{tr}} R_{[\text{N II}]} + 1} \quad (3)$$

where $R_{[\text{N II}]}$ is the adopted [N II]/H α ratio for the PN and K_{tr} is a dimensionless constant which takes into account the transmission of the filter at H α and for each [N II] line. Note that the [N II] flux refers to the sum of the $\lambda 6548$ and $\lambda 6584$ lines, and the ratio of the two is quantum mechanically fixed to be ~ 3 . For the SHASSA filter we determine $K_{\text{tr}} = 0.375$ using the transmission coefficients of the filter given by GMR01. If only the brighter $\lambda 6584$ line is measurable in a spectrum, $F_{[\text{N II}]}$ is estimated as $4/3 \times F(\lambda 6584)$.

A smaller number of PNe were measured from the VTSS survey (Dennison et al. 1998). The procedure for VTSS (including the treatment of the uncertainties) is identical to that used for the SHASSA measurements with the important simplification that a correction for [N II] emission is not necessary as these lines are not passed by the narrowband VTSS H α filter, unless the radial velocity of the PN is significant. The native units of the VTSS are Rayleighs, so the adopted equation is:

$$F(\text{H}\alpha)_{\text{VTSS}} = 5.66 \times 10^{-18} \times P_S^2 \times \text{SUM} \quad \text{erg cm}^{-2} \text{s}^{-1} \quad (4)$$

where in this case $P_S = 96.4'' \text{pix}^{-1}$. The VTSS fluxes were then brightened by 0.04 dex (or 12%) based on a comparison between SHASSA and VTSS fluxes (see §4.1.2).

3.4 Analysis of Photometric Errors

The measured nebular flux for any PN is expected to have a Poissonian uncertainty. The total uncertainty in each flux measurement is a quadratic summation of the uncertainties due to photon statistics (i.e. shot noise from the nebula and sky), dark current noise, readout noise, the survey calibration uncertainty, and the uncertainty in the adopted [NII]/H α ratio of the PN. Additional terms are due to the PN's heliocentric radial velocity and the angular offset of the PN from the camera's optical axis (which causes a shift in the effective wavelength of the filter).

A further potential uncertainty depends on any error in the angular position of the PN, which leads to vignetting of the photometric aperture automatically placed around the catalogued PN position. GMR01 found that the instrumental positions of several stars on each field matched the catalogued positions to 0.18 pixel ($8''$) rms, derived from first-order plate equations. However, we found that a non-trivial fraction of Galactic PNe have uncertainties of up to $20''$ in the positions catalogued by SIMBAD. For a small number of PNe with more severe positional errors, we manually re-centered the aperture to accept all of the flux from the PN.

The uncertainty due to shot noise scales as the square-root of the flux. Following Masci (2008), the resulting uncertainty in the integrated red flux due to all noise terms, including the uncertainty from the fixed minimum aperture (σ_{aper}), is given as:

$$\sigma_{\text{phot}}^2 = \frac{1}{g} \sum_i^{N_A} \frac{(S_i - \bar{B})}{N_i} + \left(N_A + k \frac{N_A^2}{N_B} \right) \sigma_{B/\text{pix}}^2 + \sigma_{\text{aper}}^2 \quad (5)$$

where S_i is the recorded intensity, g is the gain in electrons/ADU, N_A is the number of pixels in the nebular aperture, N_B is the number of pixels in the sky annulus, N_i is the depth-of-coverage at pixel i (for SHASSA, each survey field is the combination of five individual exposures so $N_i = 5$), S_i is the signal in pixel i , \bar{B} is the mean sky background count per pixel in the annulus, and $\sigma_{B/\text{pix}}^2$ is the variance in the sky background annulus in [image units]²/pixel. We use an intensity-weighted mean, or centroid of the background pixel histogram in the sky annulus to use as the correction for the aperture; hence $k = 1$ in the formula above (following Masci 2008). Bad pixels or pixels with an intensity value $> 3\sigma_{\text{sky}}$ from the mean were rejected from the sky pixel distribution.

Fluxes were automatically flagged if the PN is confused with adjacent objects and stellar residuals (based on a variance cut in pixel values), or shows unphysical pixel values within the aperture. While SHASSA is linear up to the full-well capacity (60 000 ADU), the variance increases non-linearly above 20 000 ADU (GMR01). Consequently, 25 bright PNe on SHASSA were flagged because the maximum pixel value was $> 20 000$ ADU. Two PNe (IC 418 and NGC 6572) had a maximum pixel value slightly above 60 000 ADU. Any additional uncertainty added to the H α flux, however, must be small, as our derived fluxes are in good agreement with published values.

An additional source of uncertainty follows from the shift in effective wavelength of the filter if the incident flux is not normal to its surface. Because the H α filter was placed in front of the lens, light entered the filter as a parallel beam at an angle of incidence equal to the angular distance of the object from the optical axis. For a simple interference filter, and at angles $\leq 10^\circ$ (Parker & Bland-Hawthorn 1998), the wavelength, λ_Θ at angle of incidence, Θ is given by :

$$\lambda_\Theta = \lambda_0 \left(1 - \frac{\sin^2 \Theta}{n_e^2} \right)^{1/2} \quad (6)$$

where λ_0 is the central wavelength of the filter bandpass and n_e is the refractive index of the spacer layers (usually ~ 2). As the angle of incidence increases, the H α and [NII] lines shift toward the red with respect to the filter's central wavelength, altering the transmission coefficients of the filter (GMR01). For $\Theta \simeq 9^\circ$, near the SHASSA image corners, the wavelength shift at H α is approximately 10 Å, significant compared to the filter FWHM of 32 Å. GMR01 found that the intensity-weighted average transmission of the two [N II] lines is a weakly varying function of angle of incidence but did not consider this in their calibration. However, to mitigate this effect, we do not measure the flux for any PNe that are more than 6° from a field centre, unless this is the only available measurement. There were such 18 cases, and these are flagged in Table 1.

To calibrate the SHASSA data in ADUs per unit H α flux, GMR01 compared their measured H α fluxes for 18 compact PNe to the accurate H α fluxes of DH97. The fluxes were corrected for the two [N II] emission lines adjacent to H α .

By definition, the mean difference between the PN fluxes in the GMR01 calibrating sample and those from DH97 is zero. From this comparison, the gain factor of the survey was determined: $g = 6.8 \pm 0.3 \text{ ADU R}^{-1} \text{ pix}^{-1}$ at $\text{H}\alpha$. The calibration uncertainty (σ_{cal}) of 8% was attributed to uncorrected atmospheric extinction and the undersampling of the instrumental PSF by the $12\mu\text{m}$ pixels. Including an independent comparison of the integrated $\text{H}\alpha$ flux of the Rosette nebula with that from Celnik (1983), the overall calibration uncertainty was found to be better than $\pm 9\%$ (GMR01).

A further term is the uncertainty in the deconvolved $\text{H}\alpha$ flux due to the uncertainty in the adopted $[\text{N II}]/\text{H}\alpha$ ratio. This is defined as:

$$\sigma_R = \frac{0.375 R}{(0.375 R + 1)} \times \frac{dR}{R} \quad (7)$$

where R and dR are the adopted $[\text{N II}]/\text{H}\alpha$ ratio and its proportional uncertainty respectively. The total uncertainty on the $\text{H}\alpha$ flux is then given by the following expression:

$$\sigma_{F(\text{H}\alpha), \text{SHASSA}}^2 = \sigma_{\text{phot}}^2 + \sigma_R^2 + \sigma_{\text{cal}}^2 \quad (8)$$

where σ_{phot} is the proportional uncertainty in the photometry measurement, σ_R is the uncertainty in the deconvolved $\text{H}\alpha$ flux due to the uncertainty in $R_{[\text{N II}]}$, and σ_{cal} is the calibration uncertainty of $\pm 8\%$.

As described in §3.3, the VTSS fluxes were corrected based on zero-point offset between SHASSA/WHAM and VTSS (GMR01; F03; see §4.2), noting that the WHAM survey provides a stable zero-point over 70% of the sky (F03). After applying this offset, the adopted VTSS calibration uncertainty was assumed to be equivalent to SHASSA, or 10%. This has been added in quadrature to the measurement uncertainty determined from the photometry routine to determine the final uncertainty on the $\text{H}\alpha$ flux, viz:

$$\sigma_{F(\text{H}\alpha), \text{VTSS}}^2 = \sigma_{\text{phot}}^2 + \sigma_{\text{cal}}^2 \quad (9)$$

where as before σ_{phot} and σ_{cal} are the measurement and calibration uncertainties respectively.

3.5 Radial Velocity Corrections

For PNe with known heliocentric radial velocities (e.g. Durand, Acker & Zijlstra 1998), we calculated the expected shift of the $\text{H}\alpha$ line in order to determine the filter transmission at that wavelength. The vast majority of disk PNe have heliocentric radial velocities, $v_{\text{hel}} \leq \pm 100 \text{ kms}^{-1}$ but bulge PNe can have relatively high velocities (up to $\pm 270 \text{ kms}^{-1}$; Durand et al. 1998), which can shift the observed wavelength by up to 6\AA . The original calibration of GMR01 made no correction for the observed RV of the calibrating PNe, so any uncertainty introduced by this simplification should be already accounted for by the calibration uncertainty term, σ_{cal} . Because the exact filter transmission of the $\text{H}\alpha$ and flanking $[\text{N II}]$ lines is difficult to model as the velocity changes, we simply add quadratically a further uncertainty of 6 per cent for bulge PNe with $|v_{\text{hel}}| = 100\text{--}200 \text{ kms}^{-1}$, and 15 per cent for bulge PNe with $|v_{\text{hel}}| > 200 \text{ kms}^{-1}$.

For VTSS the change in filter transmission with wavelength is more rapid, due to the narrow FWHM of the filter. For a PN with a velocity of -150 kms^{-1} , the $\text{H}\alpha$ line is shifted toward the blue edge of the filter, and the $[\text{N II}]\lambda 6584$ is potentially brought into the filter bandpass. Fortunately most northern PNe have relatively sedate radial velocities (only 5% of PN have $v_{\text{hel}} < -100 \text{ kms}^{-1}$). Again we assume that the calibration term, σ_{cal} , accounts for this additional uncertainty.

3.6 The effect of $[\text{S II}]$ emission in the SHASSA continuum filter

It is important to note that the $[\text{S II}] \lambda\lambda 6717, 6731\text{\AA}$ lines are transmitted by the blue wing of the 6770\AA filter with throughputs of ~ 16 and ~ 3 per cent respectively, increasing towards the field edges. The median $[\text{S II}]/\text{H}\alpha$ ratio for PNe from the data presented in FP10 is ~ 0.10 , and while some PNe can have $[\text{S II}]/\text{H}\alpha$ ratios approaching unity (FP10), these are evolved PNe with the $[\text{S II}] \lambda 6717/\lambda 6731$ ratio in the low-density limit so any $[\text{S II}]$ contamination is lessened. Fortunately the uncertainty in the $\text{H}\alpha$ flux due to $[\text{S II}]$ over-subtraction is at the $\sim 1\text{--}2$ per cent level for a typical PN, and can be safely neglected. We assume any residual uncertainty is incorporated in the zero-point error of the survey (see later, §3.4). However, for strongly shock-excited nebulae such as supernova remnants and Herbig-Haro objects, the fluxes derived from the SHASSA images will be less accurate, perhaps with an uncertainty of up to 25% for objects near the edge of the fields (see GMR01).

3.7 Contamination of the nebular $\text{H}\alpha$ flux by ionized helium

We have made no correction to the $\text{H}\alpha$ flux for the nebular He II 6-4 line at 46560\AA , which typically has an intensity of about 14% of the He II 4-3 line at 4686\AA (Brocklehurst 1971; Hummer & Storey 1987). Given the range of excitation seen in PNe, this corresponds to a $46560/46863$ ratio ranging between zero for very low-excitation (VLE) PNe (Sanduleak & Stephenson 1972), up to $\sim 5\%$ for the highest excitation objects (e.g. Kaler 1981). Given the average intensity of the 4686 line seen in PNe (CKS92; Tylenda et al. 1994), the $\text{H}\alpha$ flux for most PNe is overestimated by $\lesssim 2\%$. This correction (~ 0.01 dex) is smaller than the observational uncertainties.

3.8 Stellar contamination of the $\text{H}\alpha$ flux

PNe exhibit a wide diversity of central star types, with both emission-line and absorption-line spectra represented (Smith & Aller 1969; Méndez 1991; Tylenda, Acker & Stenholm 1993; Werner & Herwig 2006; DePew et al. 2011; Weidmann & Gamen 2011; Werner 2012; Frew & Parker 2012; Todt et al. 2012; Miszalski et al. 2012b; Bojčić et al. 2012b). It is possible that PNe with bright central stars relative to the surrounding shell have integrated $\text{H}\alpha$ fluxes slightly in error. While the continuum subtraction process should largely alleviate this, there remains the possibility that contamination by strong emission-line central stars (e.g. [WC] stars) will lead to an overestimated flux for the PN. We examined

the spectra of several [WC] stars presented by DePew et al. (2011) and measured the strengths of the Pickering 6 He II line at $\lambda 6560\text{\AA}$. We found this line is typically at an intensity level of $\lesssim 2$ per cent of the nebular H α flux, so we made no change to the integrated fluxes as this correction (~ 0.01 dex) is also smaller than the observational uncertainties for most of the PNe considered.

Similarly, for PN with central binaries dominated by bright B-, A- or F-type companions with strong Balmer absorption lines, the nebular H α flux may be underestimated. The PNe affected are NGC 2346 (A5 V), NGC 3132 (A2 IV-V), Hen 2-36 (A2 III), Abell 14 (B7 V), Abell 79 (F0 V) and SuWt 2 (A1 IV sb2); there is no available VTSS image for NGC 1514 (A0 III). We estimated a magnitude offset (H $\alpha - R$) from the typical equivalent width of the H α line for each spectral type (e.g. Jaschek & Jaschek 1987), and then derived a correction factor to the H α flux for each PN based on a comparison of the apparent stellar R -band magnitude with the integrated nebular magnitude. The correction factors are relatively small, ranging from 0.04 dex (Abell 79) to 0.12 dex (SuWt 2), and have been applied to the H α fluxes presented in Tables 1 and 4.

However, for luminous LBV, B[e], and WR stars in ejecta nebulae, the contribution of the emission line star to the total H α flux is potentially significantly greater. For those objects listed in Table B1, we have made no attempt to deconvolve the H α (or He II $\lambda 6560$) flux of the ionizing star from the total H α flux, so the nebular fluxes should be considered as firm upper limits.

4 RESULTS

Our new homogeneously measured H α fluxes for 1230 true and possible PNe, derived from both the SHASSA and VTSS data, are presented in the following sections.

4.1 SHASSA H α Fluxes

The final H α fluxes for each PN from n separate SHASSA fields are combined to give a weighted mean:

$$\bar{F}_w = \frac{\sum_{i=1}^n w_i F_i}{\sum_{i=1}^n w_i} \quad (10)$$

where $[F_1, F_2 \dots F_n]$ are the individual flux estimates, with associated weights $[w_1, w_2 \dots w_n]$ determined from the inverse variances, $w_i = 1/\sigma_i^2$, via equation 8. It follows that the variance of the weighted mean is:

$$\sigma_{\bar{F}}^2 = \frac{V_1}{V_1^2 - V_2} \sum_{i=1}^n w_i (F_i - \bar{F}_w)^2 \quad (11)$$

where $V_1 = \sum_{i=1}^n w_i$ and $V_2 = \sum_{i=1}^n w_i^2$.

Table 1 contains the mean H α fluxes for ~ 1120 PNe derived from SHASSA images. Columns 1 and 2 give the standard *PNG* designation and the common name respectively, and columns 3 and 4 give the right ascension and declination (epoch J2000.0). The adopted [N II]/H α ratio is given in column 5, and the logarithms of the averaged red flux and the corrected H α flux are given in columns 6 and

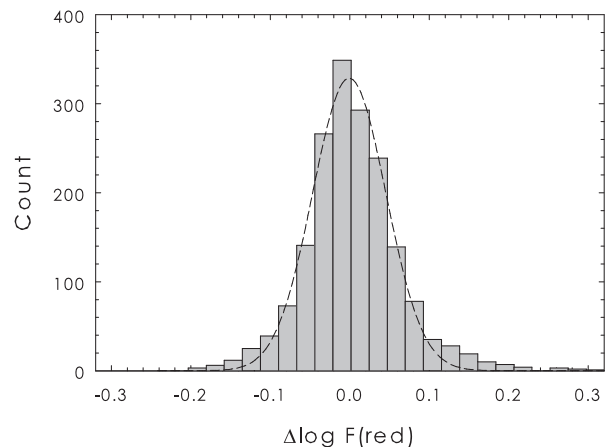


Figure 2. A difference histogram of individual flux measurements from SHASSA. The abscissa plots the difference between an individual flux measurement and the mean for that object ($\Delta \log F$), and the ordinate shows the number of separate determinations. The distribution is approximately Gaussian, with a standard deviation of 0.05 dex, in excellent agreement with the nominal zero-point error of the Survey.

7 respectively. Column 8 lists the adopted aperture radius in arcmin, and column 9 gives the number of independent fields from which a measurement is obtained. The derived extinction is given in column 10 and any notes are indexed in column 11, including noting if the PN has a central star with Wolf-Rayet features (see §3.8).

If we do not have any information on the [N II]/H α for an individual PN, we simply list the integrated red flux as measured from the images. An H α flux can be derived using equation 3 once spectroscopic data becomes available in the future.

4.1.1 Comparison of fluxes from different SHASSA fields

For each PN detected on SHASSA, we compared the individual flux measurements from separate fields with the mean flux of each PN to ascertain the repeatability of our procedure. In the difference histogram (Figure 2) the abscissa plots the difference between an individual flux measurement and the mean for that object ($\Delta \log F$), and the ordinate shows the number of determinations based on our measurements of all PNe detected in at least three SHASSA fields. The distribution is approximately Gaussian, with a dispersion of 0.05 dex, in excellent agreement with the nominal zero-point error of the survey.

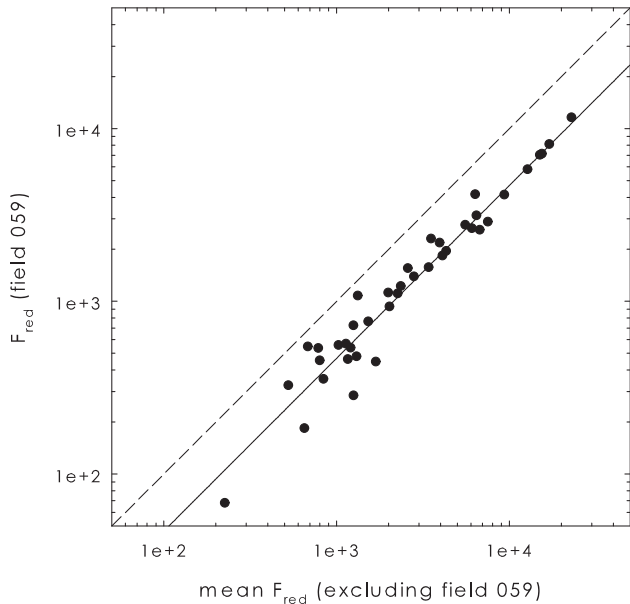
During this process it was noticed that the integrated fluxes measured from SHASSA field #059 were discrepant compared to the fluxes measured from overlapping fields. This field has an erroneous zero-point calibration, and gives nebular H α fluxes too faint by a factor of 2.14 (see Figure 3). We found smaller offsets for eight other fields. The correction factors for these fields are presented in Table 2. Five of the nine fields are below $\delta = -60^\circ$, where a cross-check with WHAM data is unavailable (GMR01). The source of error for the four fields north of this limit is not clear.

From equation 3 it follows that at $R_{[\text{N II}]} = 2.7$, the con-

Table 1. $H\alpha$ fluxes for 1120 true and possible PNe measured from SHASSA. The table is published in its entirety as an online supplement. A portion is shown here for guidance regarding its form and content.

PN G	Name	RAJ2000	DEJ2000	$R_{[N\text{II}]}$	$\log F_{\text{red}}$	$\log F(H\alpha)$	r_{aper}	N_f	c_β	Note
108.4–76.1	BoBn 1	00:37:16.0	–13:42:58	0.2	–12.03	–12.05±0.06	1.8	3	0.00	C
118.8–74.7	NGC 246	00:47:03.4	–11:52:19	0.0	–10.07	–10.07±0.03	6.1	2	0.02	
255.3–59.6	Lo 1	02:56:58.4	–44:10:18	1.1	–10.99	–11.14±0.06	4.5	4	...	
220.3–53.9	NGC 1360	03:33:14.6	–25:52:18	0.0	–9.78	–9.78±0.03	9.4	2	0.00	6
206.4–40.5	NGC 1535	04:14:15.8	–12:44:22	0.0	–9.95	–9.95±0.03	5.0	1	0.04	
...	Fr 2-3	04:56:20.0	–28:07:48	1.6	–10.89	–11.09±0.12	9.5	1	...	1
243.8–37.1	PRTM 1	05:03:01.7	–39:45:44	0.0	–12.02	–12.02±0.07	1.8	3	...	5
215.5–30.8	Abell 7	05:03:07.5	–15:36:23	0.8	–10.30	–10.41±0.06	11.0	1	...	
205.8–26.7	MaC 2-1	05:03:41.9	–06:10:03	0.0	–11.77	–11.77±0.05	1.8	3	...	
190.3–17.7	J 320	05:05:34.3	10:42:23	0.0	–10.91	–10.92±0.04	1.8	3	0.04	

Notes: (1) Possible PN; (2) pre-PN; (3) transition object; (4) uncertain counts; (5) confused with nearby object; (6) bad pixels in aperture; (7) object near field edge; (8) flux excludes halo; (9) flux corrected for CSPN; (10) Wolf-Rayet CSPN; (N) previously unpublished object; (V) very low excitation PN; (C) specific comment given.

**Figure 3.** A comparison of the $H\alpha+[N\text{II}]$ fluxes from SHASSA field #059 with the remainder. The abscissa plots the mean fluxes of 32 PNe from overlapping fields (excluding field #059) and the ordinate plots the fluxes for these PNe measured from field #059. The dashed and dotted lines show the 1:1 relation and the least squares fit to the data respectively. The fluxes from field #059 are a factor of 2.14 too low (or offset by 0.33 dex).

tribution from the two $[N\text{II}]$ lines in the overall flux is equal to $H\alpha$. We use this value to divide our PN sample into two groups, $[N\text{II}]$ -dominated and $H\alpha$ -dominated, and compare the SHASSA $H\alpha$ fluxes with our own VTSS measurements and with independent literature values. We found no significant difference between the samples, but did find that the $H\alpha$ fluxes from the Illinois group tend to be overestimated for PNe with $R_{[N\text{II}]} \geq 2$. We attribute this to their $H\alpha$ filter passing an uncorrected amount of $[N\text{II}]$ emission (Kaler, Pratap & Kwitter 1987; SK89).

Table 2. Offsets applied to nine discrepant SHASSA fields. The correction factor was found by dividing the mean flux of all PNe in fields excluding the affected field by the mean flux of the same PNe in that field.

SHASSA field	Field centre (J2000)	Corr. factor	Offset (dex)
031	08 ^h 53 ^m –60°11′	0.80	0.10
059	16 ^h 04 ^m –50°08′	2.14	–0.33
172	06 ^h 42 ^m –10°03′	0.81	0.09
190	18 ^h 43 ^m –09°57′	1.34	–0.13
518	14 ^h 49 ^m –75°12′	1.17	–0.07
536	15 ^h 55 ^m –65°09′	1.40	–0.15
584	15 ^h 13 ^m –45°11′	1.50	–0.18
653	18 ^h 36 ^m –24°57′	1.33	–0.12
708	07 ^h 02 ^m –05°04′	1.25	–0.10

4.1.2 Comparison of SHASSA and literature $H\alpha$ fluxes

In this section we present a detailed comparison between our new SHASSA $H\alpha$ fluxes and the equivalent measurements for the same PNe available in the literature. We demonstrate the validity of these new SHASSA fluxes and highlight some problems with previous determinations. The early study of Pierce et al. (2004) showed that the deconvolved SHASSA $H\alpha$ fluxes agreed with published data to $\Delta F(H\alpha) = -0.00$ dex, $\sigma = 0.07$ dex in the sense of SHASSA minus literature fluxes (see also Parker et al. 2005). Since GMR01 used 18 bright PNe from DH97 as SHASSA calibrators, it was expected that a comparison between the full set of DH97 fluxes and those derived here would have a negligible zero-point offset. We indeed found no offset for the 18 PNe of the original calibrating sample, and $\Delta F(H\alpha) = -0.02$ dex for the full set of 36 objects, excluding PN G307.2-09.0 (Hen 2-97) as it has an erroneous $H\alpha$ flux (M. Dopita, pers. comm. 2012). Not only does our expanded analysis here give a useful cross-check to the GMR01 intensity calibration, but it also allows the veracity of the adopted aperture photometry technique used here to be ascertained, including the treatment of the deconvolution of the $[N\text{II}]$ lines from the red flux for each PN.

In order to undertake the comparison, we have carefully

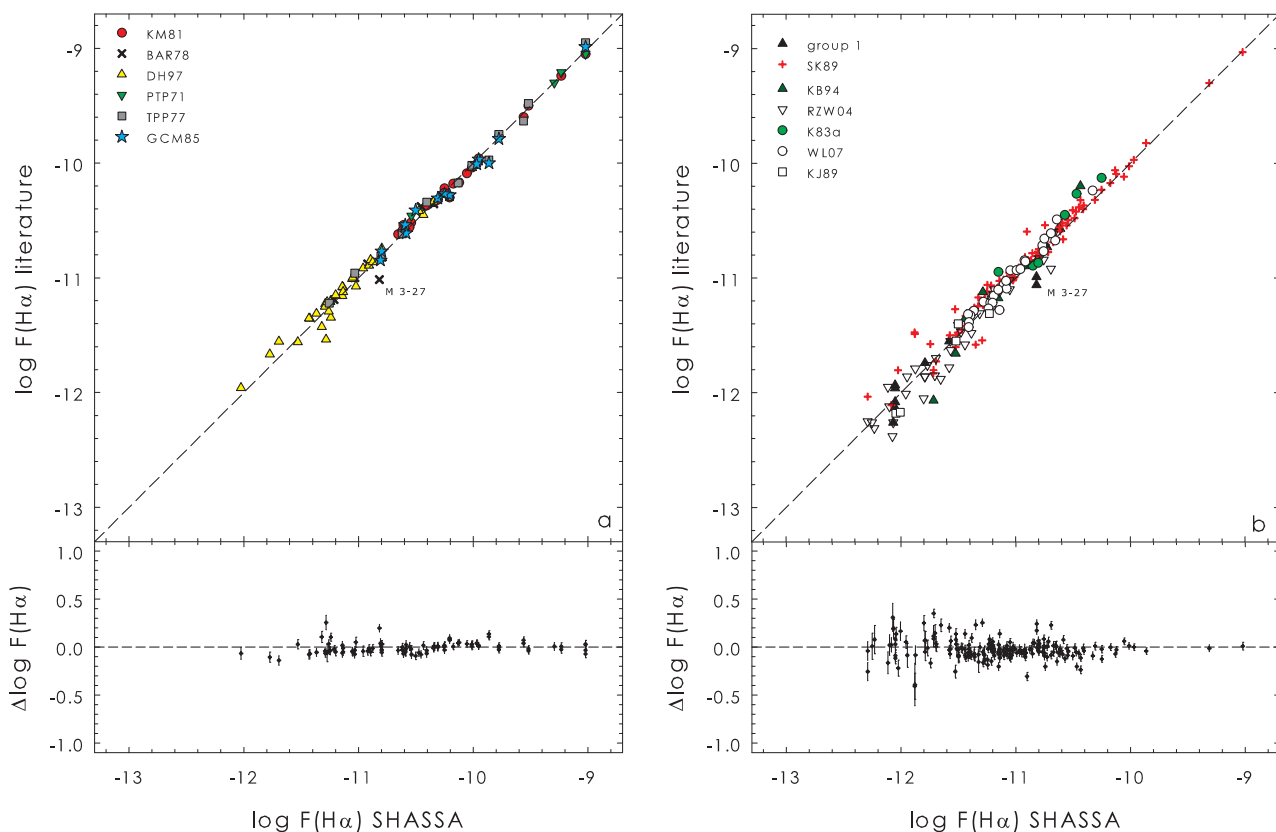


Figure 4. A comparison of our $H\alpha$ fluxes determined from SHASSA with those from the literature. The left panel shows fluxes from sources deemed to have the highest level of precision and accuracy, as defined in the text. The agreement between our fluxes and those from the literature is excellent over more than three orders of magnitude. The right panel compares our $H\alpha$ fluxes with the fluxes from sources with a somewhat lower accuracy, or reliable data-sets with less than three objects in common. A colour version of this figure is available in the online journal.

compiled a large database of $H\alpha$ and other line fluxes from the literature. The literature fluxes have been measured using a variety of methods, with a range of observational uncertainties. In several references (e.g. Barker 1978; Kaler 1980; Kaler & Lutz 1985; SK89), we readily calculated the integrated $H\alpha$ fluxes from the tabulated $H\beta$ fluxes and quoted $H\alpha/H\beta$ ratios. However, in other references (Peimbert & Torres-Peimbert 1971; Torres-Peimbert & Peimbert 1977; Gutiérrez-Moreno, Cortes & Moreno 1985), only the observed $H\beta$ flux was given along with the reddening-corrected $H\alpha/H\beta$ ratio for each object. We re-determined the observed $H\alpha/H\beta$ ratio, and hence the observed $H\alpha$ flux, by using the logarithmic extinctions given for each PN and applying the reddening law used by the authors. In some cases, only the $H\alpha$ surface brightnesses were provided (Boumis 2003, 2006). We calculated the $H\alpha$ fluxes using the nebular diameters given in these papers. In addition, some studies only provide global $H\alpha + [N\text{ II}]$ fluxes (e.g. Xilouris et al. 1994, 1996). The treatment of these data is described in Appendix A.

A correction was then applied to the older $H\alpha$ values due to the flux recalibration of Vega (Hayes & Latham 1975; Oke & Gunn 1983). Those fluxes published before 1975 were decreased by 0.02 dex (0.03 dex for PTP71), while the fluxes tied to the fainter calibration of Miller & Mathews (1972),

e.g. Ahern (1978), were brightened by 0.07 dex (see Shaw & Kaler 1982; SK89, and CKS92 for further comments).

For completeness we also provide the references which had three or less PNe in common with our catalogue (and for which we did not include any statistical information in the tables). For plotting purposes, we group these sources into two groups, based on the relative accuracy of the data sets. The first group includes $H\alpha$ fluxes from Adams (1975), Ahern (1978), Cuisinier et al. (1996), Dufour (1984), Hippelein, Baessgen & Grewing (1985), Hawley & Miller (1978a), Kaler (1980), Kaler & Lutz (1985), Kelly et al. (1992), Mavromatakis et al. (2001b), Miszalski et al. (2011), Moreno et al. (1994), Peimbert et al. (1991), Peña et al. (1990), Torres-Peimbert et al. (1981), WCP05, Wesson & Liu (2004), Zhang & Liu (2003), and Zijlstra et al. (2006).

The second group includes fluxes from Ali & Pfeiderer (1997), Goldman et al. (2004), Hawley (1981), Hawley & Miller (1978b), Hua (1988), Hua & Grundseth (1985), Jacoby & Van de Steene (2004), Kaler (1981), Kaler & Hartkopf (1981), Kistiakowsky & Helfand (1993), Kwitter et al. (2003), Lame & Pogge (1996), Liu et al. (2006), Louise & Hua (1984), Sahai et al. (1999), Peña, Torres-Peimbert & Ruiz (1991), Sahai, Nyman & Wootten (2000), Shen, Liu & Danziger (2004), Torres-Peimbert, Peimbert & Peña (1990),

Table 3. Statistical comparison of our H α fluxes measured from the SHASSA with independent values from the literature. Only data-sets with more than three PNe in common are listed. The table is organized into four tranches according to the contents of Figure 4 and Figure 5 (see text for details).

Reference	ΔF	σ	n	Meth.	Det.	Fig.
BAR78	-0.03	0.03	5	Spec	IDS	4a
DH97	-0.02	0.08	37	Spec	CCD	4a
GCM85	0.01	0.06	13	Spec	PEP	4a
KM81	0.00	0.03	25	Aper	PEP	4a
PTP71	-0.02	0.05	4	Spec	PEP	4a
TPP77	-0.02	0.09	14	Spec	IDS	4a
K83a	-0.09	0.12	6	Aper	PEP	4b
KB94	-0.03	0.19	12	Spec	IDS	4b
KJ89	0.06	0.11	5	Aper	CCD	4b
RZW04	0.03	0.11	43	Aper	CCD	4b
SK89	-0.05	0.10	98	Aper	PEP	4b
WL07	-0.06	0.08	30	Spec	CCD	4b
B01, B03	-0.25	0.29	15	Sp/Ap	CCD	5a
BDF99	0.04	0.35	11	Aper	CCD	5a
Bm03, Bm06	0.26	0.28	10	Aper	CCD	5a
CSBT	-0.03	0.48	5	Aper	CCD	5a
HDM98	0.03	0.16	14	Aper	CCD	5a
HK99	0.10	0.21	4	Aper	CCD	5a
K81	0.06	0.13	5	Aper	PEP	5a
K83b	-0.02	0.14	16	Aper	PEP	5a
KSK90	0.06	0.34	26	Spec	IDS	5a
MFP06	-0.12	0.12	10	F-P	CCD	5a
RCM05	0.01	0.11	16	F-P	CCD	5a
ASTR91A	0.00	0.18	207	Spec	IDS	5b
ASTR91B	0.09	0.26	225	Spec	IDS	5b
ASTR91C	0.21	0.44	161	Spec	IDS	5b
VV68	-0.37	0.28	105	ObP	pg	5b
VV75	-0.28	0.20	16	ObP	pg	5b

Reference codes for Table 3, Table 5, Figure 4 and Figure 5:

ASTR91: Acker et al. (1991); B01: Bohigas (2001); B03: Bohigas (2003); BAR78: Barker (1978); BDF99: Beaulieu et al. (1999); Bm03: Boumris et al. (2003); Bm06: Boumris et al. (2006); CSBT: Cappellaro et al. (2001); DH97: Dopita & Hua (1997); GCM85: Gutiérrez-Moreno et al. (1985); HDM98: Hua et al. (1998); K83a: Kaler (1983a); K83b: Kaler (1983b); KJ89: Kwitter & Jacoby (1989); KM81: Kohoutek & Martin (1981a); KSK90: Kaler et al. (1990); KB94: Kingsburgh & Barlow (1994); MFP06: Madsen et al. (2006); PTP71: Peimbert & Torres-Peimbert (1971); RCM05: Reynolds et al. (2005); RZW04: Ruffe et al. (2004); SK89: Shaw & Kaler (1989); TPP77: Torres-Peimbert et al. (1977); VV68: Vorontsov-Vel'yaminov et al. (1968); VV75: Vorontsov-Vel'yaminov et al. (1975); WL07: Wang & Liu (2007).

Turatto et al. (1990), Xilouris et al. (1994), and the corrected fluxes from Ali, Pfeleiderer & Saurer (1997) and Xilouris et al. (1996). Also included here for plotting purposes are the fluxes from Bm03, Bm06, CSBT, and HK99 (see Table 3 for details on these data sets).

Table 3 presents a detailed statistical comparison between our SHASSA H α fluxes and those from the most important literature sources. The columns give respectively the comparison dataset, the mean $\Delta \log F(\text{H}\alpha)$ between data-sets (in the sense SHASSA – literature fluxes), the standard deviation of the difference, the number of PNe in common,

and the technique and detector used for each data-set. A positive value of the offset means our fluxes are brighter. This table can be compared with Table 3 of Kovacevic et al. (2011), which details a comparison of the integrated [O III] fluxes for ~ 170 PNe between various sources.

Figure 4 and Figure 5 graphically illustrate these comparisons, with each sample being identified with a different symbol. These samples are separated according to our opinion on their reliability, the PN’s surface brightness, and the measurement techniques employed. In Figure 4a (left panel) we plot our H α fluxes (excluding those flagged as less certain) for 101 mostly compact PNe against fluxes from independent data sets that meet two quality criteria: (i) a mean flux difference from ours, $\Delta F(\text{H}\alpha) \leq 0.05$ dex and (ii) a dispersion around this mean, $\sigma \leq 0.10$ dex. These data sets include the SHASSA calibrating measurements of DH97, the high-quality aperture fluxes of Kohoutek and Martin (1981), and other reliable H α fluxes in a series of papers by the Peimberts (refer to Table 3). The lower panels of the figure give the difference between the data-sets, in the sense SHASSA minus literature fluxes. The statistical results from these comparisons appear in the first tranche of entries in Table 3. The H α fluxes from KM81 show the best agreement with our data, with a negligible offset and a dispersion around the mean of only 0.03 dex.

Other than the calibrating sample of GMR01 and our own work, we are not aware of any other published H α fluxes for PNe using SHASSA data, with the exception of McCullough et al. (2001) who determined a flux for Abell 36 of $F(\text{H}\alpha) = 2.8 \times 10^{-11} \text{ erg cm}^{-2} \text{ s}^{-1}$, which is 28% lower than our own determination of $3.9 \times 10^{-11} \text{ erg cm}^{-2} \text{ s}^{-1}$. We attribute this difference to the smaller (4.8 diameter) aperture used by McCullough et al. (2001), which missed some flux from this 6.0×4.7 planetary.

In Figure 4b (right panel), we plot the H α fluxes of 150 PNe which we deem to be of slightly lower accuracy, based on the data-set meeting only one of the above criteria. Some objects were excluded from the comparison, as the published measurement is not an integrated flux, e.g. NGC 5189 (SK89). The statistical results appear as the second tranche of entries in Table 3. The literature H α fluxes have their own associated uncertainties (typically ± 0.01 – 0.05 dex), but based on the 252 fluxes presented in Figure 4, we find SHASSA to be calibrated to better than $\pm 10\%$ across nearly the whole survey. This is in agreement with the nominal error supplied by GMR01, excluding those fields with an incorrect zero point (see Table 2).

Of the brighter PNe ($\log F(\text{H}\alpha) > -11.0$) plotted in Figure 4, the most discrepant point is M 3-27, an unusual object in several respects. The three previous H α fluxes in the literature that are deemed to be reliable (Adams 1975; Ahern 1978; Barker 1978) agree within their respective uncertainties,¹³ but our H α measurement is about 0.2 dex brighter (Figure 4). While our measurement is only from one SHASSA field (#262),¹⁴ which has no zero-point offset,

¹³ The H β flux of Kohoutek & Martin (1981b) also agrees with the H β fluxes from Adams (1975), Barker (1978) and Ahern (1978). The H α flux of Kohoutek (1968) agrees with our own, but is derived from photographic plates and has a substantial uncertainty.

¹⁴ The PN is at the very edge of field 261, and some flux is lost.

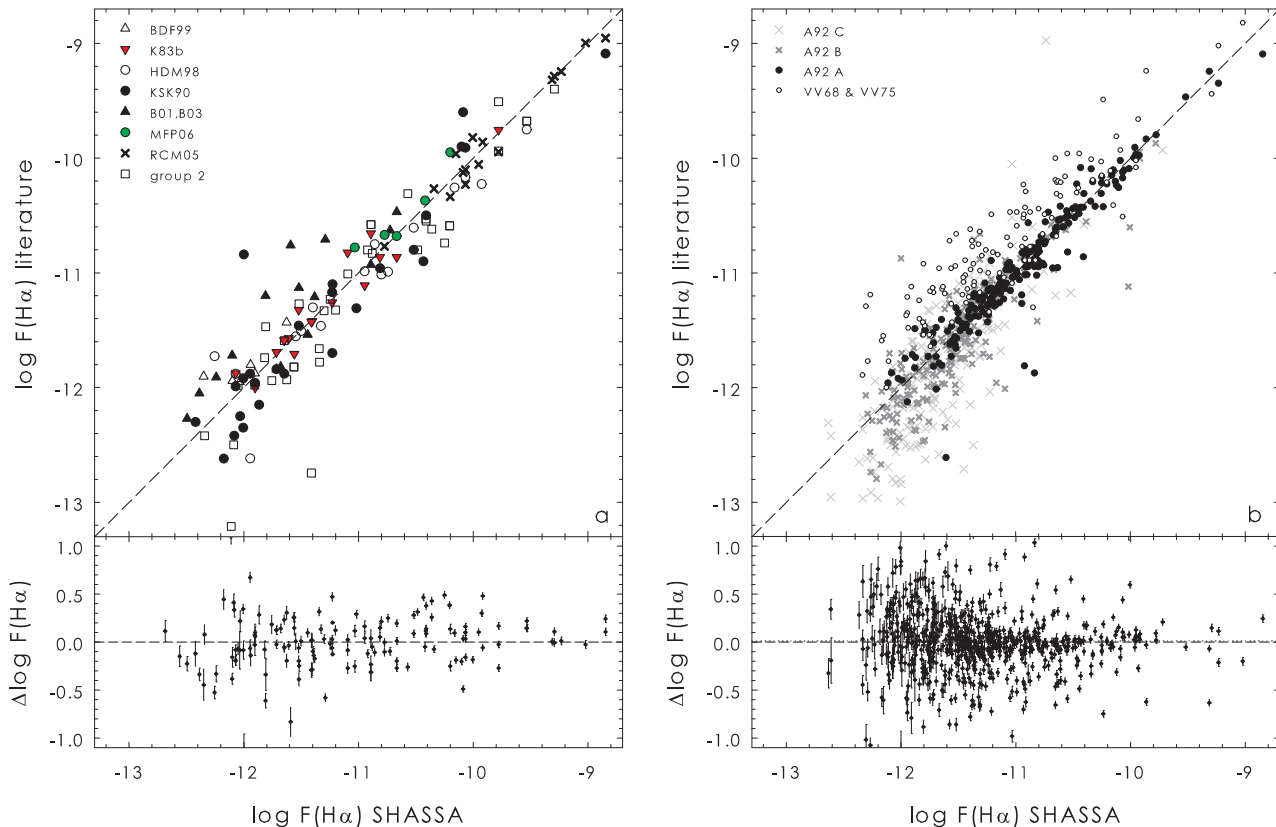


Figure 5. The left panel compares our SHASSA with literature H α fluxes for PNe of low surface brightness (see the text for details). The right panel compares our H α fluxes with the two largest data-sets from the literature (VV and ASTR91), as described in the text. A colour version of this figure is available in the online journal.

the detection is good and there is no confusion of the PN with any nearby sources. This observation (epoch 1999.30) is ~ 25 years after the earlier measurements, suggesting a secular change in the flux with time. This is a very compact, dense and presumably young object (Adams 1975; Miranda et al. 1997) and we initially thought that the change was due to the possible evolution of the central star, a situation seen in the very young object Hen 3-1357 (Parthasarathy et al. 1993; Bobrowsky 1994). However, M 3-27 shows evidence for Balmer self-absorption (Adams 1975; Ahern 1978; Barker 1978), and the bulk of the H α (and radio-continuum emission) originates in an ionized, optically-thick stellar wind which appears variable with time (Miranda et al. 1997). M 3-27 also exhibits large variations in the measured electron densities and temperatures (Barker 1978; Feibelman 1985), similar characteristics to the well-known variable PN, IC 4997 (Aller & Liller 1966; Hyung, Aller & Feibelman 1994). Both these nebulae have very high [O III] $\lambda 4663/\text{H}\gamma$ ratios, overlapping with the symbiotic stars in the diagnostic plot of Gutiérrez-Moreno, Moreno & Cortes (1995). Interestingly, the fluxes for M 3-27 presented by Wesson, Liu & Barlow (2005) show that some line ratios have changed markedly between the mid-1970s and 2001, however, Wang & Liu (2007) state that the “fluxes for a number of lines published by WLB05 ... seem to be incorrect.” Unfortunately the latter authors did not provide any updated data. Notwithstanding

this, our new flux adds weight to the conclusion of Miranda et al. (1997) that the H α emission is variable. This is certainly an interesting object, and warrants further study.

In Figure 5, we present two panels of lower quality flux comparisons. In Figure 5a (left panel), we compare our SHASSA fluxes for 138 mostly LSB PNe ($S_{\text{H}\alpha} < 10^{-4}$ erg cm $^{-2}$ s $^{-1}$ sr $^{-1}$) with the equivalent measurements from different literature sources. The ability to recover fluxes for these faint PNe depends on an accurate background subtraction, given the often low data counts recorded above sky. Such LSB PNe are generally quite extended and may have an asymmetric or irregular morphology, further complicating flux measurement. The statistical summary of these comparisons appear in the third tranche of results in Table 3. Unsurprisingly the mean offsets and dispersions are up to a factor of four larger for these samples than those of Figure 4, along with several large outliers. We excluded some literature fluxes from this comparison because the largest photometer aperture used was much smaller than the nebular diameter. This leads to very uncertain values in the estimated total flux in these cases (e.g. Abell 21, Abell 35, Jones 1 and K 2-2; Kaler 1983b). The WHAM H α fluxes (Reynolds et al. 2005; Madsen et al. 2006) are measured with a 1° beam, so contaminating background emission may occur for some PNe. One example is Abell 74, where diffuse background emission is located near to the PN. This object

is omitted from the comparison table. We also omit the flux for Abell 60 from Hua et al. (1998), which is too faint. The SHASSA $H\alpha$ fluxes determined here are all integrated fluxes, measured through an aperture that was always larger than the nebula on the CCD image. They are to be preferred for these large evolved PNe.

In Figure 5b (right panel), we present 760 lower quality fluxes from ASTR91 and Vorontsov-Vel'yaminov et al. (1968, 1975). The comparison of our $H\alpha$ fluxes with the older photographic determinations of Vorontsov-Vel'yaminov et al. (1968, 1975) was done primarily for historical interest. These fluxes were derived from objective-prism plates which suffered from high non-linearity (e.g. Torres-Peimbert 2011). The fluxes are not reliable and are systematically brighter than our data by 0.2 – 0.4 dex, increasing in offset at faint flux levels.

ASTR91 determined integrated $H\beta$ fluxes for 880 PNe, with the majority scaled up from small-aperture slit spectroscopic measurements. We calculated $H\alpha$ fluxes from these data using the observed $H\alpha/H\beta$ ratios given by ASTR91. These authors also compiled $H\beta$ fluxes for ~ 350 PNe with accurate independent measurements from the literature. We then calculated $H\alpha$ fluxes for these objects using the $H\alpha/H\beta$ ratios from ASTR91. These make up ASTR91 sample ‘A’, with typical flux errors of ≤ 0.08 dex. This subsample gives the best agreement with our SHASSA data, with a small offset and a reasonably low dispersion of 0.14 dex. For PNe that were larger than the slit aperture used (typically $\theta > 5''$), ASTR91 determined the integrated $H\beta$ flux by scaling up the observed flux by a geometric ratio (ratio of the PN area to the aperture area), before applying an empirical correction factor. Again we determine the integrated $H\alpha$ flux for each PN using their published $H\alpha/H\beta$ ratio. These objects make up sample ‘B’, including 224 PNe with an uncertainty ≤ 0.15 dex.

For the larger PNe ($\theta > 1'$), the slit covered only a small fraction of the object, so the derived integrated fluxes become very uncertain. These lower-quality fluxes (ASTR91, sample ‘C’) have errors > 0.15 dex, and are not reliable, as the extrapolation from the observed flux through a small aperture to the full dimensions of the PN introduces a large uncertainty. Figure 5b shows that errors of 0.5 – 1.0 dex are not uncommon, so we recommend that the data from ASTR91 B and C samples be only used if there is no other data source. Their quoted uncertainties also appear to have been underestimated for these objects, a point previously noted by Ruffle et al. (2004) and WCP05. A similar effect, though less severe, is seen in the data from Kaler et al. (1990) and Bohigas (2001, 2003). These samples form the final tranche of entries in Table 3.

Lastly, as SHASSA provides nearly 90 per cent of the new $H\alpha$ fluxes in our catalogue, we show in Figure 6 the spatial distribution of PNe measured on SHASSA, plus non-detections over a greyscale $H\alpha$ map of the southern Galactic plane. The green circles represent detections, while the red circles are non-detections. As expected the non-detections are mostly faint PNe, concentrated in regions of high extinction close to the mid-plane, in the crowded star fields of the Galactic bulge, or in areas of complex emission where the poor resolution prevents detection against the bright ambient background. The SHASSA flux limit is $\log F(H\alpha) \simeq -12.8$, and this limit is ~ 0.5 –1 dex brighter for areas

close to the Galactic plane with a high level of diffuse $H\alpha$ emission. As an example of an object near the plane, we note the faint bipolar PHR 1315-6555 with $\log F(H\alpha) = -12.45 \pm 0.01$ (Parker et al. 2011). This PN resides in an area of background $H\alpha$ emission and is only barely detected on SHASSA at the 1σ level.

4.2 VTSS $H\alpha$ Fluxes

In a similar fashion to the SHASSA fluxes, we present VTSS $H\alpha$ fluxes for 178 northern PNe. The resolution of VTSS is coarser than SHASSA and owing to the increased level of confusion at low intensities, the VTSS flux limit is brighter; for regions with low uniform sky background, the VTSS limit is $\log F(H\alpha) \simeq -12.2$ compared to $\log F(H\alpha) \simeq -12.8$ for SHASSA. As noted previously, the median intensity in each VTSS image has been set equal to zero, so the survey can be considered to have an arbitrary zero point (Dennison et al. 1998). From a comparison of two VTSS fields, Aql04 and Ori11, with the equivalent binned SHASSA data, GMR01 estimated correction factors of 0.10 and 0.07 dex respectively, which one needs to apply to the VTSS data in order to get the same surface brightness for diffuse emission measured in both surveys. F03 applied this same factor to all VTSS images in order to compare the VTSS data with SHASSA, using available WHAM data as a cross-check, finding the resulting agreement between VTSS and SHASSA to be good (see his figure 7). This offset factor was then assumed to be constant across the whole VTSS survey.

However, from a detailed comparison between our VTSS $H\alpha$ data and independent fluxes for 21 bright PNe, we noticed that with this correction, the VTSS integrated fluxes appear to be slightly overestimated (cf. GMR01; F03; Frew 2008). By fitting a simple linear function to the available data in common, we estimate a new VTSS correction factor of 0.07 dex (in the sense that the VTSS data need to be brightened by 17 per cent). We applied this correction to all of our VTSS fluxes, except for the objects in fields Aql04 and Ori11 where the original corrections of GMR01 are applied.

Table 4 contains the $H\alpha$ fluxes for ~ 162 PNe measured from the VTSS, brightened by 0.07 dex. Columns 1 and 2 give the *PNG* designation and the common name respectively, columns 3 and 4 give the J2000.0 coordinates, while the logarithm of the $H\alpha$ flux is given in column 5. The adopted aperture radius in arcmin is given in column 6, the number of measurements from separate fields is given in column 7, the derived extinction in column 7, and any notes are indexed in column 9.

4.2.1 Comparison of VTSS and literature $H\alpha$ fluxes

We made a comparison of the VTSS $H\alpha$ fluxes with literature data, evaluated in the same way as for SHASSA. Table 5 presents a statistical comparison between literature $H\alpha$ fluxes and our $H\alpha$ fluxes measured from VTSS after brightening by 0.07 dex. The columns give the comparison dataset, the mean $\Delta \log F(H\alpha)$ between measurements in the sense VTSS – literature fluxes, the standard deviation of the difference, the number of PNe in common, and the technique and detector used by each data-set. These can

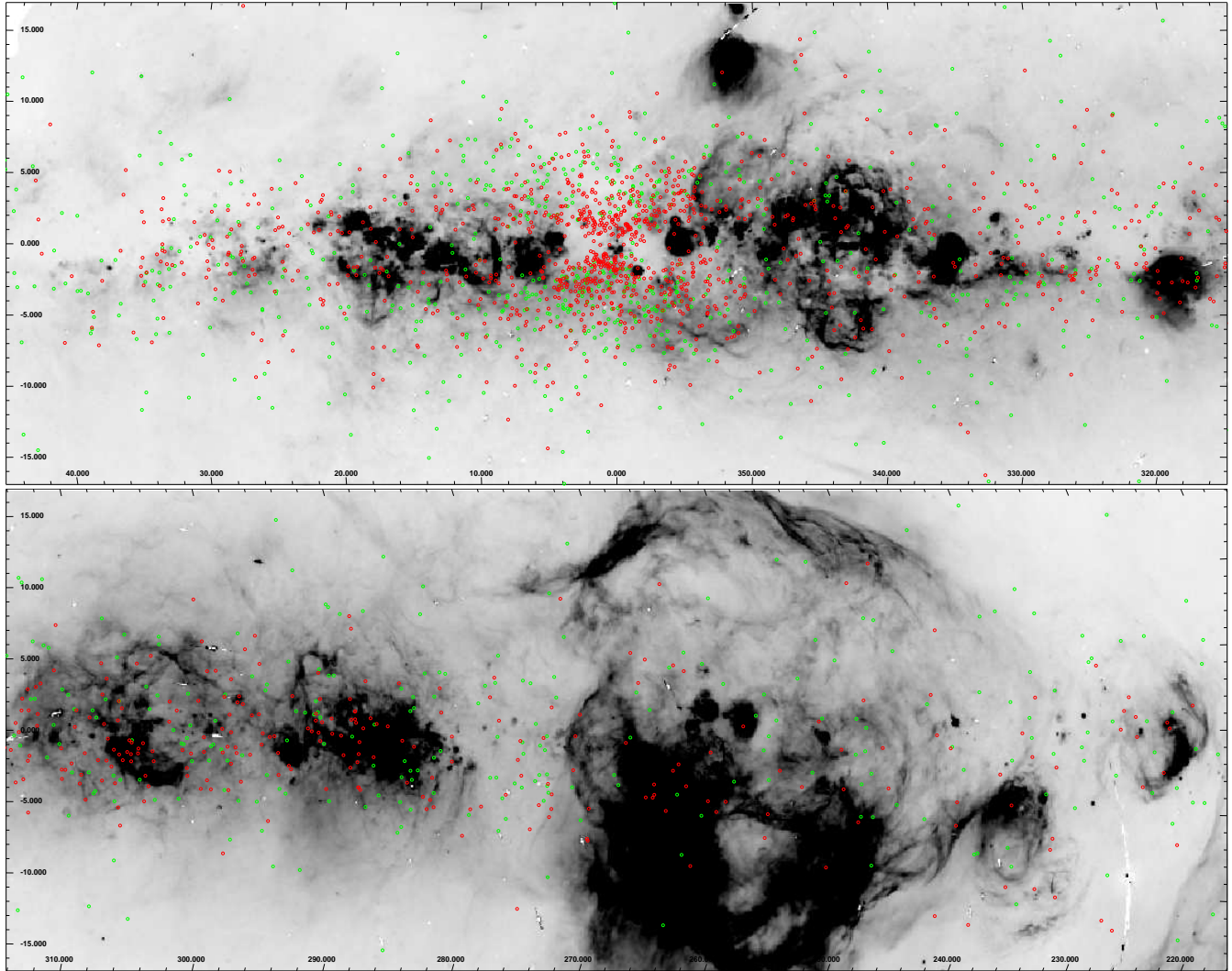


Figure 6. The spatial distribution of PNe overlaid on a greyscale H α map of the southern Galactic plane generated from SHASSA data. The top panel is centred on the Galactic Bulge ($l = 0^\circ$), while the lower panel is centered at $l = 270^\circ$, in the vicinity of the Gum nebula. The green circles represent SHASSA-detected PNe, while red circles mark non-detections. As expected the latter are concentrated in high-extinction regions close to the mid-plane, in the crowded star fields of the Bulge, or in areas of bright background H α emission. A colour version of this figure is available in the online journal.

Table 4. H α fluxes for 178 true and possible PNe measured from VTSS. The table is published in its entirety as an online supplement. A portion is given here for guidance regarding its form and content.

PN G	Name	RAJ2000	DEJ2000	logF(H α)	r_{aper}	N_f	c_β	Notes
118.0-08.6	Vy 1-1	00:18:42.2	53:52:20	-10.95 ± 0.09	4.8	1	0.38	6,10
119.3+00.3	BV 5-1	00:20:00.5	62:59:03	-11.62 ± 0.18	5.0	1	...	4,5
119.6-06.1	Hu 1-1	00:28:15.6	55:57:55	-11.00 ± 0.08	3.2	1	0.44	
121.6+00.0	BV 5-2	00:40:21.6	62:51:34	-11.60 ± 0.14	3.2	1	...	1,4
122.1-04.9	Abell 2	00:45:34.7	57:57:35	-11.61 ± 0.10	3.2	2	...	6
124.3-07.7	WeSb 1	01:00:53.3	55:03:48	-12.1 ± 0.2	9.3	1	...	
126.3+02.9	K 3-90	01:24:58.6	65:38:36	-11.90 ± 0.12	3.2	1	...	5,6
130.3-11.7	M 1-1	01:37:19.4	50:28:12	-11.33 ± 0.10	3.2	1	...	
130.9-10.5	NGC 650/1	01:42:20.0	51:34:31	-10.19 ± 0.05	3.2	1	0.10	
138.8+02.8	IC 289	03:10:19.3	61:19:01	-10.82 ± 0.07	3.2	1	1.29	

Notes: (1) Possible PN; (2) pre-PN; (3) transition object; (4) uncertain counts; (5) confused with nearby object; (6) bad pixels in aperture; (7) object near field edge; (8) flux excludes halo; (9) flux corrected for CSPN; (10) Wolf-Rayet CSPN; (N) previously unpublished object; (V) very low excitation PN; (C) specific comment given.

Table 5. Statistical comparison of our VTSS H α fluxes with independent literature values. Only data-sets with more than three PNe in common are listed, and the offsets are in the sense VTSS fluxes minus literature. The reference codes are given in the footnotes to Table 3.

Reference	ΔF	σ	n	Meth.	Det.	Fig.
SHASSA	0.01	0.09	47	Aper	CCD	7a
BAR78	0.03	0.06	9	Spec	IDS	7b
KM81	0.05	0.03	4	Aper	PEP	7b
PTP71	0.01	0.03	4	Spec	PEP	7b
B01, B03	-0.17	0.29	6	Sp/Ap	CCD	...
H97	-0.13	0.14	5	Aper	CCD	...
HGM93	-0.03	0.23	7	Aper	PCC	...
K83a	0.10	0.12	9	Aper	PEP	...
K83b	-0.03	0.17	17	Aper	PEP	...
KSK90	0.13	0.33	14	Spec	IDS	...
RCM05	0.11	0.14	4	F-P	CCD	...

be compared with the comparisons presented in Table 3 for SHASSA fluxes.

Figure 7 shows a comparison between our independent VTSS H α fluxes and SHASSA H α fluxes for 47 PNe in common (Figure 7a; left panel). The relation between our VTSS and SHASSA fluxes is linear, with a low dispersion, especially for PNe with $\log F(\text{H}\alpha) > -11.0$. This independently demonstrates the reliability of our SHASSA fluxes. In Figure 7b (right panel) we compare our new VTSS measurements to 179 measurements from 17 independent literature sources which mostly provide small numbers (<15) of comparison fluxes. The abbreviated symbol codes in the right panel are the same as before. The flux differences vary according to the quality of the published source fluxes, but are generally larger than the SHASSA comparisons plotted in Figure 4. We measure a dispersion around the mean between our SHASSA and VTSS fluxes of ± 0.09 dex. Assuming a dispersion in our SHASSA fluxes of 0.04 dex, then the mean VTSS uncertainty can be estimated to be approximately ± 0.08 dex.

5 EXTINCTION DETERMINATIONS

We use our homogenous catalogue of H α fluxes to calculate independent extinction determinations for a subset of ~ 270 PNe with reliable integrated H β fluxes in the literature. We take these from Copetti (1990), ASTR91, CKS92, DH97 and WCP05, and exclude any with an uncertainty in $\log F(\text{H}\beta)$ of > 0.06 dex. We also exclude any objects with an uncertainty in H α of > 0.08 dex. The logarithmic extinction at H β , $c_\beta = \log F(\text{H}\beta) - \log I(\text{H}\beta)$, is derived for each PN by comparing the observed Balmer decrement with the theoretical one for case B recombination. In this study, we have used the $R = 3.1$ Galactic reddening law of Howarth (1983) and adopt an intrinsic line ratio of $I(\text{H}\alpha)/I(\text{H}\beta) = 2.86$ (Hummer & Storey 1987), or $\log I(\text{H}\alpha/\text{H}\beta) = 0.456$. This value is appropriate for $T_e = 10^4$ K and the range of densities seen in most PNe. The logarithmic extinction is then given by the following expression:

$$c_\beta = 3.125 \times \log \left[\frac{F(\text{H}\alpha)}{F(\text{H}\beta)} \right] - 1.43 \quad (12)$$

where as before, $F(\text{H}\alpha)$ and $F(\text{H}\beta)$ are the observed integrated fluxes. The logarithmic extinction at H α , c_α , can also be derived using:

$$c_\alpha = 0.70 \times c_\beta \quad (13)$$

Our H β logarithmic extinctions should be accurate to better than 0.10 dex, and should not be affected by the unknown intensity of the He II Pickering lines which contribute to the H α and H β fluxes, as to first order, the intrinsic Pi6/Pi8 ratio of ~ 2.7 is nearly identical to the intrinsic H α /H β ratio (Hummer & Storey 1987). The calculated extinctions are given in column 11 of Table 1 and column 9 of Table 4. There were a few formally negative values for the extinction arising from measurement errors in both the H α and H β fluxes, and these have been reset to zero in the tables.

Our extinction determinations are generally in very good agreement with other values taken from the literature (Pottasch et al. 1977; Feibelman 1982; Kaler & Lutz 1985; Gathier, Pottasch & Pel 1986; CKS92; Stasińska et al. 1992; Tylanda et al. 1992; Giammanco et al. 2011) and with the total line-of-sight extinction to each object (Schlafly & Finkbeiner 2011). In a follow-up paper, we will undertake a comprehensive analysis of the optical and radio extinctions for a large number of Galactic PNe (Bojčić et al. 2011a; Bojčić et al., in preparation).

6 FUTURE WORK

This paper is the first in an ambitious project which plans to determine an integrated hydrogen-line flux for almost all of the currently-known Galactic PNe, and the new discoveries coming on-stream (e.g. Parker & Frew 2011), especially from the IPHAS survey. It is important to note that the SHASSA survey only covers the southern hemisphere, and that the VTSS is unlikely to be reborn. Furthermore, these surveys are of low angular resolution and cannot provide reliable fluxes nor, in many cases, detections for faint PNe in complex regions of high background emission. Alternative sources for determining H α fluxes for these PNe are required.

In this vein, Parker et al. (2012c) demonstrated that the SHS survey, though photographic in origin, can never the less be used to provide flux estimates for resolved nebulae. As part of a pilot study, moderate-precision integrated H α fluxes for ~ 50 faint PNe were measured. This is important as the 900 or so MASH PNe not detected in SHASSA were all discovered on the SHS. We are now extending this pilot to undertake a larger project to determine H α fluxes for a large number of MASH PNe that have no short-term prospects of alternative flux measurements. These include the faintest PNe detectable by the SHS including those with an interstellar V -band extinction exceeding 10 magnitudes (see Parker et al. 2012b). The SHS should extend the flux limit for Galactic PNe down to $\log F(\text{H}\alpha) \simeq -15$, or a factor of a few hundred fainter than the SHASSA limit.

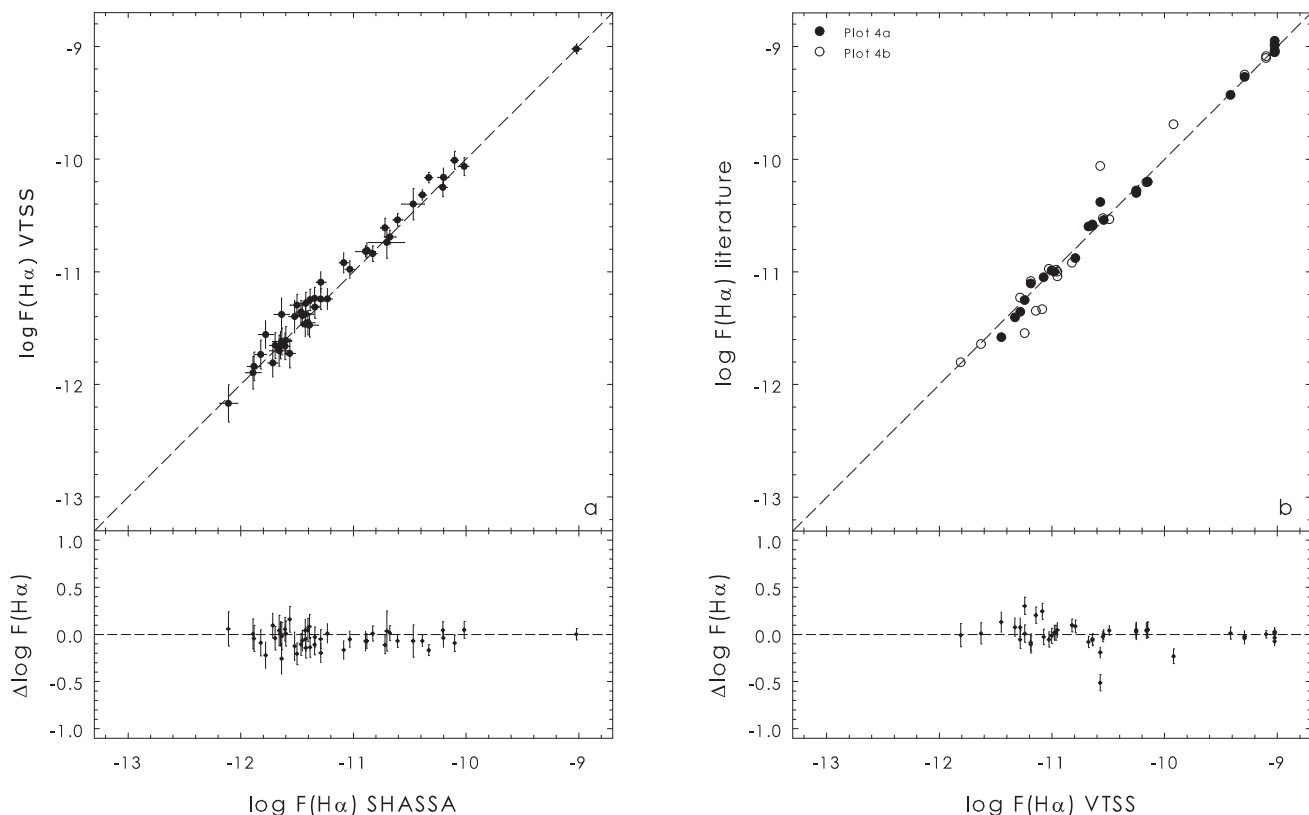


Figure 7. The left panel (a) compares our fluxes measured from SHASSA with the corrected VTSS fluxes for 47 PNe in common. The dispersion is very small for fluxes brighter than $\log F(H\alpha) = -11.0$. The right panel (b) compares our VTSS $H\alpha$ fluxes with the most accurate subset of literature fluxes, and the symbol codes refer to the data-sets plotted on Figures 4a and 4b.

In the near future, many more global $H\alpha$ fluxes will be determined for PNe from the IPHAS survey (Drew et al. 2005), within 5° of the northern Galactic plane. The digital IPHAS images, like the SHS data, are not only a powerful discovery medium, but have the advantage of providing accurate $H\alpha$ fluxes for the hundreds of PNe located within the 1800 square degree footprint. The initial IPHAS point source catalogues (González-Solares et al. 2008; Witham et al. 2008) hold few compact PNe, but many more extended nebulae are being discovered from visual examination of the imaging data (e.g. Viironen et al. 2009b, 2011; Sabin et al. 2010). A uniform flux calibration across the whole survey, accurate to ≈ 0.01 dex, is in progress. This will allow the determination of precise $H\alpha$ fluxes for many northern extended PNe. To date, only a handful of $H\alpha$ fluxes for PNe from the IPHAS survey have been published (Mampaso et al. 2006; Wesson et al. 2008; Viironen et al. 2009a, 2011; Corradi et al. 2011).

The southern counterpart of the digital IPHAS Survey is the new VST/OmegaCam Photometric $H\alpha$ Survey of the Southern Galactic Plane (VPHAS+; Drew & Raddi 2012; J. Drew et al., in preparation)¹⁵. This survey commenced in 2012 using the recently completed VLT Survey Telescope, equipped with OmegaCam (Kuijken et al. 2004).

VPHAS+ will have a depth about two magnitudes fainter than the SHS for point sources, and comparable sensitivity to diffuse emission. Besides finding new PNe missed by the SHS, VPHAS+ should provide accurate $H\alpha$ fluxes for many southern PNe below the flux limit of SHASSA. However, its areal coverage is only ~ 50 per cent of the SHS survey, so the SHS remains the only $H\alpha$ survey able to cover most of the southern Galactic plane at good sensitivity and resolution for the foreseeable future.

We also note the Palomar Transient Factory (PTF; Rau et al. 2009), a series of wide-field surveys that will investigate the variable sky on time scales from minutes to years. Amongst many science goals, a set of narrowband ($H\alpha$, $H\alpha$ -off and [O III]) surveys will be conducted, covering the sky north of $\delta = -28^\circ$. The estimated 5σ intensity limit for the PTF $H\alpha$ survey will be ~ 0.6 R, allowing the discovery of new faint PNe, and providing new integrated fluxes for faint PNe and other emission-line objects.

We also plan to derive a set of independent $H\alpha$ fluxes from narrowband archival images taken with HST and the F656N filter. Few of these fluxes have been published to date (e.g. Sahai, Nyman & Wootten 2000; Wesson & Liu 2004; Miszalski et al. 2011), so any further data will be worthwhile.

Our catalogue is complementary to fluxes obtained from imaging surveys at other wavelengths, such as the very bright [O III] line at $\lambda 5007\text{\AA}$ (e.g. Kovacevic et al. 2011), or

¹⁵ <http://www.vphasplus.org/>

in the light of [S III] $\lambda 9532\text{\AA}$ (Kistiakowsky & Helfand 1993, 1995; Jacoby & Van de Steene 2004; Shiode et al. 2006). With the exception of the VLE PNe, the [S III] $\lambda 9532\text{\AA}$ line essentially becomes the brightest apparent line when the total *V*-band extinction is between 5 and 12 mag (Van de Steene, Sahu & Pottasch 1996; Jacoby & Van de Steene 2004). If NIR spectra are available, then the integrated flux in an atomic hydrogen line such as Paschen- γ can then be bootstrapped from the observed $\lambda 9532\text{\AA}$ flux.

For the many PNe expected to be completely hidden in the optical due to very high extinction, global fluxes in a longer wavelength hydrogen line will be needed. Brackett- γ is recommended as it one of the brightest lines accessible from the ground when the visual extinction exceeds ~ 12 magnitudes (Jacoby & Van de Steene 2004; Jacoby et al. 2010); at this level of extinction $H\alpha$ is rapidly becoming undetectable.¹⁶ Brackett- α (e.g. Forrest et al. 1987) might also be a useful secondary choice for very reddened PNe. The intrinsically brighter Paschen- α line is only accessible from space, but will prove useful when available (e.g. Wang et al. 2010; Dong et al. 2011).

7 SUMMARY

We present reliable $H\alpha$ fluxes for 1258 unique PNe, including fluxes for 1234 PNe measured from SHASSA and VTSS images. This is the largest compilation of homogeneously derived fluxes yet measured. In Appendix A, we list the corrected $H\alpha$ fluxes for 49 PNe taken from the literature, including 24 PNe not detected on our SHASSA or VTSS images, all set to a common zero-point.

Aperture photometry on the digital images was performed to extract integrated $H\alpha$ + [N II] fluxes in the case of SHASSA, and $H\alpha$ fluxes from VTSS. The [N II] contribution was then deconvolved from the SHASSA flux using spectrophotometric data taken from the literature or derived by us. Comparison with previous work shows that our flux scale has no significant zero-point error. Including literature flux measurements for another 200 PNe that were either too faint, or fell outside of the combined survey coverage, there are now reliable integrated $H\alpha$ fluxes for nearly 45% of the Galactic PN population. We also list new independent reddening determinations for ~ 270 PNe, derived from a comparison of our $H\alpha$ data with the best literature $H\beta$ fluxes, and in Appendix B, we provide integrated $H\alpha$ fluxes for another 76 nebulae formerly classified as PNe.

Along with providing the community with an legacy resource with many applications, our benchmark catalogue of $H\alpha$ fluxes can be used to calculate surface-brightness distances for each PN (Frew 2008), estimate new Zanstra temperatures for PN central stars with accurate photometry (e.g. De Marco et al. 2012), provide baseline data for photoionization modelling, and allow a comparison with data at radio (Condon & Kaplan 1998; Bojičić et al. 2011a), mid-infrared (e.g. Chu et al. 2009; Zhang, Hsia & Kwok 2012), near-IR (Guerrero et al. 2000; Schmeja & Kimeswenger 2001; Speck et al. 2002; Hora et al. 2006; Cohen et al. 2011;

Froebrich et al. 2011) and ultraviolet and X-ray wavelengths (Bianchi 2012; Kastner et al. 2012) in order to better understand the physical processes occurring within PNe. Lastly, we will determine new absolute $H\alpha$ magnitudes for delineating the faint end of the PNLf (Ciardullo 2010). Such an $H\alpha$ PNLf can be compared with the widely-used [O III] $\lambda 5007\text{\AA}$ PNLf, both within and outside the Milky Way (e.g. Méndez et al. 1993; Jacoby & De Marco 2002; Schönberner et al. 2007; Reid & Parker 2010; Kovacevic et al. 2011; Ciardullo 2012).

Ultimately, we hope to conduct a multi-wavelength statistical analysis of the Galactic PN population in a way that has not yet been achieved. This analysis will be crucial to our overall understanding of the origin of PNe, including the role of binary companions in their shaping and evolution (De Marco 2009; De Marco & Soker 2011), the physics of AGB mass loss, and the return of metals to the ISM. This paper is a first step towards this goal.

ACKNOWLEDGEMENTS

We thank the referee, C.R. O’Dell, for comments which helped to improve the paper. D.J.F. thanks Macquarie University for a MQ Research Fellowship and I.S.B. is the recipient of an Australian Research Council Super Science Fellowship (project ID FS100100019). This research has made use of the SIMBAD database and the VizieR service, operated at CDS, Strasbourg, France, and also utilized imaging data from the Southern $H\alpha$ Sky Survey Atlas (SHASSA) and the Virginia-Tech Spectral Line Survey (VTSS), which were produced with support from the National Science Foundation (USA). Additional data were used from the AAO/UKST $H\alpha$ Survey, produced with the support of the Anglo-Australian Telescope Board and the Particle Physics and Astronomy Research Council (UK), and the Wisconsin H-Alpha Mapper (WHAM), produced with support from the National Science Foundation. This project also made use of APLpy, an open-source plotting package for Python. We thank Greg Madsen for his help with the WHAM data, and Warren Reid for his assistance in measuring the line fluxes from our unpublished spectra.

REFERENCES

- Abell G.O., 1966, ApJ, 144, 259
- Acker A., Stenholm B., 1990, A&AS, 86, 219
- Acker A., Chopinet M., Pottasch S. R., Stenholm B., 1987, A&AS, 71, 163
- Acker A., Lundström I., Stenholm B., 1988, A&AS, 73, 325
- Acker A., Stenholm B., Tylenda R., 1989, A&AS, 77, 487
- Acker A., Stenholm B., Tylenda R., Raytchev, B., 1991, A&AS, 90, 89 (ASTR91)
- Acker A., Ochsnein F., Stenholm B., Tylenda R., Marcout J., Schohn C., 1992, Strasbourg-ESO Catalogue of Galactic Planetary Nebulae (Garching: ESO)
- Acker A., Marcout J., Ochsnein F., Beaulieu S., García-Lario P., Jacoby G., 1996, Strasbourg-ESO Catalogue of Galactic Planetary Nebulae, First Supplement (Observatoire de Strasbourg)
- Acker A., Boffin H.M.J., Outters N., Miszalski B., Sabin L., Le Du P., Alves F., 2012, RMxAA, 48, 223
- Adams T.F., 1975, ApJ, 202, 114

¹⁶ Except for the most compact PNe, the $H\beta$ line becomes undetectable when the *V*-band extinction exceeds 8–9 mags.

- Ahern F.J., 1978, *ApJ*, 223, 901
 Ali A., 1999, *NewA*, 4, 95
 Ali A., Pfeiderer J., 1997, *MNRAS*, 289, 589
 Ali A., Pfeiderer J., Saurer W., 1997, *IAUS*, 180, 204
 Ali A., Sabin L., Snaid S., Basurah H.M., 2012, *A&A*, 541, A98
 Allen C.W., 1973, *Astrophysical Quantities*, 3rd edition (The Athlone Press)
 Aller L.H., Faulkner D.J., 1964, *IAUS*, 20, 45
 Aller L.H., Liller W., 1966, *MNRAS*, 132, 337
 Anderson L.D., Zavagno A., Barlow M.J., Garca-Lario P., Noriega-Crespo A., 2012, *A&A*, 537, A1
 Balick B., 2007, *APN IV Conf. Proc.*, published online at <http://www.iac.es/proyect/apn4>, article #3
 Balick B., Perinotto M., Maccioni A., Terzian Y., Hajian A., 1994, *ApJ*, 424, 800
 Barker T., 1978, *ApJ*, 219, 914
 Barker T., Cudworth K.M., 1984, *ApJ*, 278, 610
 Beaulieu S.F., Dopita M.A., Freeman K.C., 1999, *ApJ*, 515, 610
 Beer S.H., Vaughan A.E., 1999, *PASA*, 16, 134
 Belczyński K., Mikołajewska J., Munari U., Ivison R.J., Friedjung M., 2000, *A&AS*, 146, 407
 Bensby T., Lundström I., 2001, *A&A*, 374, 599
 Bianchi L., 2012, *IAUS*, 283, 45
 Blair W.P., Feibelman W.A., Michalitsianos A.G., Stencil R.E., 1983, *ApJS*, 53, 573
 Bobrowsky M., 1994, *ApJ*, 426, L47
 Bohigas J., 2001, *RMxAA*, 37, 237
 Bohigas J., 2003, *RMxAA*, 39, 149
 Boissay R., Parker Q.A., Frew D.J., Bojičić I., 2012, *IAUS*, 283, 316
 Bojičić I.S., Parker Q.A., Filipović M.D., Frew D.J., 2011a, *MNRAS*, 412, 223
 Bojičić I.S., Parker Q.A., Frew D.J., Vaughan A.E., Filipović M.D., Gunawardhana M.L.P., 2011b, *AN*, 332, 697
 Bojičić I.S., Frew D.J., Parker Q.A., 2012a, *IAUS*, 283, 318
 Bojičić I.S., Frew D.J., Parker Q.A., Stupar M., Wachter S., DePew K., 2012b, *ASP Conf. Proc.*, in press
 Bond H.E., 1981, *PASP*, 93, 429
 Bond H.E., Pollacco D.L., Webbink R.F., 2003, *AJ*, 125, 260
 Boumis P., Paleologou E.V., Mavromatakis F., Papamastorakis J., 2003, *MNRAS*, 339, 735
 Boumis P., Akras S., Xilouris E.M., Mavromatakis F., Kapakos E., Papamastorakis J., Goudis C.D., 2006, *MNRAS*, 367, 1551
 Braxton K.M., Balick B., Jacob R., Steffen M., Schönberner D., 2012, *AAS Meeting #220, #431.10*
 Brocklehurst M., 1971, *MNRAS*, 153, 471
 Buxton M., Bessell M., Watson B., 1998, *PASA*, 15, 24
 Cahn J.H., Kaler J.B., 1971, *ApJS*, 22, 319
 Cahn J.H., Kaler J.B., Stanghellini L., 1992, *A&AS*, 94, 399 (CKS92)
 Cantó J., 1981, *ASSL*, 91, 95
 Caplan J., Deharveng L., Peña M., Costero R., Blondel C., 2000, *MNRAS*, 311, 317
 Cappellaro E., Benetti S., Sabbadin F., Salvadori L., Turatto M., Zanin C., 1994, *MNRAS*, 267, 871
 Cappellaro E., Sabbadin F., Benetti S., Turatto M., 2001, *A&A*, 377, 1035
 Capriotti E.R., Daub C.T., 1960, *ApJ*, 132, 677
 Carrasco L., Serrano A., Costero R., 1983, *RMxAA*, 8, 187
 Carrasco L., Serrano A., Costero R., 1984, *RMxAA*, 9, 111
 Celnik W.E., 1983, *A&AS*, 53, 403
 Chu Y.-H., 2003, *IAUS*, 212, 585
 Chu Y.-H., Gruendl R.A., Williams R.M., Gull T.R., Werner K., 2004, *AJ*, 128, 2357
 Chu Y.-H. et al., 2009, *AJ*, 138, 691
 Ciardullo R., 2010, *PASA*, 27, 149
 Ciardullo R., 2012, *Ap&SS*, 341, 151
 Cohen M., Barlow M.J., 1975, *ApL*, 16, 165
 Cohen M., Parker Q.A., Green A.J., 2005a, *MNRAS*, 360, 1439
 Cohen M. et al., 2005b, *ApJ*, 627, 446
 Cohen M. et al., 2007, *ApJ*, 669, 343
 Cohen M., Parker Q.A., Green A.J., Miszalski B., Frew D.J., Murphy T., 2011, *MNRAS*, 413, 514
 Collins G.W., Daub C.T., O'Dell C.R., 1961, *ApJ*, 133, 471
 Condon J.J., Kaplan D.L., 1998, *ApJS*, 117, 361
 Condon J.J., Kaplan D.L., Terzian Y., 1999, *ApJS*, 123, 219
 Copetti M.V.F., 1990, *PASP*, 102, 77
 Copetti M.V.F., Oliveira V.A., Riffel R., Castañeda H.O., Sanmartim D., 2007, *A&A*, 472, 847
 Corradi R.L.M., 1995, *MNRAS*, 276, 521
 Corradi R.L.M., Schwarz H.E., 1993, *A&A*, 268, 714
 Corradi R.L.M., Villaver E., Mampaso A., Perinotto M., 1997, *A&A*, 324, 276
 Corradi R.L.M., Schönberner D., Steffen M., Perinotto M., 2003, *MNRAS*, 340, 417
 Corradi R.L.M. et al., 2008, *A&A*, 480, 409
 Corradi R.L.M. et al., 2010, *A&A*, 509, A41
 Corradi R.L.M. et al., 2011, *MNRAS*, 410, 1349
 Costa R.D.D., Uchida M.M.M., Maciel W.J., 2004, *A&A*, 423, 199
 Crawford I.A., Barlow M.J., 1991a, *A&A*, 249, 518
 Crawford I.A., Barlow M.J., 1991b, *A&A*, 251, L39
 Cuisinier F., Acker A., Köppen J., 1996, *A&A*, 307, 215
 Daub C.T., 1982, *ApJ*, 260, 612
 De Marco O., 2009, *PASP*, 121, 316
 De Marco O., Soker N., 2011, *PASP*, 123, 402
 De Marco O., Passy J.-C., Frew D.J., Moe M.M., Jacoby G.H., 2012, *MNRAS*, in press (arXiv:1210.2841)
 Dennison B., Simonetti J.H., Topasna G.A., 1998, *PASA*, 15, 14
 DePew K., Parker Q.A., Miszalski B., De Marco O., Frew D.J., Acker A., Kovacevic A.V., Sharp R.G., 2011, *MNRAS*, 414, 2812
 Dong H. et al., 2011, *MNRAS*, 417, 114
 Dopita M.A. & Hua C.T., 1997, *ApJS*, 108, 515 (DH97)
 Drew J.E. et al., 2005, *MNRAS*, 362, 753
 Drew J.E., Raddi R., EGAPS Consortia, 2012, *Ap&SS Proc.*, 1, 3
 Duerbeck H.W., Reipurth B., 1990, *A&A*, 231, L11
 Dufour R.J., 1984, *ApJ*, 287, 341
 Durand S., Acker A., Zijlstra A., 1998, *A&AS*, 132, 13
 Egan M.P., Clark J.S., Mizuno D.R., Carey S.J., Steele I.A., Price S.D., 2002, *ApJ*, 572, 288
 Emprechtinger M., Forveille T., Kimeswenger S., 2004, *A&A*, 423, 1017
 Eracleous M., Wade R.A., Mateen M., Lanning H.H., 2002, *PASP*, 114, 207
 Escudero A.V., Costa R.D.D., 2001, *A&A*, 380, 300
 Esteban C., Vilchez J.M., Manchado A., Smith L.J., 1991, *A&A*, 244, 205
 Exter K.M., Barlow M.J., Walton N.A., 2004, *MNRAS*, 349, 1291
 Fang X., Liu X.-W., 2011, *MNRAS*, 415, 181
 Feibelman W.A., 1982, *AJ*, 87, 555
 Feibelman W.A., 1985, *PASP*, 97, 404
 Fesen R.A., Milisavljevic D., 2010, *AJ*, 139, 2595
 Finkbeiner D.P., 2003, *ApJS*, 146, 407 (F03)
 Forrest W.J., Shure M.A., Pipher J.L., Woodward C.E., 1987, *AIPC*, 155, 153
 Frew D.J., 2008, PhD thesis, Macquarie University
 Frew D.J., Parker Q.A., 2006, *IAUS*, 234, 49
 Frew D.J., Parker Q.A., 2007, *APN IV Conf. Proc.*, published online at <http://www.iac.es/proyect/apn4>, article #68
 Frew D.J., Parker Q.A., 2010, *PASA*, 27, 129 (FP10)
 Frew D.J., Parker Q.A., 2011, *APN V Conf. Proc.*, 33 (eprint: arXiv:1010.5003)
 Frew D.J., Parker Q.A., 2012, *IAUS*, 283, 192
 Frew D.J., Madsen G.J., Parker Q.A., 2006, *IAUS*, 234, 395

- Frew D.J., Parker Q.A., Russeil D., 2006, *MNRAS*, 372, 1081
 Frew D.J., Madsen G.J., O'Toole S.J., Parker Q.A., 2010, *PASA*, 27, 203
 Frew D.J. et al., 2011, *PASA*, 28, 83
 Frew D.J., Bojčić I.S., Parker Q.A., 2012a, *IAUS*, 283, 362
 Frew D.J. et al. 2012b, in preparation
 Froebrich D. et al., 2011, *MNRAS*, 413, 480
 García-Rojas J., Peña M., Peimbert A., 2009, *A&A*, 496, 139
 García-Rojas J., Peña M., Morisset C., Mesa-Delgado A., Ruiz M.T., 2012, *A&A*, 538, A54
 Gathier R., Pottasch S.R., Pel J.W., 1986, *A&A*, 157, 171
 Gaustad J.E., McCullough P.R., Rosing W., Van Buren D., 2001, *PASP*, 113, 1326 (GMR01)
 Gebel W.L., 1968, *ApJ*, 153, 743
 Giammanco C. et al., 2011, *A&A*, 525, A58
 Gieseck F., Hippelein H., Weinberger R., 1986, *A&A*, 156, 101 (GHW)
 Goldman D.B., Guerrero M.A., Chu Y.-H., Gruendl R.A., 2004, *AJ*, 128, 1711
 Gonçalves D.R., Corradi R.L.M., Mampaso A., 2001, *ApJ*, 547, 302
 González-Solares E.A. et al. 2008, *MNRAS*, 388, 89
 Górný S.K., Stasińska G., Escudero A.V., Costa R.D.D., 2004, *A&A*, 427, 231
 Górný S.K., Chiappini C., Stasińska G., Cuisinier F., 2009, *A&A*, 500, 1089
 Grosdidier Y., Moffat, A.F.J., Joncas G., Acker A., 2001, *ApJ*, 562, 753
 Guerrero M.A., Villaver E., Manchado A., Garcia-Lario P., Prada F., 2000, *ApJS*, 127, 125
 Gutiérrez-Moreno A., Moreno, H., 1998, *PASP*, 110, 458
 Gutiérrez-Moreno A., Cortes G., Moreno H., 1985, *PASP*, 97, 397
 Gutiérrez-Moreno A., Moreno H., Cortes G., 1995, *PASP*, 107, 462
 Gvaramadze V.V., Kniazev A.Y., Fabrika S., 2010, *MNRAS*, 405, 1047
 Haffner L.M., Reynolds R.J., Tuftte S.L., Madsen G.J., Jaehnig K.P., Percival J.W., 2003, *ApJS*, 149, 405
 Haffner L.M. et al., 2010, *ASPC*, 438, 388
 Hawley S.A., 1981, *PASP*, 93, 93
 Hawley S.A., Miller J.S., 1978a, *ApJ*, 220, 609
 Hawley S.A., Miller J.S., 1978b, *ApJ*, 221, 851
 Hayes D.S., Latham D.W., 1975, *ApJ*, 197, 593
 Henry R.B.C., Kwitter K.B., Jaskot A.E., Balick B., Milingo J.B., 2010, *ApJ*, 724, 748
 Hewett P.C., Irwin M.J., Skillman E.D., Foltz C.B., Willis J.P., Warren S.J., Walton N.A., 2003, *ApJ*, 599, L37
 Hippelein H., Münch G., 1981, *MitAG*, 54, 193
 Hippelein H., Weinberger R., 1990, *A&A*, 232, 129 (HP90)
 Hippelein H.H., Baessgen M., Grewing M., 1985, *A&A*, 152, 213
 Hora J.L., Latter W.B., Smith H.A., Marengo M., 2006, *ApJ*, 652, 426
 Howarth I.D., 1983, *MNRAS*, 203, 301
 Hua C.T., 1988, *A&A*, 193, 273
 Hua C.T., 1997, *A&AS*, 125, 355
 Hua C.T., Grundseth B., 1985, *AJ*, 90, 2055
 Hua C.T., Kwok S., 1999, *A&AS*, 138, 275
 Hua C.T., Nguyen-Trong T., 1983, *A&A*, 117, 272
 Hua C.T., Grundseth B., Maucherat A.J., 1993, *A&AS*, 101, 541
 Hua C.T., Dopita M.A., Martinis J., 1998, *A&AS*, 133, 361
 Hummer D.G., Storey P.J., 1987, *MNRAS*, 224, 801
 Hyung S., Aller, L.H., Feibelman, W.A., 1994, *ApJS*, 93, 465
 Ishida K., Weinberger R., 1987, *A&A*, 178, 227
 Jacoby G.H., 1980, *ApJS*, 42, 1
 Jacoby G.H., De Marco O., 2002, *AJ*, 123, 269
 Jacoby G.H., Van de Steene G., 2004, *A&A*, 419, 563
 Jacoby G.H. et al., 2010, *PASA*, 27, 156
 Jaschek C., Jaschek M., 1987, *The Classification of Stars* (Cambridge: University Press)
 Jurasevich D.M., 2009, *CBET*, 1876, 1
 Kaler J.B., 1976, *ApJ*, 210, 113
 Kaler J.B., 1978, *ApJ*, 226, 947
 Kaler J.B., 1980, *ApJ*, 239, 78
 Kaler J.B., 1981, *ApJ*, 250, L31
 Kaler J.B., 1983a, *ApJ*, 264, 594
 Kaler J.B., 1983b, *ApJ*, 271, 188
 Kaler J.B., Hartkopf W.I., 1981, *ApJ*, 249, 602
 Kaler J.B., Lutz J.H., 1980, *PASP*, 92, 81
 Kaler J.B., Lutz J.H., 1985, *PASP*, 97, 700
 Kaler J.B., Pratap P., Kwitter K.B., 1987, *PASP*, 99, 952
 Kaler J.B., Shaw R.A., Kwitter K.B., 1990, *ApJ*, 359, 392
 Kaler J.B., Shaw R.A., Browning L., 1997, *PASP*, 109, 289
 Kastner J.H. et al., 2012, *AJ*, 144, 58
 Kelly D.M., Latter W.B., Rieke G.H., 1992, *ApJ*, 395, 174
 Kerber F., Gröbner H., Lercher G., Weinberger R., 1997, *A&A*, 324, 1149
 Kerber F., Roth M., Manchado A., Gröbner H., 1998, *A&AS*, 130, 501
 Kerber F., Furlan E., Roth M., Galaz G., Chaname J.C., 2000, *PASP*, 112, 542
 Kimeswenger S., 1998, *MNRAS*, 294, 312
 Kimeswenger S., 2001, *RMxAA*, 37, 115
 Kingsburgh R.L., Barlow M.J., 1994, *MNRAS*, 271, 257
 Kistiakowsky V., Helfand D.J., 1993, *AJ*, 105, 2199
 Kistiakowsky V., Helfand D.J., 1995, *AJ*, 110, 2225
 Kohoutek L., 1968, *BAC*, 19, 371
 Kohoutek L., 2001, *A&A*, 378, 843
 Kohoutek L., Martin W., 1981a, *A&AS*, 44, 325 (KM81)
 Kohoutek L., Martin W., 1981b, *A&A*, 94, 365
 Kondratyeva L.N., Denissyuk E.K., 2003, *A&A*, 411, 477
 Kovacevic A.V., Parker Q.A., Jacoby G.H., Sharp R., Miszalski B., Frew D.J., 2011, *MNRAS*, 414, 860
 Kraan-Korteweg R.C., Fairall A.P., Woudt P.A., Van de Steene G.C., 1996, *A&A*, 315, 549
 Krabbe A.C., Copetti M.V.F., 2006, *A&A*, 450, 159
 Kronberger M. et al., 2012, *IAUS*, 283, 414
 Kuijken K. et al., 2004, *SPIE Proc.*, 5492, 484
 Kwitter K.B., Jacoby G.H., 1989, *AJ*, 98, 2159
 Kwitter K.B., Henry R.B.C., Milingo J.B., 2003, *PASP*, 115, 80
 Kwok S., 2010, *PASA*, 27, 174
 Kwok S., Zhang Y., Koning N., Huang H.-H., Churchwell E., 2008, *ApJS*, 174, 426
 Lagadec E. et al., 2011, *MNRAS*, 417, 32
 Lane N.J., Pogge R.W., 1994, *AJ*, 108, 1860
 Lane N.J., Pogge R.W., 1996, *AJ*, 111, 2320
 Lamers H.J.G.L.M., Zickgraf F.-J., de Winter D., Houziaux L., Zorec J., *A&A*, 340, 117
 Lanning H.H., Meakes M., 2004, *PASP*, 116, 1039
 Leibowitz E.M., Danziger I.J., 1983, *MNRAS*, 204, 273
 Liller W., 1955, *ApJ*, 122, 240
 Liller W., Aller L.H., 1954, *ApJ*, 120, 48
 Liller W., Aller L.H., 1963, *PNAS*, 49, 675
 Liu X.-W., Storey P.J., Barlow M.J., Danziger I.J., Cohen M., Bryce M., 2000, *MNRAS*, 312, 585
 Liu Y., Liu X.-W., Luo S.-G., Barlow M.J., 2004, *MNRAS*, 353, 1231
 Liu X.-W., Barlow M.J., Zhang Y., Bastin R.J., Storey P.J., 2006, *MNRAS*, 368, 1959
 López J.A., Richer M.G., Garca-Díaz, M.T., Clark D.M., Meaburn J., Riesgo H., Steffen W., Lloyd M., 2012, *RMxAA*, 48, 3
 Lutz J.H., 1984, *ApJ*, 279, 714
 Lutz J.H., Kaler J.B., Shaw R.A., Schwarz H.E., Aspin C., 1989, *PASP*, 101, 966

- Lutz J., Fraser O., McKeever J., Tugaga D., 2010, *PASP*, 122, 524
- McCullough P.R., Bender C., Gaustad J.E., Rosing W., Van Buren D., 2001, *AJ*, 121, 1578
- Madsen G.J., Frew D.J., Parker Q.A., Reynolds R.J., Haffner L.M., 2006, *IAUS*, 234, 455
- Malin D.F., 1982, *S&T*, 63, 22
- Mampaso A. et al., 2006, *A&A*, 458, 203
- Masci F., 2008, available at <http://wise2.ipac.caltech.edu/staff/fmasci/APN.html>
- Mavromatakis F., Papamastorakis J., Paleologou E.V., Ventura J., 2000, *A&A*, 353, 371
- Mavromatakis F., Papamastorakis J., Ventura J., Becker W., Paleologou E.V., Schaudel D., 2001a, *A&A*, 370, 265
- Mavromatakis F., Papamastorakis J., Paleologou E.V., 2001b, *A&A*, 374, 280
- Meaburn J., Boumis P., López J.A., Harman D.J., Bryce M., Redman M.P., Mavromatakis F., 2005, *MNRAS*, 360, 963
- Méndez R.H., 1991, *IAUS*, 145, 375
- Méndez R.H., Kudritzki R.P., Ciardullo R., Jacoby G.H., 1993, *A&A*, 275, 534
- Merline W.J., Howell S.B., 1995, *ExA*, 6, 163
- Mikołajewska J., Acker A., Stenholm B., 1997, *A&A*, 327, 191
- Milingo J.B., Kwitter K.B., Henry R.B.C., Cohen R.E., 2002, *ApJS*, 138, 279
- Milingo J.B., Kwitter K.B., Henry R.B.C., Souza S.P., 2010, *ApJ*, 711, 619
- Miller J.S., Mathews W.G., 1972, *ApJ*, 172, 593
- Milne D.K., Aller L.H., 1975, *A&A*, 38, 183
- Miranda L.F., Vazquez R., Torrelles J.M., Eiroa C., López J.A., 1997, *MNRAS*, 288, 777
- Miranda L.F., Vázquez R., Guerrero M.A., Pereira, C.B., Iñiguez-Garín E., 2010, *PASA*, 27, 199
- Miszalski B., Parker Q.A., Acker A., Birkby J.L., Frew D.J., Kovacevic A., 2008, *MNRAS*, 384, 525
- Miszalski B., Acker A., Moffat A.F.J., Parker Q.A., Udalski A., 2009, *A&A*, 496, 813
- Miszalski B. et al., 2011, *A&A*, 528, A39
- Miszalski B., Boffin H.M.J., Frew D.J., Acker A., Köppen J., Moffat A.F.J., Parker Q.A., 2012a, *MNRAS*, 419, 39
- Miszalski B., Crowther P.A., De Marco O., Köppen J., Moffat A.F.J., Acker A., Hillwig T.C., 2012b, *MNRAS*, 423, 934
- Mizuno D.R. et al., 2010, *AJ*, 139, 1542
- Monreal-Ibero A., Roth M.M., Schönberner D., Steffen M., Böhm P., 2005, *ApJ*, 628, L139
- Moreno H., Gutierrez-Moreno A., Cortes G., Hamuy M., 1994, *PASP*, 106, 619
- Morgan D.H., Parker Q.A., Cohen M., 2003, *MNRAS*, 346, 719
- Nota A., Leitherer C., Clampin M., Greenfield P., Golimowski D.A., 1992, *ApJ*, 398, 621
- Nürnberg D., Durand S., Köppen J., Stanke Th., Sterzik M., Els S., 2001, *A&A*, 377, 241
- O'Dell C.R., 1962, *ApJ*, 135, 371
- O'Dell C.R., 1963, *ApJ*, 138, 293
- O'Dell C.R., 1998, *AJ*, 116, 1346
- O'Dell C.R., Terzian Y., 1970, *ApJ*, 160, 915
- O'Dell C.R., McCullough P.R., Meixner M., 2004, *AJ*, 128, 2339
- Oke J.B., Gunn J.E., 1983, *ApJ*, 266, 713
- Oliveira I., Overzier R.A., Pontoppidan K.M., van Dishoeck E.F., Spezzi L., 2011, *A&A*, 526, A41
- Osterbrock D.E., Stockhausen R.E., 1961, *ApJ*, 133, 2
- Papamastorakis J., Xilouris K.M., Paleologou E.V., 1994, *IAUS*, 161, 484
- Parker Q.A., Bland-Hawthorn, J., 1998, *PASA*, 15, 33
- Parker Q.A., Malin D., Tritton S., Hartley M., 2001, *AAONw*, 96, 6
- Parker Q.A. et al., 2005, *MNRAS*, 362, 689
- Parker Q.A. et al., 2006, *MNRAS*, 373, 79
- Parker Q.A., Frew D.J., 2011, *APN V Conf. Proc.*, 1
- Parker Q.A., Frew D.J., Miszalski B., Kovacevic A.V., Frinchaboy, P.M., Dobbie, P.D., Köppen J., 2011, *MNRAS*, 413, 1835
- Parker Q.A., Frew D.J., Acker A., Miszalski B., 2012a, *IAUS*, 283, 9
- Parker Q.A., et al., 2012b, *MNRAS*, in press (arXiv:1208.4164)
- Parker Q.A., Frew D.J., Gunawardhana M.L.P., Pierce M.J., Bojičić I.S., 2012c, *MNRAS*, to be submitted
- Parthasarathy M., et al., 1993, *A&A*, 267, L19
- Parthasarathy M., Drilling J.S., Vijapurkar J., Takeda Y., 2012, *PASJ*, 64, 57
- Peimbert M., 1973, *MSRSL*, 5, 307
- Peimbert M., 1978, *IAUS*, 76, 215
- Peimbert M., Serrano A., 1980, *RMxAA*, 5, 9
- Peimbert M., Torres-Peimbert S., 1971, *BOTT*, 6, 21
- Peimbert M., Torres-Peimbert S., 1983, *IAUS*, 103, 233
- Peimbert M., Torres-Peimbert S., 1987, *RMxAA*, 14, 540
- Peña M., Ruiz M.T., Torres-Peimbert S., Maza J., 1990, *A&A*, 237, 454
- Peña M., Torres-Peimbert S., Ruiz M.T., 1991, *PASP*, 103, 865
- Pereira C.B., Franco C.S., de Araújo F.X., 2003, *A&A*, 397, 927
- Perek L., 1971, *BAICz*, 22, 103
- Perek L., Kohoutek L., 1967, *Catalogue of Galactic Planetary Nebulae* (Prague: Academia Publishing House)
- Perinotto M., Corradi R.L.M. 1998, *A&A*, 332, 721
- Perinotto M., Schönberner D., Steffen M., Calonaci C., 2004, *A&A*, 414, 993
- Phillips J.P., 2004, *MNRAS*, 353, 589
- Phillips J.P., Marquez-Lugo R.A., 2011, *MNRAS*, 410, 2257
- Phillips J.P., Ramos-Larios G., 2008, *MNRAS*, 386, 995
- Phillips J.P., Ramos-Larios G., 2009, *MNRAS*, 396, 1915
- Phillips J.P., Cuesta L., Kemp S.N., 2005, *MNRAS*, 357, 548
- Phillips J.P., Ramos-Larios G., Schröder K.-P., Verbena Contreras J.L., 2009, *MNRAS*, 399, 1126
- Pierce M.J., Frew D.J., Parker Q.A., Köppen J., 2004, *PASA*, 21, 334
- Pollacco D.L., Bell S.A., 1997, *MNRAS*, 284, 32
- Pottasch S.R., 1984, *Planetary Nebulae: A Study of Late Stages of Stellar Evolution* (D. Reidel Publishing, Dordrecht: ASSL, vol. 107)
- Pottasch S.R., 1996, *A&A*, 307, 561
- Pottasch S.R., Wesselius P.R., Wu C.-C., van Duinen R. J., 1977, *A&A*, 54, 435
- Rau A. et al., 2009, *PASP*, 121, 1334
- Ramos-Larios G., Guerrero, M.A., Suárez O., Miranda L.F., Gómez J.F., 2012, *A&A*, 545, A20
- Reid W.A., Parker Q.A., 2010, *MNRAS*, 405, 1349
- Reid W.A., Parker Q.A., 2012, *MNRAS*, 425, 355
- Reynolds R.J., 1987, *ApJ*, 315, 234
- Reynolds R.J., Chaudhary V., Madsen G.J., Haffner L.M., 2005, *AJ*, 129, 927
- Rodríguez M., Corradi R.L.M., Mampaso A., 2001, *A&A*, 377, 1042
- Roth M.M., Becker T., Böhm P., Kelz A., 2004, *AN*, 325, 147
- Ruffe P.M.E., Zijlstra A.A., Walsh J.R., Gray M.D., Gesicki K., Minniti D., Comerón F., 2004, *MNRAS*, 353, 796
- Sabbadin F., 1986, *A&AS*, 65, 301
- Sabbadin F., Minello S., Bianchini A., 1977, *A&A*, 60, 147
- Sabin L., 2008, Unpublished PhD thesis, University of Manchester
- Sabin L., Zijlstra A.A., Wareing C., Corradi R.L.M., Mampaso A., Viironen K., Wright N.J., Parker Q.A., 2010, *PASA*, 27, 166
- Sabin L. et al., 2012, *MNRAS*, submitted
- Sahai R. et al., 1999, *AJ*, 118, 468
- Sahai R., Nyman L.-Å, Wootten A., 2000, *ApJ*, 543, 880
- Sahai R., Morris M., Sánchez Contreras C., Claussen M., 2007, *AJ*, 134, 2200
- Sahan M., 2011, *AN*, 332, 185

- Sandin C., Schönberner D., Roth M.M., Steffen M., Böhm P., Monreal-Ibero A., 2008, *A&A*, 486, 545
- Sandin C., Roth M.M., Schönberner D., 2010, *PASA*, 27, 214
- Sanduleak N., Stephenson C.B., 1972, *ApJ*, 178, 183
- Santander-García M., Corradi R.L.M., Mampaso A., Morisset C., Munari U., Schirmer M., Balick B., Livio M., 2008, *A&A*, 485, 117
- Saurer W., 1997a, *A&A*, 326, 1187
- Saurer W., 1997b, *A&A*, 328, 641
- Saurer W., Weinberger R., 1987, *A&AS*, 69, 527
- Schlafly E.F., Finkbeiner D.P., 2011, *ApJ*, 737, 103
- Schmeja S., Kimeswenger S., 2001, *A&A*, 377, L18
- Schönberner D., Jacob R., Steffen M., Sandin C., 2007, *A&A*, 473, 467
- Shaw R.A., Kaler J.B., 1982, *ApJ*, 261, 510
- Shaw R.A., Kaler J.B., 1985, *ApJ*, 295, 537
- Shaw R.A., Kaler J.B., 1989, *ApJS*, 69, 495 (SK89)
- Shaw R.A., Stanghellini L., Villaver E., Mutchler M., 2006, *ApJS*, 167, 201
- Shen Z.-X., Liu X.-W., Danziger I.J., 2004, *A&A*, 422, 563
- Shiode J., Clemens, D.P. Janes K.A., Pinnick, A., 2006, *IAUS*, 234, 509
- Smith L.F., Aller L.H., 1969, *ApJ*, 157, 1245
- Smith N., Bally J., Walawender J., 2007, *AJ*, 134, 846
- Speck A.K., Meixner M., Fong D., McCullough P.R., Moser D.E., Ueta T., 2002, *AJ*, 123, 346
- Stanghellini L., Shaw R.A., Villaver E., 2008, *ApJ*, 689, 194
- Stasińska G., Tylenda R., Acker A., Stenholm B., 1992, *A&A*, 266, 486
- Stock D.J., Barlow, M.J., 2010, *MNRAS*, 409, 1429
- Stupar M., Parker Q.A., Filipović M.D., Frew D.J., Bojčić I., Aschenbach B., 2007, *MNRAS*, 381, 377
- Stupar M., Parker Q.A., Filipović M.D., 2008, *MNRAS*, 390, 1037
- Su K.Y.L. et al., 2007, *ApJ*, 657, L41
- Suárez O., Garca-Lario P., Machado A., Manteiga M., Ulla A., Pottasch S. R., 2006, *A&A*, 458, 173
- Szczerba R., Siódmiak N., Stasińska G., Borkowski J., 2007, *A&A*, 469, 799
- Szczerba R. et al., 2012, *IAUS*, 283, 506
- Todt H., Peña M., Zühlke J., Oskinova L., Hamann W.-R., Gräfener G., 2012, *IAUS*, 283, 510
- Topasna G.A., 1999, PhD thesis, Virginia Polytechnic Institute and State University
- Torres-Peimbert S., 2011, *RMxAC*, 39, 87
- Torres-Peimbert S., Peimbert M., 1977, *RMxAA*, 2, 181
- Torres-Peimbert S., Peimbert M., 1979, *RMxAA*, 4, 341
- Torres-Peimbert S., Rayo J.F., Peimbert, M., 1981, *RMxAA*, 6, 315
- Torres-Peimbert S., Peimbert M., Peña M., 1990, *A&A*, 233, 540
- Tsamis Y.G., Barlow M.J., Liu X.-W., Danziger I.J., Storey P.J., 2003, *MNRAS*, 345, 186
- Tsamis Y.G., Walsh J.R., Péquignot D., Barlow M.J., Danziger I.J., Liu X.-W., 2008, *MNRAS*, 386, 22
- Turatto M., Cappellaro E., Sabbadin F., Salvadori L., 1990, *AJ*, 99, 1170
- Tweedy R.W., Kwitter K.B., 1994, *AJ*, 108, 188
- Tweedy R.W., Kwitter K.B., 1996, *ApJS*, 107, 255
- Tylenda R., Acker A., Stenholm B., 1993, *A&AS*, 102, 595
- Tylenda R., Acker A., Stenholm B., Köppen J., 1992, *A&AS*, 95, 337
- Tylenda R., Stasińska G., Acker A., Stenholm B., 1994, *A&AS*, 106, 559
- Urquhart J.S., Hoare M.G., Lumsden S.L., Oudmaijer R.D., Moore T.J.T., 2008, *ASPC*, 387, 381
- Urquhart J.S. et al., 2009, *A&A*, 501, 539
- Van de Steene G.C., Zijlstra A.A., 1994, *A&AS*, 108, 485
- Van de Steene G.C., Sahu K.C., Pottasch S.R., 1996, *A&AS*, 120, 111
- Viironen K. et al., 2009a, *A&A*, 502, 113
- Viironen K. et al., 2009b, *A&A*, 504, 291
- Viironen K. et al., 2011, *A&A*, 530, A107
- Vorontsov-Vel'yaminov B.A., Kostyakova E.B., Dokuchaeva O.D., Arkhipova V.P., 1968, *IAUS*, 34, 57
- Vorontsov-Vel'yaminov B.A., Kostyakova E.B., Dokuchaeva O.D., Arkhipova V.P., 1975, *SvA*, 19, 163
- Wachter S., Mauerhan J.C., Van Dyk S.D., Hoard D.W., Kafka S., Morris P.W., 2010, *AJ*, 139, 2330
- Wang Q.D. et al., 2010, *MNRAS*, 402, 895
- Wang W., Liu X.-W., 2007, *MNRAS*, 381, 669
- Wareing C.J., 2010, *PASA*, 27, 220
- Webster B.L., 1969, *MNRAS*, 143, 79
- Webster B.L., 1983, *PASP*, 95, 610
- Weidmann W.A., Gamen R., 2011, *A&A*, 526, A6
- Weinberger R., Hartl H., Temporin S., Zanin C., 1999, *ASPC*, 168, 142
- Weinberger R., Kerber F., Gröbner H., 1997, *A&A*, 323, 963
- Wenger M. et al., 2007, *ASPC*, 377, 197
- Werner K., 2012, *IAUS*, 283, 196
- Werner K., Herwig F., 2006, *PASP*, 118, 183
- Wesson R., Liu X.-W., 2004, *MNRAS*, 351, 1026
- Wesson R., Liu X.-W., Barlow M.J., 2005, *MNRAS*, 362, 424
- Wesson R. et al., 2008, *ApJ*, 688, L21
- Whiting A.B., Hau G.K.T., Irwin, M., 2002, *ApJS*, 141, 123
- Whiting A.B., Hau G.K.T., Irwin, M., Verdugo M., 2007, *AJ*, 133, 715
- Witham A.R., Knigge C., Drew J.E., Greimel R., Steeghs D., Gänsicke B.T., Groot P.J., Mampaso A., 2008, *MNRAS*, 384, 1277
- Wright S.A., Corradi R.L.M., Perinotto M., 2005, *A&A*, 436, 967 (WCP05)
- Xilouris K.M., Papamastorakis J., Sokolov N., Paleologou E., Reich W., 1994, *A&A*, 290, 639
- Xilouris K.M., Papamastorakis J., Paleologou E., Terzian Y., 1996, *A&A*, 310, 603 (XPPT)
- Zanin C., Cappellaro E., Sabbadin F., Turatto M., 1997, *IAUS*, 180, 26
- Zhang C.Y., 1995, *ApJS*, 98, 659
- Zhang Y., Liu X.-W., 2003, *A&A*, 404, 545
- Zhang Y., Hsia C.-H., Kwok S., 2012, *ApJ*, 755, 53
- Zijlstra A., Pottasch S., Bignell C., 1990, *A&AS*, 82, 273
- Zijlstra A.A., Gesicki K., Walsh J.R., Péquignot D., van Hoof P.A.M., Minniti D., 2006, *MNRAS*, 369, 875

APPENDIX A: RECALIBRATED H α FLUXES

Other potentially useful integrated H α + [N II] fluxes have been published in the literature, especially for several large, evolved PNe. In particular, Xilouris et al. (1996; XPPT) presented H α + [N II] and [O III] fluxes for eight evolved PNe (see also Papamastorakis, Xilouris & Paleologou 1994), while Xilouris et al. (1994) and Ali et al. (1997) presented integrated H α + [N II] fluxes for another five PNe. However, we found that the XPPT fluxes to be inconsistent with other measurements. A comparison between their quoted surface brightness data and independent SHASSA measurements show the XPPT surface brightness data to be accurate, but the integrated fluxes were found to be too faint by a factor of ~ 20 , presumably the result of a simple reduction error. In order to make a comparison with other sources, firstly H α fluxes were derived from their quoted 'red' fluxes by deconvolving the [N II] emission for each PN, using the references from Section 3.2. The characteristics of the broad H α + [N II] filter ($\lambda_{\text{eff}} = 6570\text{\AA}$, FWHM = 75 \AA) are described

Table A1. Summary details of the H α + [N II] filters used in various studies, and the adopted transmission coefficients used in Equation 3. These were calculated from the filter transmission characteristics given in the references.

Reference	λ_{eff} (Å)	FWHM (Å)	K_{tr}
SHASSA	6563	32	0.375
VTSS	6566	17.5	0.00
SHS	6590	70	0.725
APS97	6574	104	1.00
JaSt	6569	80	1.00
XPS94	6570	75	1.00
XPPT	6570	75	1.00

by XPPT and Mavromatakis et al. (2000) which indicates the transmission for the [N II] doublet is identical to H α making the deconvolution calculation straightforward (i.e. $K_{\text{tr}} = 1$; see Table A1). We then compared the H α fluxes from our SHASSA and other literature data with the XPPT fluxes; they were found to be offset in the mean by 1.32 ± 0.08 dex ($n = 7$) and this correction was hence applied to all their original fluxes.

Table A2 gives the original H α + [N II] fluxes adopted from these sources and our derived H α fluxes. The [N II]/H α ratios were taken from the references described in Section 3.2 and we used the filter transmission coefficients from Table A1, and the principles adopted previously. The H α fluxes from XPPT corrected for the zero-point offset are presented in the last column.

Another set of useful emission-line data in H α , [N II] and [O III] is presented by Giesekeing, Hippelein & Weinberger (1986; GHW) and Hippelein & Weinberger (1990; HW90). These authors used a Fabry-Perot spectrometer using 1' or 2' apertures (i.e. smaller than most of the PNe they studied), presenting surface brightness values (given in mag per arcsec²) for each PN. These surface brightness values were not immediately reconcilable with the fluxes of XPPT and Kaler (1983b) for the evolved PNe in common, nor with our SHASSA data, as the adopted formula to convert from magnitudes to cgs units is not given by either GHW nor HW90. However, a comparison of the surface brightness measurements of GHW for IsWe 1 and IsWe 2 with the absolute surface fluxes for these same PNe presented by Ishida & Weinberger (1987), allowed the determination of the transformation equation used, which is that given by Pottasch (1984), viz:

$$m_{\lambda} = -2.5 \log F(\lambda) - 15.77 \quad (\text{A1})$$

where λ is the emission line species of interest. Consequently the same zero-point was used for [O III], [N II] and H α , despite the range in wavelength of these emission lines (cf. Allen 1973, p. 197). Using equation A1, the surface brightnesses in $\text{erg cm}^{-2} \text{s}^{-1} \text{arcsec}^{-2}$ in each line were then determined. However, to get the integrated flux, one needs to know the angular size of these PNe. The dimensions were generally taken from Frew (2008). Table A3 summarises the adopted dimensions and derived H α fluxes for these PNe.

There are a few other moderately-sized PNe from Abell (1966) which have no flux data at present, either because

they are too faint for SHASSA and VTSS, or because they are located outside the bounds of the available survey fields. Since any flux data on these poorly-studied objects are welcome, a re-investigation of the Abell (1966) photographic data is warranted. Nebular magnitudes were estimated from the POSS I survey blue and red plates. The nebular surface brightness of a PN was compared with spots of different densities on film strips exposed with a sensitometer, in turn calibrated with extra-focal images of standard stars. Further details on the method are given in Abell (1966).

From the calibrated surface brightness and the angular size of the nebula in each passband, integrated photographic and photo-red magnitudes were determined for each object, but we are only concerned with the photo-red magnitudes here. These were adjusted following Jacoby (1980) and then corrected here for the contribution of the nitrogen lines, assuming equal throughput for the H α and [N II] lines from the broadband Plexiglass filter used in conjunction with red-sensitive (Kodak 103a-E) photographic plates. The conversion to 'H α ' magnitudes is given by:

$$m_{(\text{H}\alpha)} = m_{\text{pr}} - 2.5 \log \left(\frac{1}{R_{[\text{N II}]} + 1} \right) \quad (\text{A2})$$

where $R_{[\text{N II}]}$ is defined as before. The resulting 'H α ' magnitudes were then compared with the mean of all available integrated H α fluxes from our database. A least-squares linear fit to the flux-magnitude relation gave:

$$m_{(\text{H}\alpha)} = -2.5 \log F(\text{H}\alpha) - 14.35 \quad (\text{A3})$$

which can be compared with the expressions given by Ciardullo (2010) and Reid & Parker (2012). Equation A3 was used to determine approximate H α fluxes for all the PNe with m_{pr} magnitudes listed in Abell (1966) that have [N II]/H α ratios available. We compared the derived fluxes with literature H α data, and with our SHASSA and VTSSH α fluxes, finding a dispersion of the Abell 'H α ' fluxes compared to our independent SHASSA and VTSS fluxes of ± 0.22 dex ($n = 44$) and ± 0.21 dex ($n = 20$) respectively. The Abell 'H α ' fluxes derived in this way are surprisingly good, and better than some modern CCD studies (see Table 3). Rather than listing the full list of derived H α fluxes, we present in Table A4 data for the 14 PNe and two mimics which either have no measurements from elsewhere in this paper, or have inconsistent fluxes in the literature.

APPENDIX B: H α FLUXES FOR MISCLASSIFIED NEBULAE

Many different kinds of objects can masquerade as PNe in extant catalogues (see FP10 for a detailed review). These objects include compact H II regions (e.g. Kimeswenger 1998; Copetti et al. 2007; Cohen et al. 2011; Anderson et al. 2012), Strömgren zones around low-mass stars (Reynolds 1987; Hewett et al. 2003; Chu et al. 2004; Madsen et al. 2006; Frew 2008; Frew et al. 2010; De Marco et al. 2012; cf. Wareing 2010), ejecta shells around Wolf-Rayet and other massive stars (e.g. Duerbeck & Reipurth 1990; Cohen & Barlow 1975; Crawford & Barlow 1991a,b; Chu 2003; Egan et al. 2002; Morgan, Parker & Cohen 2003; Cohen et al.

Table A2. Integrated $H\alpha + [N II]$ fluxes taken from Xilouris et al. (1994), Xilouris et al. (1996; XPPT) and Ali et al. (1997). The XPPT fluxes have been further corrected as described in the text. The flux uncertainties are estimated to be ± 0.08 dex.

Name	PN G	$R_{[N II]}$	$\log F_{red}$	$\log F(H\alpha)$	$\log F(H\alpha)$ (corrected)	Ref.	Notes
Abell 4	144.3–15.5	0.28	–11.80	–11.91	–11.91	APS97	...
Abell 7	215.5–30.8	0.9	–11.59	–11.85	–10.58	XPPT	...
Abell 8	167.0–00.9	0.97	–11.60	–11.90	–11.90	APS97	...
Abell 62	047.1–04.2	1.5	–11.96	–12.29	–11.02	XPPT	...
Abell 74	072.7–17.1	1.3	–11.51	–11.80	–10.52	XPPT	...
G4.4+6.4	004.3+06.4	2.4	–10.70	–11.23	–11.23	XPS94	a
HFG 1	136.3+05.5	0.4	–11.59	–11.77	–10.49	XPPT	...
IsWe 1	149.7–03.3	0.75	–11.96	–12.07	–10.80	XPPT	...
IsWe 2	107.7+07.8	1.45	–11.37	–11.76	–10.48	XPPT	...
J 320	190.3–17.7	0.04	–10.80	–10.82	–10.82	APS97	...
M 2-55	116.2+08.5	1.7	–10.74	–11.17	–11.17	APS97	...
Sh 2-68	030.6+06.2	0.5	–11.66	–11.84	–10.56	XPPT	a,b
Sh 2-176	120.2–05.3	2.3	–11.41	–11.93	–10.65	XPPT	...
Sh 2-188	128.0–04.1	1.9	–10.87	–11.35	–10.07	XPPT	...

Notes: (a) PN status uncertain; (b) flux excludes outer halo.

Table A3. Integrated $H\alpha$ fluxes derived from the surface brightness data presented by Giesekeing, Hippelein & Weinberger (1986, GHW), Hippelein & Weinberger (1990, HW90), and Saurer & Weinberger (1987, SW87), who utilised the MPI Fabry-Perot Interferometer (Hippelein & Münch 1981). For completeness, we also quote the integrated $H\alpha$ fluxes taken with this instrument for two smaller PNe (Saurer 1997a,b). The flux uncertainties are estimated to be ± 0.05 dex for the smaller objects up to ± 0.25 dex for the largest.

Name	PN G	Size ($''$)	$S(H\alpha)$ (mag/ \square'')	$\log S(H\alpha)$ (erg/cm ² /s/ \square'')	$\log F(H\alpha)$ (erg/cm ² /s)	Ref.	Notes
Abell 28	158.8+37.1	320	25.1	–12.79	–11.44	HW90	...
Abell 34	248.7+29.5	292	24.1	–12.39	–11.12	HW90	...
Abell 39	047.0+42.4	174	23.9	–12.31	–11.49	HW90	...
Abell 61	077.6+14.7	199	23.6	–12.19	–11.26	GHW	...
Abell 62	047.1–04.2	160	22.8	–11.87	–11.12	HW90	...
Abell 71	084.9+04.4	157	22.0	–11.55	–10.82	HW90	...
Abell 74	072.7–17.1	795	24.5	–12.55	–10.41	GHW	...
DHW 5	111.0+11.6	595	24.3	–12.47	–10.58	GHW	a
EGB 6	221.5+46.3	780	26.3	–13.27	–11.15	HW90	...
IsWe 1	149.7–03.3	745	25.6	–12.99	–10.91	GHW	...
IsWe 2	107.7+07.8	970	25.1	–12.79	–10.48	GHW	...
JnEr 1	164.8+31.1	380	23.5	–12.15	–10.65	HW90	...
K 3-82	093.3-00.9	20	–11.60	S97b	...
M 1-79	093.3-02.4	33	–11.04	S97a	...
PuWe 1	158.9+17.8	1210	25.2	–12.83	–10.33	GHW	...
SaWe 3	013.8–02.8	95	...	–11.58	–11.19	SW87	b
Sh 2-68	030.6+06.2	410	24.0	–12.35	–10.79	HW90	c,d
We 1-10	086.1+05.4	190	24.0	–12.35	–11.46	HW90	...
We 3-1	044.3+10.4	166	23.2	–12.03	–11.25	HW90	...

Notes: (a) HII region; (b) the $S(H\alpha)$ and total $F(H\alpha)$ values are derived from the measured $H\alpha$ flux of 5.5×10^{-13} erg cm^{–2} s^{–1} observed through a 31 $''$ aperture; (c) PN status uncertain; (d) Flux excludes outer halo.

2005a; Stock & Barlow 2010), B[e] and related stars (e.g. Lamers et al. 1998), symbiotic systems (Blair et al. 1983; Lutz 1984; Acker, Lundström & Stenholm 1988; Corradi 1995; Belczyński et al. 2000; Corradi et al. 2008, 2010; Lutz et al. 2010), Herbig-Haro objects (Cantó 1981; Cappellaro et al. 1994), evolved supernova remnants (e.g. Mavromatakis et al. 2001a,b; Stupar et al. 2007, 2008; Sabin et al. 2012), as well as old nova shells and bow-shock nebulae (see FP10, and references therein).

For reviews of the problem, the reader is referred to

Acker & Stenholm (1990), Kohoutek (2001), Parker et al. (2006), Cohen et al. (2007, 2011), Kwok (2010), FP10, and Frew & Parker (2011), while individual lists of misclassified PNe have been published by Sabbadin (1986), Acker et al. (1987), Acker & Stenholm (1990), Zijlstra, Pottasch & Bignell (1990), Kohoutek (2001), Frew (2008), and Miszalski et al. (2009). Since our input database drew on the older PN catalogues (Acker et al. 1992, 1996; Kohoutek 2001), we measured $H\alpha$ fluxes for 76 objects of various kinds that were formerly classified as PNe.

Table A4. Magnitudes and derived H α fluxes for 23 PNe and two mimics from Abell (1966) following the method described in the text. The flux uncertainties are estimated to be ± 0.22 dex.

Name	PN G	Other	$R_{[\text{N II}]}$	m_{pr}	$m_{(\text{H}\alpha)}$	F(H α)	Note
Abell 1	119.4+06.5	...	0.7	15.7	16.3	-12.21	a
Abell 3	131.5+02.6	...	0.4	14.3	14.6	-11.61	...
Abell 5	141.7-07.8	...	4.0	13.7	15.4	-11.98	...
Abell 6	136.1+04.9	...	0.2	13.6	13.8	-11.26	...
Abell 8	167.0-00.9	...	1.0	15.0	16.0	-12.00	...
Abell 9	172.1+00.8	...	1.6	16.3	17.3	-12.69	...
Abell 19	200.7+08.4	...	1.7	15.8	16.9	-12.43	...
Abell 30	208.5+33.2	...	0.1	14.5	14.6	-11.58	...
Abell 33	238.0+34.8	...	0.2	12.1	12.3	-10.68	...
Abell 49	027.3-03.4	...	1.3	14.2	15.1	-11.80	...
Abell 54	055.3+06.6	...	1.2	15.5	16.3	-12.29	...
Abell 55	033.0-05.3	...	1.0	13.0	13.8	-11.26	...
Abell 59	053.3+03.0	...	2.1	13.2	14.4	-11.52	...
Abell 60	025.0-11.6	...	0.0	14.7	14.7	-11.64	...
Abell 69	076.3+01.1	...	5.2	15.3	17.3	-12.67	a
Abell 72	059.7-18.7	...	0.1	13.8	13.9	-11.30	...
Abell 73	095.2+07.8	...	1.3	14.7	15.6	-11.99	...
Abell 75	101.8+08.7	NGC 7076	0.0	15.2	15.2	-11.85	...
Abell 77	097.5+03.1	Sh 2-128	0.2	12.5	12.7	-10.83	b
Abell 78	081.2-14.9	...	0.1	15.3	15.4	-11.91	...
Abell 79	102.9-02.3	...	6.9	12.1	14.4	-11.49	...
Abell 81	117.5+18.9	IC 1454	0.3	13.6	13.9	-11.32	...
Abell 83	113.6-06.9	...	0.8	15.9	16.6	-12.31	...
Abell 85	...	CTB 1	0.6	8.6	9.1	-9.5 :	a,c
Abell 86	118.7+08.2	...	0.0:	14.8	14.8	-11.67	a

Notes: (a) No other integrated flux determination in the literature; (b) H II region; (c) supernova remnant.

We do not provide an exhaustive list of mimics but only include those 76 objects that were cleanly detected with our pipeline. Nonetheless, many well-known objects are included, such as the symbiotic outflow Hen 2-104 (Lutz et al. 1989; Corradi & Schwarz 1993; Santander-García et al. 2008), the WR nebula M 1-67 (Cohen & Barlow 1975; Crawford & Barlow 1991a; Esteban et al. 1991; Grosdidier et al. 2001), and Kepler’s supernova remnant (Leibowitz & Danziger 1983), for which integrated H α fluxes should be of interest to the wider community. Table B1 lists the H α fluxes for these objects. Columns 1 and 2 give the *PNG* designation and the common name respectively, columns 3 and 4 give the J2000.0 coordinates, while the adopted value of $R_{[\text{N II}]}$, the logarithm of the red flux and the logarithm of the H α flux are given in column 5, 6 and 7. The adopted aperture radius in arcmin is given in column 8, the number of measurements from separate fields is given in column 9, the classification of the object in column 10, and any notes are indexed in column 11. Objects that are likely to be mimics, but which are still considered to be PNe by some authors are kept in the main tables for now, and are flagged accordingly (see Tables 1 and 4).

The abbreviations used for the classification are as follows: H II: H II region; ELS: emission-line star; SNR: supernova remnant; BCD: blue compact dwarf; SyS: symbiotic star; post-RSG: post-red supergiant; WR neb: Wolf-Rayet nebula; (c)LBV: (candidate) luminous blue variable; CV: cataclysmic variable.

Table B1: H α fluxes for 76 objects that have been misclassified as PNe in the literature. The top section contains 71 fluxes determined from SHASSA, and the bottom section contains eight fluxes from VTSS. Sh 2-266 and Ap 2-1 are in both lists.

PNG	Name	RAJ2000	DEJ2000	$R_{[NII]}$	$\log F_{\text{red}}$	$\log F(\text{H}\alpha)$	r_{aper}	N_f	Type	Note
125.9–47.0	PK 125-47 1	00:59:56.7	15:44:14	0.7	-10.67	-10.77±0.04	7.4	2	H II	
...	Reynolds 1	01:11:06.6	10:21:39	...	-10.9	-10.9±0.2	31.4	2	H II	4
...	Sh 2-266	06:18:45.5	15:16:52	0.7	-10.23	-10.33±0.04	2.9	2	H II	
...	Min 2-62	06:43:48.5	-01:08:20	0.3	-11.14	-11.19±0.04	1.9	4	H II	
...	MWC 819	06:44:37.7	01:19:32	...	-11.32	...	1.8	4	ELS	1
...	PHR J0712-0950	07:12:34.8	-09:50:44	0.4	-9.7	-9.7±0.2	9.5	3	H II	
...	EGB 9	07:18:57.9	07:22:23	0.4	-11.18	-11.25±0.06	5.4	1	H II	
211.9+22.6	EGB 5	08:11:12.8	10:57:17	0.4	-11.59	-11.65±0.08	2.8	1	H II	4
...	NGC 2579	08:20:55.3	-36:13:23	0.9	-9.58	-9.71±0.05	4.7	2	H II	
260.7–03.3	Wray 16-20	08:23:40.7	-43:12:47	6.1	-11.39	-11.91±0.05	1.9	3	SNR	6
...	Hen 2-10	08:36:14.9	-26:24:32	0.4	-11.60	-11.66±0.06	2.0	2	BCD galaxy	
...	K 2-15	08:48:38.7	-42:53:46	0.4	-10.34	-10.41±0.04	2.8	3	H II	
274.1+02.5	Hen 2-34	09:41:14.0	-49:22:47	0.2	-11.97	-11.99±0.07	1.9	5	SyS	
...	Hen 2-38	09:54:43.3	-57:18:52	0.0	-10.19	-10.19±0.04	2.3	3	SyS	
...	AFGL 4106	10:23:19.5	-59:32:05	...	-10.91	...	1.8	3	post-RSG	
...	PHR J1025-5805	10:25:35.0	-58:05:23	0.5	-10.50	-10.58±0.08	3.3	2	H II	
...	Hewett 1	10:37:00.0	00:18:00	0.6	-10.00	-10.08±0.10	40.0	1	H II	
288.9–00.8	Hf 39	10:53:59.6	-60:26:44	1.4	-10.55	-10.74±0.04	2.0	5	WR neb	
...	Hen 2-58	10:56:11.6	-60:27:13	0.9	-9.31	-9.43±0.03	2.6	4	LBV neb	
...	Hen 2-61	11:06:30.0	-54:48:29	0.0	-11.63	-11.63±0.05	1.8	4	B[e]?	1
...	Wray 15-751	11:08:40.1	-60:42:52	1.5	-11.03	-11.23±0.08	1.8	3	LBV neb	4
...	MeWe 2-3	11:56:43.5	-34:25:42	...	-11.66	...	2.0	4	galaxy	
298.1–00.7	Hen 2-77	12:09:01.3	-63:15:60	0.1	-11.33	-11.35±0.05	3.8	1	H II	
...	RCW 64	12:19:53.5	-62:55:08	0.3	-10.19	-10.24±0.04	2.9	3	H II	6
...	Gum 43	12:34:54.4	-61:39:00	0.3	-10.19	-10.24±0.03	2.9	3	H II	
302.3–01.3	DuRe 1	12:45:51.2	-64:09:38	1.1	-11.67	-11.80±0.10	2.0	4	WR neb	
...	Hen 2-91	13:10:04.9	-63:11:30	0.0	-11.29	-11.29±0.06	1.8	2	B[e]pec	
311.1+03.4	Hen 2-101	13:54:55.7	-58:27:16	0.0	-12.3	-12.3±0.2	1.8	4	SyS	4
312.6+05.9	PHR J1400-5536	14:00:56.0	-55:36:58	0.3	-11.21	-11.25±0.09	4.4	3	H II?	1,4
315.4+09.4	Hen 2-104	14:11:52.1	-51:26:24	0.1	-10.77	-10.79±0.04	2.1	2	SyS	
312.0–02.0	Hen 2-106	14:14:09.4	-63:25:46	0.3	-10.49	-10.53±0.04	1.8	3	SyS	
...	ESO 223-9	15:01:07.0	-48:17:30	0.8	-12.29	-12.40±0.14	2.4	1	dwf galaxy	1
326.7+00.6	Wray 16-185	15:44:59.1	-54:02:06	0.9	-11.54	-11.66±0.09	1.8	2	H II	
323.6–03.8	PHR J1547-5929	15:47:26.6	-59:29:46	0.8	-11.15	-11.27±0.07	2.7	5	H II	
328.8–01.1	PHR J1603-5402	16:03:41.4	-54:02:04	0.4	-11.94	-12.00±0.08	1.8	2	H II	
328.9–02.4	Hen 2-146	16:10:41.3	-54:57:33	0.2	-10.80	-10.84±0.04	1.8	2	H II	6
327.9–04.3	Hen 2-147	16:14:01.0	-56:59:28	1.6	-12.4	-12.6±0.3	1.8	3	SyS	4
333.9+00.6	PMR 5	16:19:40.1	-49:14:00	2.5	-12.6	-12.9±0.3	1.8	3	WR neb	4
...	PCG 11	16:33:48.7	-49:28:44	0.8	-12.1	-12.3±0.2	1.8	1	WR neb	
...	NGC 6164/5	16:33:52.4	-48:06:41	1.2	-9.29	-9.45±0.03	4.9	4	ejecta	
346.0+08.5	Hen 2-171	16:34:04.2	-35:05:27	0.2	-11.47	-11.49±0.05	1.8	4	SyS?	1
...	vBe 1	16:45:18.0	-46:09:11	0.8	-9.90	-10.02±0.08	5.2	2	H II	
...	Hen 2-183	16:53:24.0	-44:52:48	0.0	-11.51	-11.51±0.06	1.8	4	B[e]	
...	Fr 2-11	16:57:48.0	-63:12:00	0.8	-10.87	-10.99±0.06	5.4	2	CV neb	6
...	H 2-3	17:09:34.0	-41:36:12	0.3	-10.28	-10.32±0.04	2.9	2	H II	
...	H 2-6	17:18:23.9	-39:19:10	0.3	-9.94	-9.98±0.03	2.9	4	H II	
...	Hen 3-1383	17:20:35.1	-33:10:06	...	-11.32	...	3.3	3	cLBV	
004.5+06.8	H 2-12	17:30:36.0	-21:28:56	2.4	-11.57	-11.85±0.05	1.8	3	SNR	
...	Wray 17-96	17:41:35.4	-30:06:38	0.0	-12.3	-12.3±0.2	2.1	4	LBV	
358.8+00.0	Terz N 124	17:42:42.5	-29:51:35	0.1	-12.20	-12.21±0.13	1.8	4	H II	
...	Sh 2-20	17:47:08.0	-28:46:30	0.3	-10.25	-10.30±0.04	2.9	2	H II	6
...	HD 316285	17:48:14.0	-28:00:52	0.0	-9.40	-9.40±0.05	7.7	2	LBV	
008.3+03.7	Th 4-4	17:50:23.8	-19:53:43	0.0	-11.68	-11.68±0.07	1.8	3	SyS	C
...	M 3-18	17:57:16.0	-21:41:29	0.0	-11.19	-11.19±0.05	1.9	3	SyS	
002.0–02.0	H 1-45	17:58:21.9	-28:14:52	0.0	-11.9	-11.9±0.2	1.8	2	SyS?	1
...	H 1-49	18:03:23.9	-32:42:22	...	-11.20	...	1.8	3	SyS	
003.7–02.7	KFL 6	18:04:41.3	-27:09:12	0.0	-10.99	-11.00±0.06	1.8	3	SyS?	1
003.6–04.0	IRAS 18067-2746	18:09:51.8	-27:45:54	0.0	-11.94	-11.94±0.08	1.8	2	ELS	1,4
...	Ap 1-10	18:10:43.7	-27:57:49	...	-11.17	...	1.8	3	SyS	

Table B1 – Continued

PNG	Name	RAJ2000	DEJ2000	$R_{[N\text{II}]}$	$\log F_{\text{red}}$	$\log F(\text{H}\alpha)$	r_{aper}	N_f	Type	Note
...	CnMy 17	18:15:24.7	-30:31:55	0.0	-10.90	-10.90±0.05	2.6	4	SyS	
...	Hen 2-374	18:15:31.1	-21:35:23	...	-11.73	...	1.8	3	ELS	1
...	Hen 2-376	18:15:46.3	-27:53:46	0.0	-11.68	-11.68±0.05	1.8	3	ELS	1
...	RAFGL 2139	18:23:18.0	-13:42:49	...	-11.48	...	1.8	4	post-RSG	
...	RY Sct	18:25:31.3	-12:41:26	...	-10.60	...	2.6	3	B[e] neb	
...	Sh 2-61	18:33:21.2	-04:58:02	0.3	-10.63	-10.67±0.04	2.9	3	H II	
...	Vy 1-3	18:41:00.9	-04:26:14	0.0	-11.75	-11.75±0.10	1.8	4	WR	
...	NaSt 1	18:52:17.4	00:59:44	0.3	-11.62	-11.66±0.04	1.8	3	WR	6
035.1-00.7	Ap 2-1	18:58:10.5	01:36:57	0.7	-11.19	-11.29±0.06	2.6	2	H II	5,6
...	ALS 1	19:16:16.1	-08:17:46	0.0	-11.49	-11.49±0.07	1.8	2	SyS	6
...	GK Per	03:31:12.0	43:54:15	-11.65±0.10	5.0	1	Nova shell	1,C
...	Sh 2-266	06:18:45.5	15:16:52	-10.19±0.05	3.9	1	H II	
035.1-00.7	Ap 2-1	18:58:10.5	01:36:57	-11.25±0.10	3.2	1	H II	
050.1+03.3	M 1-67	19:11:30.9	16:51:38	-10.45±0.08	4.8	1	WR neb	
...	HM Sge	19:41:57.1	16:44:40	-10.17±0.08	4.8	1	symb. nova	
...	EGB 10	20:04:24.0	71:48:00	-11.3±0.2	3.7	1	galaxy	4
...	Fr 2-14	20:25:40.0	76:40:00	-9.86±0.10	45.0	1	H II	
111.0+11.6	DeHt 5	22:19:33.7	70:56:03	-10.54±0.07	7.2	2	H II	8

Notes to Table B1 follow the format of Table 1 and Table 4; (C) specific comment given here: Wray 16-20 — part of the Vela SNR; H 2-12 — part of Kepler’s SNR; Th 4-4 — flux is variable; GK Per — flux includes part of outer bipolar nebula.

Supplementary Online Tables:

Table B2: (**Table 1**): H α fluxes for 1120 true and possible PNe measured from SHASSA

PNG	Name	RAJ2000	DEJ2000	$R_{[\text{N II}]}$	$\log F_{\text{red}}$	$\log F(\text{H}\alpha)$	r_{aper}	N_{f}	c_{β}	Note
108.4–76.1	BoBn 1	00:37:16.0	–13:42:58	0.2	–12.03	–12.05 \pm 0.06	1.8	3	0.00	C
118.8–74.7	NGC 246	00:47:03.4	–11:52:19	0.0	–10.07	–10.07 \pm 0.03	6.1	2	0.02	
255.3–59.6	Lo 1	02:56:58.4	–44:10:18	1.1	–10.99	–11.14 \pm 0.06	4.5	4	...	
220.3–53.9	NGC 1360	03:33:14.6	–25:52:18	0.0	–9.78	–9.78 \pm 0.03	9.4	2	0.00	6
206.4–40.5	NGC 1535	04:14:15.8	–12:44:22	0.0	–9.95	–9.95 \pm 0.03	5.0	1	0.04	
...	Fr 2-3	04:56:20.0	–28:07:48	1.6	–10.89	–11.09 \pm 0.12	9.5	1	...	1
243.8–37.1	PRTM 1	05:03:01.7	–39:45:44	0.0	–12.02	–12.02 \pm 0.07	1.8	3	...	
215.5–30.8	Abell 7	05:03:07.5	–15:36:23	0.8	–10.30	–10.41 \pm 0.06	11.0	1	...	
205.8–26.7	MaC 2-1	05:03:41.9	–06:10:03	0.0	–11.77	–11.77 \pm 0.05	1.8	3	...	
190.3–17.7	J 320	05:05:34.3	10:42:23	0.0	–10.91	–10.92 \pm 0.04	1.8	3	0.04	
215.2–24.2	IC 418	05:27:28.2	–12:41:50	0.8	–8.92	–9.02 \pm 0.04	5.1	1	0.32	6
197.2–14.2	Abell 10	05:31:45.5	06:56:02	0.8	–11.41	–11.52 \pm 0.05	1.8	2	0.48	
193.6–09.5	H 3-75	05:40:45.0	12:21:23	0.3	–11.38	–11.43 \pm 0.04	1.8	2	1.13	
196.6–10.9	NGC 2022	05:42:06.2	09:05:11	0.0	–10.61	–10.61 \pm 0.04	2.2	2	0.20	
...	Te 11	05:45:58.2	02:21:06	0.8	–11.65	–11.76 \pm 0.08	1.8	3	...	1,C
228.2–22.1	DeHt 1	05:55:06.7	–22:54:02	0.0	–11.87	–11.87 \pm 0.10	2.5	2	...	
286.8–29.5	K 1-27	05:57:02.1	–75:40:23	0.0	–12.08	–12.08 \pm 0.12	3.8	1	...	
193.0–04.5	KLSS 1-5	05:57:08.0	15:25:31	...	–11.92	...	1.8	1	...	
197.4–06.4	WDHS 1	05:59:24.8	10:41:41	4.0	–10.07	–10.47 \pm 0.10	11.5	1	...	
198.6–06.3	Abell 12	06:02:20.0	09:39:14	1.1	> –11.8	> –12.0 \pm 0.2	1.8	1	...	5,C
204.0–08.5	Abell 13	06:04:47.9	03:56:36	3.5	–11.04	–11.40 \pm 0.06	2.7	3	...	
197.8–03.3	Abell 14	06:11:08.7	11:46:43	6.2	–11.97	–12.45 \pm 0.09	1.8	1	...	9
201.9–04.6	We 1-4	06:14:33.7	07:34:30	5.0	–11.93	–12.39 \pm 0.07	1.8	2	...	
209.1–08.2	PHR J0615-0025	06:15:20.4	00:25:49	0.0	–11.9	–11.9 \pm 0.2	3.0	1	...	
221.3–12.3	IC 2165	06:21:42.8	–12:59:14	0.2	–10.18	–10.21 \pm 0.03	4.6	1	0.74	
218.9–10.7	HDW 5	06:23:37.1	–10:13:24	0.8	–11.18	–11.29 \pm 0.06	2.2	4	...	1,V
204.8–03.5	K 3-72	06:23:54.9	05:30:13	6.7	–11.56	–12.10 \pm 0.06	1.8	3	...	
233.5–16.3	Abell 15	06:27:01.9	–25:22:50	0.1	–11.89	–11.90 \pm 0.06	1.8	2	0.35	
211.2–03.5	M 1-6	06:35:45.1	00:05:37	0.6	–11.20	–11.29 \pm 0.04	1.8	3	1.63	V
216.9–05.2	MPA J0639-0554	06:39:58.1	–05:54:57	...	–12.08	...	1.8	3	...	
216.3–04.4	We 1-5	06:41:34.6	–05:02:35	0.0	–12.17	–12.17 \pm 0.10	1.8	4	...	
229.0–08.7	MPA J0649-1816	06:49:02.7	–18:16:38	...	–12.39	...	1.8	3	...	
212.6–00.0	PHR J0650+0013	06:50:40.5	00:13:40	2.6	–11.67	–11.96 \pm 0.06	2.0	3	...	
...	PHR J0652-0951	06:52:19.4	–09:51:36	0.9	–12.40	–12.52 \pm 0.13	1.9	3	...	1,4
224.3–05.5	PHR J0652-1240	06:52:20.3	–12:40:34	0.9	–11.51	–11.64 \pm 0.08	2.9	2	...	1
204.1+04.7	K 2-2	06:52:23.2	09:57:56	0.3	–10.30	–10.35 \pm 0.08	6.0	2	...	1,6,8,C
210.3+01.9	M 1-8	06:53:33.8	03:08:27	1.8	–11.34	–11.57 \pm 0.04	1.8	1	1.07	
222.8–04.2	PM 1-23	06:54:13.4	–10:45:38	0.1	–12.18	–12.19 \pm 0.10	1.8	3	...	4,5,6,10
236.0–10.6	HaWe 9	06:54:20.8	–25:24:34	0.0	–11.58	–11.58 \pm 0.08	2.6	3	...	
...	Fr 2-24	06:54:28.5	–44:58:33	...	–10.32	...	11.4	4	...	1,4,6,N
216.0–00.2	Abell 18	06:56:14.7	–02:53:08	2.5	–11.72	–12.00 \pm 0.09	2.0	2	...	
291.3–26.2	Vo 1	06:59:26.4	–79:38:47	0.5	–11.95	–12.02 \pm 0.06	1.8	5	1.43	10,V
200.7+08.4	Abell 19	06:59:56.4	14:36:34	1.7	–11.84	–12.05 \pm 0.08	1.9	2	...	4
224.3–03.4	PHR J0700-1144	07:00:05.8	–11:43:51	2.0	–12.2	–12.5 \pm 0.2	1.8	2	...	
210.0+03.9	We 2-34	07:00:28.4	04:20:30	4.0	–11.74	–12.14 \pm 0.10	3.3	3	...	6
221.0–01.4	PHR J0701-0749	07:01:09.3	–07:49:21	2.0	–11.95	–12.19 \pm 0.08	1.9	3	...	6
226.4–03.7	PB 1	07:02:46.8	–13:42:35	0.0	–11.68	–11.68 \pm 0.07	1.8	4	0.0:	5,6
242.6–11.6	M 3-1	07:02:50.0	–31:35:32	0.3	–10.75	–10.80 \pm 0.04	1.8	2	0.18	5,6
212.0+04.3	M 1-9	07:05:19.2	02:46:59	0.3	–11.04	–11.09 \pm 0.04	1.8	1	0.37	
237.3–08.4	BMP J0705-2528	07:05:45.5	–25:28:50	...	–12.14	...	2.4	4	...	4
222.9–01.1	PHR J0705-0924	07:05:51.4	–09:24:11	5.3	–11.84	–12.31 \pm 0.13	2.1	4	...	
...	Sa 2-4	07:06:44.9	–11:45:21	...	–11.56	...	1.8	3	...	1
217.4+02.0	St 3-1	07:06:50.9	–03:05:10	1.0	–11.47	–11.60 \pm 0.04	1.8	3	...	
...	K 1-9	07:07:15.6	–05:10:07	6.1	–11.78	–12.42 \pm 0.13	2.0	1	...	
215.6+03.6	NGC 2346	07:09:22.6	00:48:23	2.0	–10.39	–10.60 \pm 0.08	4.0	1	0.61	9
232.8–04.7	M 1-11	07:11:16.7	–19:51:03	0.9	–10.68	–10.80 \pm 0.04	1.8	3	1.63	6,V
237.9–07.2	FP J0711-2531	07:11:31.9	–25:31:24	0.9	–10.56	–10.69 \pm 0.04	6.2	1	...	1,6
226.4–01.3	PHR J0711-1238	07:11:43.3	–12:38:03	0.6	–12.4	–12.5 \pm 0.2	1.9	2	...	

Table B2 – Continued

PNG	Name	RAJ2000	DEJ2000	$R_{[N\ II]}$	$\log F_{\text{red}}$	$\log F(\text{H}\alpha)$	r_{aper}	N_f	c_β	Note
...	Fr 2-4	07:11:52.0	-82:03:03	...	-10.00	...	23.0	4	...	1,4,6
229.6-02.7	K 1-10	07:12:35.5	-16:05:60	7.1	-11.87	-12.44±0.06	1.8	3	...	
219.1+03.0	MPA J0713-0405	07:13:47.9	-04:05:08	...	-12.13	...	2.0	3	...	4
258.0-15.7	Lo 3	07:14:49.4	-46:57:40	0.3	-11.19	-11.23±0.06	2.1	2	...	
240.3-07.6	M 3-2	07:14:49.8	-27:50:23	4.3	-11.67	-12.08±0.07	1.8	2	0.22	
240.6-07.7	BMP J0715-2805	07:15:02.3	-28:05:44	0.1	-12.07	-12.09±0.14	1.8	2	...	
224.9+01.0	We 1-6	07:17:26.0	-10:10:38	0.0	-11.64	-11.64±0.07	1.9	3	...	
235.3-03.9	M 1-12	07:19:21.5	-21:43:55	0.7	-10.86	-10.96±0.05	1.8	3	0.72	V
...	WHI B0717-07	07:19:40.3	-07:13:11	...	-11.93	...	2.1	3	...	1,4
227.1+00.5	PHR J0719-1222	07:19:46.7	-12:22:47	2.7	-11.68	-11.99±0.10	3.0	2	...	6
232.4-01.8	M 1-13	07:21:15.0	-18:08:37	2.1	-10.90	-11.15±0.04	1.8	4	0.76	
215.0+07.4	FP J0721+0133	07:21:41.0	01:33:32	1.0	-11.11	-11.18±0.08	7.5	1	...	1
222.1+03.9	PFP 1	07:22:17.7	-06:21:46	1.5	-10.5	-10.7±0.2	11.5	1	...	
214.9+07.8	Abell 20	07:22:57.7	01:45:33	0.0	-11.64	-11.65±0.05	2.0	2	0.00	
216.0+07.4	PHR J0723+0036	07:23:48.1	00:36:48	0.0	-12.27	-12.27±0.14	2.1	5	...	4,10
232.6-01.0	PHR J0724-1757	07:24:43.4	-17:57:51	8.0	-12.3	-12.9±0.2	2.8	4	...	4
230.0+00.5	PHR J0725-1457	07:25:23.6	-14:57:10	1.4	-12.05	-12.23±0.10	2.2	5	...	4
221.7+05.3	M 3-3	07:26:34.2	-05:21:52	4.4	-11.29	-11.72±0.04	1.8	4	0.43	
232.1-00.1	PHR J0727-1707	07:27:08.3	-17:07:14	1.9	-12.6	-12.8±0.2	1.8	2	...	4
234.9-01.4	M 1-14	07:27:56.5	-20:13:23	0.4	-11.03	-11.09±0.04	2.1	1	0.13	5
248.8-08.5	M 4-2	07:28:53.8	-35:45:14	0.1	-11.34	-11.35±0.05	1.8	3	...	
205.1+14.2	Abell 21	07:29:02.7	13:14:49	2.2	-9.64	-9.91±0.03	9.2	1	...	8
245.1-05.5	BMP J0733-3108	07:33:24.1	-31:08:05	6.0	-10.91	-11.42±0.08	7.2	2	...	
238.4-01.8	KLSS 1-8	07:33:25.0	-23:26:09	13.9	-11.19	-12.0±0.2	3.2	1	...	6, C
236.8-00.4	PHR J0735-2122	07:35:23.3	-21:22:42	0.7	-12.3	-12.4±0.2	1.9	2	...	
215.6+11.1	Abell 22	07:36:07.9	02:42:28	1.8	-11.29	-11.51±0.09	3.8	1	...	
222.5+07.6	BMP J0736-0500	07:36:23.1	-05:00:20	...	-12.47	...	2.1	3	...	
226.7+05.6	M 1-16	07:37:19.0	-09:38:50	3.4	-10.93	-11.29±0.04	1.8	3	0.61	
242.3-02.4	FP J0739-2709	07:39:35.9	-27:09:54	3.0	-11.00	-11.33±0.06	5.1	3	...	
228.8+05.3	M 1-17	07:40:22.2	-11:32:30	1.1	-11.28	-11.42±0.04	1.8	2	0.56	
237.0+00.7	PHR J0740-2055	07:40:22.9	-20:55:54	1.0	-12.19	-12.33±0.12	3.2	1	...	
231.8+04.1	NGC 2438	07:41:50.5	-14:44:08	1.0	-10.25	-10.39±0.04	3.5	3	0.61	
234.8+02.4	NGC 2440	07:41:55.4	-18:12:33	3.7	-9.49	-9.86±0.03	4.4	2	0.56	6
231.4+04.3	M 1-18	07:42:04.2	-14:21:13	2.5	-11.52	-11.81±0.05	1.8	3	...	
247.5-04.7	HFG 2	07:42:23.6	-32:47:45	0.1	-10.95	-10.97±0.07	2.9	3	...	C
249.3-05.4	Abell 23	07:43:18.0	-34:45:16	1.0	-11.72	-11.86±0.09	1.8	4	...	
236.5+02.0	PHR J0743-1951	07:43:53.5	-19:51:49	1.5	-11.23	-11.42±0.07	4.7	4	...	
250.3-05.4	PHR J0745-3535	07:45:41.1	-35:35:04	1.4	-11.90	-12.09±0.10	1.9	4	...	4
238.5+01.7	PHR J0747-2146	07:47:18.8	-21:46:50	0.6	-11.56	-11.64±0.08	2.6	3	...	
264.4-12.7	Hen 2-5	07:47:20.0	-51:15:03	0.2	-10.76	-10.80±0.04	1.8	2	0.18	
243.3-01.0	NGC 2452	07:47:26.3	-27:20:07	0.6	-10.72	-10.80±0.04	1.8	3	0.73	10
232.0+05.7	SaSt 2-3	07:48:03.7	-14:07:40	0.5	-11.62	-11.69±0.05	1.8	1	0.73	
236.7+03.5	K 1-12	07:50:11.6	-19:18:16	1.2	-11.96	-12.12±0.08	1.8	3	...	
217.1+14.7	Abell 24	07:51:37.6	03:00:21	7.4	-10.09	-10.67±0.03	4.4	2	...	
250.5-03.4	PHR J0754-3444	07:54:55.7	-34:44:09	0.4	-11.73	-11.79±0.09	1.9	3	...	1
211.4+18.4	HaWe 10	07:55:11.3	09:33:09	0.0	-12.02	-12.02±0.09	2.2	2	...	
241.0+02.3	M 3-4	07:55:11.4	-23:38:12	0.8	-11.35	-11.46±0.05	1.8	3	...	
249.8-02.7	PHR J0755-3346	07:55:55.5	-33:46:00	0.8	-12.13	-12.24±0.13	2.2	3	...	
235.7+07.1	PHR J0800-1635	08:00:59.1	-16:35:37	1.8	-11.82	-12.04±0.10	2.7	3	...	6
245.4+01.6	M 3-5	08:02:28.9	-27:41:55	1.8	-11.22	-11.44±0.04	1.8	2	0.94	6
250.4-01.3	NeVe 3-3	08:03:12.5	-33:31:02	3.2	-11.72	-12.07±0.06	2.0	3	...	
...	Fr 2-25	08:04:04.4	-06:30:57	...	-11.20	...	7.4	3	...	1,4,N
251.1-01.5	K 1-21	08:04:14.2	-34:16:07	1.5	-11.85	-12.05±0.08	1.8	3	...	
224.3+15.3	Abell 25	08:06:46.5	-02:52:35	1.9	-11.71	-11.95±0.09	2.8	3	...	
254.5-02.7	PHR J0808-3745	08:08:24.2	-37:45:21	0.8	-11.76	-11.87±0.12	3.3	1	...	
238.9+07.3	Sa 2-21	08:08:44.3	-19:14:03	0.9	-11.36	-11.49±0.05	1.8	1	...	6
236.9+08.6	PHR J0809-1650	08:09:01.4	-16:50:03	0.0	-12.39	-12.39±0.13	1.8	3	...	
250.3+00.1	Abell 26	08:09:01.6	-32:40:25	1.4	-12.06	-12.24±0.08	1.8	2	...	
240.3+07.0	Y-C 2-5	08:10:41.6	-20:31:32	0.0	-11.44	-11.44±0.04	1.8	4	...	
264.1-08.1	Hen 2-7	08:11:31.9	-48:43:17	0.3	-10.76	-10.81±0.05	1.8	2	0.39	
251.1+00.7	CSST 2	08:13:21.3	-33:01:05	1.2	-11.98	-12.13±0.09	1.8	2	...	
258.0-03.2	BMP J0815-4053	08:15:56.9	-40:53:08	...	-11.41	...	4.8	3	...	

Table B2 – Continued

PNG	Name	RAJ2000	DEJ2000	$R_{[N\ II]}$	$\log F_{\text{red}}$	$\log F(\text{H}\alpha)$	r_{aper}	N_f	c_β	Note
263.0–05.5	PB 2	08:20:40.2	–46:22:59	0.4	–11.51	–11.58±0.07	1.8	2	...	
253.9+00.7	MeWe 2-1	08:20:52.4	–35:16:33	0.6	–12.02	–12.11±0.12	1.8	4	...	
247.8+04.9	FP J0821-2755	08:21:18.3	–27:55:36	10.0	–11.57	–12.24±0.10	3.8	3	...	1
258.5–01.3	RCW 24	08:25:46.3	–40:13:52	6.2	–10.37	–10.90±0.04	9.8	4	...	6
258.1–00.3	Hen 2-9	08:28:28.0	–39:23:40	0.3	–11.08	–11.13±0.04	1.8	4	1.98	
257.5+00.6	RCW 21	08:30:54.2	–38:18:07	5.6	–11.03	–11.52±0.06	2.8	2	...	
249.0+06.9	SaSt 1-1	08:31:42.9	–27:45:32	0.0	–11.65	–11.65±0.04	1.1	1	...	1
252.6+04.4	Abell 27	08:31:52.6	–32:06:09	4.6	–11.57	–12.01±0.05	1.8	3	...	
239.6+13.9	NGC 2610	08:33:23.3	–16:08:58	0.0	–10.84	–10.84±0.04	1.8	1	0.27	6
265.1–04.2	LoTr 3	08:34:07.1	–47:16:37	1.0	–11.63	–11.76±0.10	1.8	4	...	
249.8+07.1	PHR J0834-2819	08:34:18.1	–28:19:03	1.0	–11.96	–12.10±0.13	2.7	2	...	
255.7+03.3	Wray 16-22	08:36:16.7	–35:15:03	0.8	–11.85	–11.97±0.07	1.8	3	...	
259.1+00.9	Hen 2-11	08:37:08.4	–39:25:08	0.3	–10.92	–10.97±0.06	2.4	5	2.24	
244.5+12.5	Abell 29	08:40:18.9	–20:54:36	6.2	–10.52	–11.04±0.04	4.9	1	...	
274.2–09.7	Fr 2-6	08:40:23.0	–57:54:49	0.9	–10.61	–10.74±0.04	4.3	2	...	1,5,6
258.4+02.3	PHR J0840-3801	08:40:29.9	–38:01:26	0.8	–12.04	–12.15±0.11	1.8	2	...	4
253.9+05.7	M 3-6	08:40:40.2	–32:22:33	0.0	–10.35	–10.36±0.04	2.6	2	0.0	
...	Sa 3-7	08:43:29.3	–48:54:48	...	–11.42	...	1.8	4	...	1
261.6+03.0	Hen 2-15	08:53:30.7	–40:03:42	4.5	–10.79	–11.21±0.04	1.8	3	2.07	
272.4–05.9	MeWe 1-1	08:53:36.9	–54:05:10	1.1	–11.28	–11.42±0.05	2.3	4	...	
219.1+31.2	Abell 31	08:54:13.2	08:53:53	0.7	–10.07	–10.20±0.05	11.5	1	...	
269.7–03.6	PB 3	08:54:18.3	–50:32:22	1.5	–11.17	–11.36±0.05	1.8	5	1.22	
253.5+10.7	K 1-2	08:57:46.0	–28:57:36	0.1	–11.76	–11.78±0.06	1.9	3	...	
270.1–02.9	Wray 17-23	08:59:03.0	–50:23:40	0.2	–12.07	–12.11±0.15	1.8	4	...	10
263.1+04.3	FP J0904-4023	09:04:02.3	–40:22:20	1.0	–10.83	–10.97±0.06	6.9	4	...	1
255.8+10.9	FP J0905-3033	09:05:05.3	–30:33:12	1.0	–10.43	–10.57±0.10	11.9	3	...	5
268.9–00.4	BRAN 229	09:05:41.1	–47:54:05	2.1	–11.45	–11.70±0.09	2.1	2	...	1
285.7–14.9	IC 2448	09:07:06.3	–69:56:31	0.0	–10.40	–10.41±0.04	1.8	2	0.00	6
267.4+01.3	PHR J0907-4532	09:07:33.1	–45:32:53	0.5	–11.51	–11.58±0.09	3.0	3	...	1
273.2–03.7	Hen 2-18	09:08:40.1	–53:19:14	1.3	–11.47	–11.64±0.06	1.8	4	1.37	
264.5+05.0	FP J0911-4051	09:11:45.6	–40:51:58	...	–12.02	...	3.3	4	...	1,4
265.7+04.1	NGC 2792	09:12:26.6	–42:25:40	0.0	–10.66	–10.66±0.04	2.6	2	0.9	
275.3–04.7	Hen 2-21	09:13:52.8	–55:28:17	0.0	–11.32	–11.32±0.06	1.8	3	0.87	
275.0–04.1	PB 4	09:15:07.8	–54:52:44	0.1	–11.02	–11.03±0.04	1.8	2	0.53	
261.9+08.5	NGC 2818	09:16:01.7	–36:37:39	2.5	–10.44	–10.73±0.04	2.3	2	0.32	
268.4+02.4	PB 5	09:16:09.6	–45:28:43	0.3	–11.37	–11.42±0.05	1.8	3	2.03	
275.2–03.7	Hen 2-25	09:18:01.3	–54:39:29	0.1	–11.26	–11.27±0.05	1.8	3	2.67	1,C
278.6–06.7	Hen 2-26	09:19:27.5	–59:12:00	0.2	–10.88	–10.91±0.04	1.8	3	0.38	
278.1–05.9	NGC 2867	09:21:25.3	–58:18:41	0.3	–9.92	–9.97±0.03	4.6	2	0.48	6,10
275.2–02.9	Hen 2-28	09:22:06.8	–54:09:39	1.0	–11.58	–11.71±0.06	1.8	2	1.16	5,6
276.1–03.3	PHR J0924-5506	09:24:15.1	–55:06:25	1.7	–12.05	–12.26±0.15	2.0	3	...	4
275.8–02.9	Hen 2-29	09:24:45.8	–54:36:15	1.1	–11.25	–11.40±0.04	1.8	5	1	6
277.1–03.8	NGC 2899	09:27:03.1	–56:06:21	3.8	–10.16	–10.55±0.03	2.9	2	1.08	
275.5–01.3	Pe 2-4	09:30:48.4	–53:09:59	0.3	–11.64	–11.69±0.06	1.8	3	...	
278.5–04.5	Hen 2-32	09:30:54.9	–57:36:52	6.2	–11.55	–12.07±0.08	2.6	2	...	
277.7–03.5	Wray 17-31	09:31:20.5	–56:17:39	2.9	–10.89	–11.20±0.04	2.3	2	...	
275.9–01.0	NeVe 3-1	09:34:01.4	–53:11:58	2.1	–12.07	–12.32±0.10	1.8	1	...	4
275.3–00.4	PHR J0934-5223	09:34:17.2	–52:23:20	1.0	–11.75	–11.89±0.08	1.9	3	...	
277.1–01.5	Wray 16-55	09:37:51.9	–54:27:09	0.3	–12.02	–12.07±0.08	1.8	1	...	4
281.0–05.6	IC 2501	09:38:47.2	–60:05:31	0.3	–9.96	–10.01±0.03	3.8	2	0.59	
238.0+34.8	Abell 33	09:39:09.1	–02:48:31	0.2	> –11.2	> –11.2±0.1	2.0	1	...	5,C
279.1–03.1	VBRC 3	09:40:52.5	–56:57:60	3.4	–11.60	–11.96±0.08	1.9	3	...	
274.6+02.1	Hen 2-35	09:41:37.5	–49:57:59	0.0	–11.43	–11.43±0.05	1.8	5	0.64	
277.2–00.8	PHR J0941-5356	09:41:47.0	–53:56:27	0.5	–10.88	–10.95±0.07	6.4	3	...	1
276.2+00.4	PHR J0942-5220	09:42:01.2	–52:20:42	0.6	–11.50	–11.58±0.09	2.8	2	...	
279.6–03.1	Hen 2-36	09:43:25.5	–57:16:55	0.3	–10.88	–10.85±0.06	1.8	2	1.34	9
248.7+29.5	Abell 34	09:45:35.3	–13:10:16	0.6	–11.32	–11.41±0.07	6.2	2	1.34	6
274.6+03.5	Hen 2-37	09:47:25.0	–48:58:12	1.5	–11.34	–11.53±0.04	1.8	1	...	6
273.6+06.1	HbDr 1	09:52:44.5	–46:16:47	0.0	–11.55	–11.55±0.10	2.5	1	...	
221.6+46.4	EGB 6	09:52:59.0	13:44:34	0.4	–10.97	–11.03±0.06	7.4	1	...	
279.1–00.4	IRAS 09517-5438	09:53:27.1	–54:52:40	0.6	–12.13	–12.22±0.12	1.8	4	...	
276.5+03.1	MPA J0954-5026	09:54:37.5	–50:26:57	...	–12.02	...	1.8	4	...	

Table B2 – Continued

PNG	Name	RAJ2000	DEJ2000	$R_{[N\ II]}$	$\log F_{\text{red}}$	$\log F(\text{H}\alpha)$	r_{aper}	N_f	c_β	Note
277.1+03.3	MeWe 2-2	09:58:10.2	-50:39:35	0.7	-12.3	-12.4±0.2	1.8	4	...	4
283.8-04.2	Hen 2-39	10:03:49.2	-60:43:48	0.7	-11.48	-11.58±0.07	1.6	5	...	
274.3+09.1	Lo 4	10:05:45.8	-44:21:33	0.2	-12.01	-12.03±0.11	1.8	4	...	10,C
286.2-06.9	Wray 17-40	10:06:59.6	-64:21:50	0.7	-11.19	-11.29±0.05	1.9	4	...	
272.1+12.3	NGC 3132	10:07:01.8	-40:26:11	3.1	-9.59	-9.84±0.06	5.2	2	0.23	6,9
286.0-06.5	Hen 2-41	10:07:23.6	-63:54:30	0.2	-11.21	-11.24±0.04	1.8	4	0.32	
279.2+03.1	MPA J1008-5202	10:08:30.4	-52:02:16	...	-12.10	...	1.8	3	...	
285.4-05.3	IC 2553	10:09:20.9	-62:36:48	0.2	-10.22	-10.25±0.04	1.8	2	0.35	
296.6-20.0	NGC 3195	10:09:20.9	-80:51:31	1.3	-10.28	-10.45±0.04	3.4	2	0.48	6
280.5+01.8	KLSS 1-12	10:10:34.4	-53:56:07	...	-11.84	...	1.8	3	...	
280.0+02.9	Sa 2-56	10:11:57.7	-52:38:17	0.0	-11.85	-11.85±0.07	1.8	2	...	4
278.8+04.9	PB 6	10:13:16.0	-50:19:59	1.1	-11.11	-11.26±0.04	1.8	3	0.5	10
283.4-01.3	MeWe 1-2	10:14:25.1	-58:11:48	1.8	-11.13	-11.35±0.12	3.6	3	...	
283.9-01.8	Hf 4	10:15:33.9	-58:51:11	3.7	-11.57	-11.94±0.09	1.8	4	...	
286.3-04.8	NGC 3211	10:17:50.6	-62:40:15	0.1	-10.53	-10.54±0.04	1.8	3	0.2	
285.5-03.3	PHR J1019-6059	10:19:27.6	-60:59:10	0.3	-11.89	-11.93±0.13	1.9	2	...	
285.1-02.7	Hen 3-401	10:19:32.5	-60:13:29	0.1	-10.97	-10.98±0.06	1.8	4	...	3
...	Roberts 22	10:21:33.8	-58:05:48	0.0	-11.54	-11.54±0.11	1.8	2	...	3
285.6-02.7	My 59	10:23:09.1	-60:32:42	1.2	-10.19	-10.35±0.04	1.8	3	0.84	V
261.0+32.0	NGC 3242	10:24:46.1	-18:38:32	0.0	-9.31	-9.31±0.03	4.2	1	0.07	6
286.3-03.1	PHR J1025-6115	10:25:46.3	-61:15:23	2.5	-11.76	-12.05±0.13	1.9	3	...	
286.1-02.0	MPA J1029-6014	10:29:07.7	-60:14:04	...	-11.16	...	2.1	3	...	
282.9+03.8	Hen 2-48	10:31:32.0	-53:33:31	0.8	-11.50	-11.62±0.05	1.8	4	...	
283.8+02.2	My 60	10:31:33.4	-55:20:51	0.1	-11.02	-11.03±0.04	1.8	4	0.92	
287.9-04.4	PHR J1032-6310	10:32:14.4	-63:10:22	1.5	-11.20	-11.40±0.07	2.9	2	...	
283.3+03.9	Hen 2-50	10:34:19.0	-53:41:04	1.4	-11.18	-11.36±0.04	1.8	4	...	
270.1+24.8	K 1-28	10:34:30.6	-29:11:15	0.0	-12.26	-12.26±0.10	1.8	4	...	
288.8-05.2	Hen 2-51	10:35:45.8	-64:19:12	1.2	-11.37	-11.52±0.05	1.8	1	1.26	
285.4+01.5	Pe 1-1	10:38:27.6	-56:47:06	0.5	-11.20	-11.27±0.09	1.8	2	...	10
285.4+01.2	Pe 1-2	10:39:32.7	-57:06:14	0.1	-11.27	-11.28±0.07	1.8	2	2.9	
284.5+03.8	PHR J1040-5417	10:40:46.8	-54:17:59	1.3	-11.38	-11.56±0.09	2.8	4	...	
288.4-02.4	Pe 1-3	10:44:31.1	-61:39:38	1.8	-11.47	-11.69±0.10	1.8	3	...	
286.3+02.8	Hen 2-55	10:48:43.2	-56:03:10	0.1	-11.58	-11.58±0.06	1.8	5	...	10
284.4+07.8	PHR J1052-5042	10:52:26.7	-50:42:01	0.5	-11.60	-11.68±0.05	1.6	3	...	1
293.2-09.5	Fr 2-7	10:54:27.3	-70:13:12	...	-10.82	...	5.7	4	...	1,6
288.4+00.3	Hf 38	10:54:34.9	-59:09:49	2.5	-10.81	-11.10±0.06	1.8	5	...	
283.9+09.7	DS 1	10:54:40.6	-48:47:03	0.0	-10.50	-10.50±0.04	6.4	2	...	6
291.6-04.8	IC 2621	11:00:20.1	-65:14:58	0.7	-10.49	-10.59±0.04	1.8	4	0.77	
290.1-00.4	Hf 48	11:03:56.0	-60:36:05	8.0	-11.33	-11.93±0.13	1.8	4	...	
289.0+03.3	PHR J1107-5642	11:07:42.9	-56:42:28	...	-11.19	...	3.0	2	...	
286.5+11.6	Lo 5	11:13:54.1	-47:57:01	1.0	-10.89	-11.03±0.05	3.2	3	...	
295.3-09.3	Hen 2-62	11:17:43.2	-70:49:32	0.2	-11.33	-11.37±0.04	1.8	3	0.18	
288.7+08.1	ESO 216-2	11:18:09.7	-52:10:02	0.0	-12.33	-12.33±0.12	1.8	2	...	
292.2-00.9	PHR J1118-6150	11:18:32.0	-61:50:57	0.0	-11.3	-11.5±0.2	5.1	1	...	
291.3+03.7	PHR J1124-5711	11:24:50.9	-57:11:10	2.0	-11.80	-12.04±0.14	2.1	2	...	4
292.5+00.9	NeVe 3-6	11:25:42.2	-60:14:35	1.2	-11.84	-12.00±0.12	1.8	4	...	
283.6+25.3	K 1-22	11:26:43.8	-34:22:11	0.3	-10.76	-10.81±0.05	2.9	4	...	
291.7+03.7	Hen 2-64	11:27:24.3	-57:17:59	0.8	-11.53	-11.64±0.07	1.8	2	...	V
292.6+01.2	NGC 3699	11:27:57.7	-59:57:28	2.9	-10.42	-10.74±0.04	1.8	4	0.04	
290.5+07.9	Fg 1	11:28:36.2	-52:56:04	0.1	-10.47	-10.49±0.04	1.8	2	0.36	
292.8+01.1	Hen 2-67	11:28:47.4	-60:06:37	0.9	-10.94	-11.06±0.04	1.8	4	1.45	5
292.9+01.0	PHR J1129-6012	11:29:50.4	-60:12:08	2.5	-12.1	-12.4±0.2	1.8	4	...	4,5,6
292.7+01.9	Wray 16-93	11:30:48.3	-59:17:05	0.0	-12.2	-12.2±0.2	1.8	3	...	4
294.9-04.3	Hen 2-68	11:31:45.4	-65:58:14	0.8	-10.98	-11.09±0.04	1.8	4	...	
292.4+04.1	PB 8	11:33:17.7	-57:06:14	0.3	-10.77	-10.82±0.04	1.8	2	0.43	10
291.3+08.4	PHR J1134-5243	11:34:38.6	-52:43:33	1.0	-12.19	-12.33±0.12	1.8	3	...	10
293.6+01.2	Hen 2-70	11:35:11.0	-60:16:60	2.7	-11.09	-11.40±0.05	1.8	3	...	
291.4+08.5	PHR J1136-5235	11:35:60.0	-52:35:33	0.4	-11.41	-11.47±0.08	3.1	3	...	
295.4-04.0	PHR J1137-6548	11:37:05.1	-65:48:11	0.5	-10.74	-10.81±0.05	4.1	2	...	1
296.4-06.9	Hen 2-71	11:39:11.2	-68:52:09	0.4	-10.99	-11.05±0.04	1.8	3	0.39	6,V
294.2+01.3	PHR J1140-6022	11:40:36.8	-60:22:10	2.7	-12.3	-12.6±0.2	1.8	2	...	4
294.9-00.6	Hf 69	11:41:37.4	-62:28:54	2.1	-10.91	-11.15±0.05	2.0	2	...	

Table B2 – Continued

PNG	Name	RAJ2000	DEJ2000	$R_{[N\,II]}$	$\log F_{\text{red}}$	$\log F(\text{H}\alpha)$	r_{aper}	N_f	c_β	Note
296.3–03.0	Hen 2-73	11:48:38.2	–65:08:37	0.4	–11.07	–11.14±0.04	1.8	3	1.1	
294.6+04.7	NGC 3918	11:50:17.7	–57:10:57	0.5	–9.45	–9.52±0.03	6.9	1	0.2	6
297.0–04.9	PHR J1150-6704	11:50:27.6	–67:04:57	1.2	–12.04	–12.20±0.11	1.9	2	...	4
291.4+19.2	LoTr 4	11:52:29.2	–42:17:39	0.0	–12.12	–12.12±0.09	1.8	3	...	
293.6+10.9	BIDz 1	11:53:06.6	–50:50:59	0.8	–10.92	–11.04±0.04	2.1	1	...	
296.3+03.1	KFR 1	12:00:16.3	–59:04:44	4.0	–11.31	–11.71±0.08	3.0	2	...	
296.5+02.7	NeVe 3-7	12:00:35.9	–59:29:49	2.1	–12.2	–12.5±0.2	1.3	5	...	
294.1+14.4	Lo 6	12:00:43.5	–47:33:12	1.5	–11.52	–11.72±0.05	2.0	2	...	
298.7–07.5	PHR J1202-7000	12:02:55.5	–70:00:57	8.0	–11.20	–11.80±0.10	4.0	3	...	
298.3–04.8	NGC 4071	12:04:14.8	–67:18:36	1.4	–10.77	–10.95±0.04	2.0	2	0.8	
299.1–08.4	MPA J1205-7101	12:05:40.0	–71:01:57	...	–12.46	...	1.8	4	...	
298.2–01.7	Hen 2-76	12:08:25.4	–64:12:09	2.5	–11.53	–11.82±0.05	1.8	4	...	
297.4+03.7	Hen 2-78	12:09:10.2	–58:42:37	0.9	–12.15	–12.28±0.14	1.8	2	...	5,V
299.4–04.1	HaTr 1	12:16:33.1	–66:45:45	0.6	–11.47	–11.55±0.05	2.0	2	...	
299.3–02.0	PHR J1217-6443	12:17:53.1	–64:43:27	0.4	–11.86	–11.92±0.11	1.8	3	...	1
298.3+06.6	Po 1	12:18:32.7	–55:54:04	0.2	–12.26	–12.29±0.13	1.8	2	...	
299.8–01.3	Hen 2-81	12:23:01.2	–64:01:46	2.7	–11.76	–12.07±0.09	1.8	5	...	
299.5+02.4	Hen 2-82	12:23:53.6	–60:13:14	1.1	–11.46	–11.60±0.05	1.8	4	...	
294.1+43.6	NGC 4361	12:24:30.8	–18:47:06	0.0	–10.09	–10.09±0.03	5.1	2	0.00	
300.2+00.6	Hen 2-83	12:28:44.0	–62:05:35	1.5	–11.57	–11.77±0.09	1.8	1	...	V
300.4–00.9	Hen 2-84	12:28:46.8	–63:44:37	1.9	–11.53	–11.77±0.06	1.8	5	...	
300.5–01.1	Hen 2-85	12:30:07.6	–63:53:00	0.3	–11.45	–11.50±0.07	1.8	5	1.86	
300.8–03.4	ESO 095-12	12:30:24.7	–66:14:23	0.4	–12.11	–12.17±0.11	1.8	2	...	
300.7–02.0	Hen 2-86	12:30:30.4	–64:52:06	0.5	–11.07	–11.14±0.04	1.8	4	2.06	10
299.0+18.4	K 1-23	12:30:52.5	–44:14:16	0.6	–11.14	–11.22±0.06	2.5	2	...	
298.0+34.8	CTIO 1230-275	12:33:13.0	–27:48:54	0.0	–12.8	–12.8±0.2	1.8	3	...	1,4
301.9–02.1	MPA J1242-6459	12:42:24.2	–64:59:25	...	–12.05	...	1.8	3	...	
302.1+00.3	RCW 69	12:44:28.5	–62:31:19	6.9	–10.40	–10.96±0.04	3.9	1	...	
302.2+02.5	Wray 16-120	12:45:54.9	–60:20:17	0.1	–12.01	–12.03±0.14	1.8	5	...	
302.3–00.5	PHR J1246-6324	12:46:26.5	–63:24:28	0.7	–12.07	–12.17±0.09	1.8	4	...	1
302.6–00.9	VBRC 4	12:48:30.6	–63:50:02	5.3	–10.97	–11.45±0.04	1.8	4	...	
302.7–00.9	PHR J1250-6346	12:50:04.4	–63:46:52	1.7	–11.77	–11.98±0.09	2.1	4	...	
303.6+40.0	Abell 35	12:53:32.8	–22:52:23	0.6	–9.91	–10.00±0.03	8.6	1	...	1,C
303.3+00.0	PHR J1255-6251	12:55:18.0	–62:51:04	10.0	–12.3	–13.0±0.3	3.2	1	...	
304.1+06.4	PHR J1300-5621	13:00:21.3	–56:21:40	1.5	–11.92	–12.12±0.08	1.8	3	...	
304.2+05.9	Wray 16-122	13:00:41.2	–56:53:40	0.1	–11.79	–11.81±0.07	1.8	3	...	
304.5+02.4	PHR J1304-6024	13:04:13.3	–60:24:57	1.5	–12.5	–12.7±0.2	1.9	1	...	1
304.8+05.1	Hen 2-88	13:05:48.2	–57:39:24	...	–11.80	...	1.8	1	...	5,6
304.5–04.8	IC 4191	13:08:47.3	–67:38:38	0.4	–10.25	–10.31±0.04	1.8	3	0.72	
305.1+01.4	Hen 2-90	13:09:36.3	–61:19:36	0.2	–10.45	–10.49±0.04	1.8	3	1.59	1,2
305.3+03.0	Wray 17-58	13:10:19.6	–59:45:11	0.0	–12.1	–12.1±0.2	1.8	3	...	
306.7+06.6	PHR J1318-5601	13:18:18.7	–56:01:12	3.0	–12.00	–12.32±0.14	2.7	3	...	
305.7–03.4	Wray 17-59	13:19:29.9	–66:09:07	0.0	–11.41	–11.41±0.07	1.8	3	...	
306.4–00.6	Th 2-A	13:22:33.9	–63:21:01	0.5	–11.05	–11.13±0.07	1.8	3	...	10
307.3+05.0	Wray 16-128	13:24:21.9	–57:31:19	0.0	–11.75	–11.75±0.07	1.8	3	...	
310.3+24.7	Lo 8	13:25:37.5	–37:36:15	0.0	–11.81	–11.81±0.10	2.8	1	...	
307.3+02.0	PHR J1327-6032	13:27:14.0	–60:32:10	3.3	–11.14	–11.49±0.07	2.9	4	...	
308.2+07.7	MeWe 1-3	13:28:04.9	–54:41:58	0.0	–12.20	–12.20±0.12	1.8	3	...	4
307.2–03.4	NGC 5189	13:33:33.0	–65:58:27	1.4	–9.74	–9.93±0.03	5.3	2	0.43	6,10
305.6–13.1	ESO 40-11	13:34:14.1	–75:46:31	0.0	–11.77	–11.77±0.06	2.0	4	...	
308.3+02.1	PHR J1335-6015	13:35:03.0	–60:15:46	2.6	–11.86	–12.15±0.12	1.8	4	...	4
...	PHR J1335-5956	13:35:23.3	–59:56:33	1.4	–11.36	–11.54±0.09	3.1	3	...	N
307.7–03.1	PHR J1337-6535	13:37:52.7	–65:35:25	4.0	–11.17	–11.56±0.07	2.8	4	...	
307.5–04.9	MyCn 18	13:39:35.1	–67:22:51	1.1	–10.28	–10.43±0.04	1.8	3	0.86	
318.4+41.4	Abell 36	13:40:41.4	–19:52:55	0.0	–10.41	–10.41±0.04	4.5	4	0.86	8
309.0+00.8	Hen 2-96	13:42:36.2	–61:22:29	0.3	–11.19	–11.24±0.04	1.8	2	2.24	
309.2+01.3	VBRC 5	13:44:00.0	–60:49:47	3.2	–11.38	–11.72±0.05	2.0	4	...	
307.2–09.0	Hen 2-97	13:45:22.4	–71:28:56	0.2	–10.77	–10.80±0.04	1.8	2	0.49	5
312.3+10.5	NGC 5307	13:51:03.3	–51:12:21	0.0	–10.61	–10.62±0.04	2.6	2	0.33	
309.0–04.2	Hen 2-99	13:52:30.7	–66:23:27	1.0	–10.97	–11.10±0.04	1.5	3	1.09	10
309.1–04.3	NGC 5315	13:53:57.0	–66:30:51	0.9	–9.62	–9.74±0.04	2.6	3	0.7	5,6,10
310.6+01.4	WKG 3	13:54:25.1	–60:27:20	4.3	–11.85	–12.26±0.12	1.9	1	...	4,5,6

Table B2 – Continued

PNG	Name	RAJ2000	DEJ2000	$R_{[N\ II]}$	$\log F_{\text{red}}$	$\log F(\text{H}\alpha)$	r_{aper}	N_f	c_β	Note
309.5−02.9	MaC 1-2	13:54:27.1	−64:59:36	1.8	−11.67	−11.89±0.08	1.8	2	...	
311.0+02.4	SuWt 2	13:55:43.2	−59:22:40	6.0	−11.07	−11.5±0.2	3.0	1	...	5,9
311.4+02.8	Hen 2-102	13:58:13.9	−58:54:32	0.0	−11.33	−11.33±0.05	1.8	5	0.93	
312.3+05.7	BMP J1358-5552	13:58:45.6	−55:52:46	...	−12.05	...	1.8	4	...	
...	Fr 2-8	14:00:41.8	−51:02:28	0.0	−11.40	−11.40±0.05	2.3	4	...	
...	MeWe 2-4	14:01:15.4	−50:40:09	3.5	−11.13	−11.49±0.07	4.7	3	...	6
326.6+42.2	IC 972	14:04:25.9	−17:13:41	1.2	−11.40	−11.56±0.07	2.6	2	0.07	
313.4+06.2	MPA J1405-5507	14:05:32.3	−55:07:45	...	−12.25	...	1.8	4	...	10
310.7−02.9	Hen 2-103	14:05:36.9	−64:40:57	1.1	−11.21	−11.36±0.04	1.8	4	0.92	
311.7−00.9	Wray 17-64	14:08:47.3	−62:29:58	8.0	−11.21	−11.79±0.10	2.1	3	...	
312.1+00.3	PHR J1408-6106	14:08:51.7	−61:06:27	1.9	−11.11	−11.34±0.07	3.9	4	...	
311.5−02.7	Wray 16-146	14:11:46.8	−64:16:25	...	−11.83	...	1.8	4	...	
313.5+02.2	PHR J1414-5857	14:14:40.9	−58:57:04	...	−12.05	...	2.0	4	...	4
310.8−05.9	LoTr 7	14:15:24.0	−67:31:56	0.1	−11.73	−11.75±0.07	1.8	2	...	
308.6−12.2	Hen 2-105	14:15:24.8	−74:12:47	0.0	−11.05	−11.05±0.04	1.8	4	0.12	
...	V417 Cen	14:15:59.7	−61:53:50	0.3	−11.77	−11.81±0.09	1.8	2	...	1
003.3+66.1	SkAc 1	14:16:22.0	13:52:24	0.0	−12.68	−12.68±0.09	1.8	1	...	6
313.1+02.1	PM 1-79	14:16:51.8	−58:53:10	...	−12.11	...	1.8	3	...	4
315.9+08.2	MeWe 1-4	14:17:32.1	−52:26:21	...	−11.59	...	2.3	2	...	
316.1+08.4	Hen 2-108	14:18:08.9	−52:10:40	0.4	−10.74	−10.80±0.04	1.8	1	0.53	
316.3+08.8	PHR J1418-5144	14:18:25.8	−51:44:39	1.4	−11.21	−11.39±0.07	4.8	2	...	
312.6−01.8	Hen 2-107	14:18:43.3	−63:07:09	1.0	−11.15	−11.28±0.04	1.8	3	...	V
...	Sa 3-25	14:19:07.4	−67:32:12	...	−11.99	...	1.8	3	...	1
315.4+05.2	Hen 2-109	14:20:48.9	−55:27:59	1.1	−11.88	−12.02±0.08	1.3	4	...	
315.7+05.5	LoTr 8	14:21:60.0	−55:02:17	0.0	−12.37	−12.37±0.14	1.4	2	...	
319.6+15.7	IC 4406	14:22:26.3	−44:09:04	2.0	−9.92	−10.16±0.03	5.4	2	0.38	
...	Fr 2-9	14:22:36.0	−09:16:00	0.9	−10.05	−10.18±0.04	41.0	3	...	1,4,6
317.2+08.6	PHR J1424-5138	14:24:32.6	−51:38:40	0.0	−11.87	−11.87±0.10	2.4	3	...	
314.5−01.0	PHR J1432-6138	14:32:05.0	−61:38:42	2.6	−10.90	−11.20±0.06	2.9	1	...	
315.0−00.3	Hen 2-111	14:33:18.4	−60:49:35	7.0	−10.34	−10.90±0.08	6.4	1	2.04	
315.9+00.3	PHR J1437-5949	14:37:53.2	−59:49:25	8.0	−12.6	−13.2±0.3	2.2	1	...	4
319.2+06.8	Hen 2-112	14:40:30.9	−52:34:57	1.3	−10.98	−11.16±0.04	1.8	3	...	
317.8+03.3	VBRC 6	14:41:36.0	−56:15:14	3.3	−11.48	−11.83±0.05	1.8	4	...	6
316.3−01.3	LoTr 10	14:46:20.2	−61:13:35	2.6	−12.10	−12.40±0.08	1	
321.0+08.3	MeWe 1-5	14:46:35.2	−50:23:26	0.0	−12.3	−12.3±0.2	1.8	1	...	
317.5+00.8	PHR J1447-5838	14:47:41.8	−58:38:41	0.9	−11.06	−11.19±0.07	3.3	2	...	1
319.8+04.3	PHR J1451-5432	14:51:37.6	−54:32:26	5.2	−12.24	−12.71±0.14	1.8	5	...	
315.7−04.2	Wray 16-158	14:52:36.2	−64:02:22	...	−12.03	...	1.8	4	...	
...	Hen 2-113	14:59:53.5	−54:18:07	0.9	−10.77	−10.89±0.04	1.8	4	1.09	10,V
318.3−02.0	Hen 2-114	15:04:08.8	−60:53:19	2.3	−11.26	−11.53±0.07	1.8	5	0.93	
321.3+02.8	Hen 2-115	15:05:16.8	−55:11:10	0.4	−11.18	−11.24±0.04	1.8	4	2.16	6
320.9+02.0	Hen 2-117	15:05:59.2	−55:59:17	0.5	−11.06	−11.13±0.04	1.8	4	2.81	
318.3−02.5	Hen 2-116	15:06:02.2	−61:21:20	2.8	−11.17	−11.49±0.04	1.8	3	...	
327.5+13.3	Hen 2-118	15:06:13.7	−42:59:56	0.1	−11.18	−11.20±0.04	1.8	2	0	
...	Mu 1	15:06:17.0	−41:45:18	0.4	−12.19	−12.24±0.12	2.6	1	...	4,C,N
316.7−05.8	MPA J1508-6455	15:08:06.4	−64:55:49	0.1	−12.06	−12.08±0.08	1.8	4	...	
318.4−03.0	ESO 135-04	15:08:43.6	−61:44:14	1.8	−11.63	−11.85±0.05	1.8	3	...	5
...	Fr 2-10	15:09:19.0	−05:20:54	1.4	−10.79	−10.98±0.05	16.4	1	...	1,4,6
321.6+02.2	CVMP 1	15:09:25.2	−55:33:05	12.0	−10.75	−11.50±0.10	4.9	2	...	
315.4−08.4	PHR J1510-6754	15:10:26.1	−67:54:54	2.4	−11.02	−11.30±0.08	4.0	3	...	
317.1−05.7	NGC 5844	15:10:40.7	−64:40:28	5.2	−10.39	−10.86±0.04	2.4	2	...	6
321.8+01.9	Hen 2-120	15:11:56.4	−55:39:47	1.4	−11.06	−11.25±0.04	1.8	3	1.62	6
331.3+16.8	NGC 5873	15:12:51.1	−38:07:34	0.1	−10.57	−10.59±0.04	2.6	2	0.15	
327.8+10.0	NGC 5882	15:16:49.9	−45:38:59	0.1	−9.76	−9.78±0.03	5.4	2	0.43	6
326.4+07.0	NeVe 3-2	15:19:43.9	−48:59:55	0.0	−11.34	−11.34±0.04	1.8	3	...	
313.8−12.6	LoTr 11	15:21:10.4	−72:13:26	0.0	−11.85	−11.85±0.08	2.3	4	...	
323.9+02.4	Hen 2-123	15:22:19.4	−54:08:13	1.2	−10.87	−11.02±0.05	2.6	2	1.81	
322.2−00.4	BMP J1522-5729	15:22:58.9	−57:29:59	...	−12.37	...	1.8	2	...	
324.2+02.5	Hen 2-125	15:23:36.3	−53:51:28	1.1	−11.38	−11.53±0.05	1.8	3	1.77	
322.4−00.1	Pe 2-8	15:23:42.9	−57:09:25	0.3	−12.07	−12.11±0.11	1.8	2	...	
325.8+04.5	Hen 2-128	15:25:07.8	−51:19:42	0.4	−11.12	−11.18±0.04	1.8	1	1.14	
325.0+03.2	Hen 2-129	15:25:32.7	−52:50:38	0.2	−11.52	−11.55±0.05	1.8	2	2.11	

Table B2 – Continued

PNG	Name	RAJ2000	DEJ2000	$R_{[N II]}$	$\log F_{\text{red}}$	$\log F(\text{H}\alpha)$	r_{aper}	N_f	c_β	Note
324.3+01.1	PHR J1529-5458	15:29:29.8	-54:58:58	3.0	-12.14	-12.47±0.13	2.3	2	...	1
328.5+06.2	PHR J1533-4824	15:33:02.0	-48:24:43	2.4	-11.72	-12.00±0.10	3.1	4	...	4
322.4-02.6	Mz 1	15:34:17.0	-59:09:09	3.1	-10.31	-10.64±0.04	1.8	3	0.66	
322.9-02.1	PHR J1534-5829	15:34:45.2	-58:29:50	1.5	-11.56	-11.75±0.11	2.4	2	...	6
329.7+06.9	PHR J1536-4711	15:36:03.7	-47:11:33	0.3	-12.19	-12.23±0.13	1.8	3	...	
315.1-13.0	Hen 2-131	15:37:11.2	-71:54:53	1.4	-9.38	-9.56±0.03	5.8	2	0.44	6,V
321.1-05.1	PHR J1537-6159	15:37:49.5	-61:59:10	1.6	-11.48	-11.68±0.13	2.8	1	...	4
323.1-02.5	Hen 2-132	15:38:01.2	-58:44:42	0.0	-11.9	-11.9±0.2	1.8	2	...	
327.1+01.9	PM 1-99	15:41:29.5	-52:43:49	...	-12.62	...	1.8	3	...	4
324.8-01.1	Hen 2-133	15:41:58.8	-56:36:26	0.6	-11.87	-11.96±0.09	1.8	2	...	
330.2+05.9	Lo 9	15:42:13.3	-47:40:46	2.6	-11.45	-11.74±0.05	2.3	3	...	
335.5+12.4	DS 2	15:43:05.0	-39:18:15	0.0	-11.55	-11.55±0.09	2.9	4	...	
322.5-05.2	NGC 5979	15:47:41.6	-61:13:06	0.1	-10.65	-10.66±0.04	1.8	3	0.34	6
332.3+07.0	PHR J1547-4533	15:47:44.2	-45:33:01	0.1	-11.82	-11.84±0.11	2.4	4	...	4
328.2+01.3	Lo 10	15:49:29.1	-52:30:16	0.5	-11.75	-11.83±0.06	1.8	1	...	
330.7+04.1	Cn 1-1	15:51:15.9	-48:44:59	0.1	-10.99	-11.01±0.04	1.8	1	1.02	1,C
325.9-01.7	vBe 2	15:51:18.9	-56:21:20	6.6	-11.73	-12.27±0.13	1.9	4	...	
330.9+04.3	Wray 16-189	15:51:19.8	-48:26:07	0.0	-11.77	-11.77±0.06	1.8	3	...	
329.0+01.9	Sp 1	15:51:40.9	-51:31:28	0.1	-10.70	-10.72±0.05	2.6	2	0.99	
322.1-06.6	Hen 2-136	15:52:10.7	-62:30:47	0.1	-11.07	-11.09±0.04	1.8	3	0.47	
325.3-02.9	PHR J1553-5738	15:53:11.2	-57:38:11	0.0	-11.45	-11.45±0.10	2.5	1	...	6
335.4+09.2	K 1-31	15:53:12.5	-41:50:26	0.6	-12.13	-12.22±0.08	1.8	2	...	5,6
330.1+02.6	MPA J1554-5022	15:54:08.9	-50:22:39	...	-12.14	...	1.8	4	...	4
326.0-02.4	FP J1554-5651	15:54:50.9	-56:51:55	...	-11.40	...	1.9	2	...	
329.5+01.7	VBRC 7	15:54:50.9	-51:22:35	1.5	-11.28	-11.48±0.07	3.1	2	...	
320.1-09.6	Hen 2-138	15:56:01.7	-66:09:09	0.8	-10.01	-10.13±0.03	3.4	2	0.35	V
330.7+02.7	FP J1556-4955	15:56:33.2	-49:55:15	...	-10.85	...	7.8	4	...	1
327.1-01.8	Hen 2-140	15:58:08.1	-55:41:50	1.4	-11.08	-11.26±0.04	1.8	5	2.23	V
325.4-04.0	Hen 2-141	15:59:08.8	-58:23:53	0.5	-10.91	-10.99±0.04	1.8	4	0.61	
327.1-02.2	Hen 2-142	15:59:57.6	-55:55:33	1.2	-10.72	-10.88±0.04	1.8	4	1.43	10,V
332.2+03.5	Wray 16-199	16:00:22.0	-48:15:35	0.0	-11.83	-11.83±0.06	1.8	2	...	
327.8-01.6	Hen 2-143	16:00:59.1	-55:05:40	0.9	-11.59	-11.72±0.07	1.8	4	2.63	
341.6+13.7	NGC 6026	16:01:21.1	-34:32:37	0.1	-11.01	-11.02±0.04	1.8	3	0.55	
336.9+08.3	Sa 1-3	16:02:13.0	-41:33:36	0.0	-12.10	-12.10±0.09	1.0	2	...	6
337.0+08.4	PHR J1602-4127	16:02:20.2	-41:27:11	1.2	-11.23	-11.39±0.07	2.7	2	...	
340.8+12.3	Lo 11	16:03:22.2	-36:00:54	0.5	-11.87	-11.95±0.06	1.9	5	...	
340.8+10.8	Lo 12	16:08:26.4	-37:08:46	0.6	-11.82	-11.91±0.07	2.1	4	...	
331.4+00.5	Hen 2-145	16:08:58.9	-51:01:58	2.3	-11.53	-11.79±0.08	2.6	2	...	
328.4-02.8	PM 1-106	16:09:20.1	-55:36:10	0.2	-12.12	-12.15±0.10	1.1	1	...	1
345.5+15.1	Lo 13	16:09:45.9	-30:55:08	0.0	-12.08	-12.08±0.11	2.0	4	...	
025.3+40.8	IC 4593	16:11:44.6	12:04:17	0.1	-10.06	-10.07±0.03	5.8	1	0.17	6
342.1+10.8	NGC 6072	16:12:58.1	-36:13:46	1.9	-10.20	-10.44±0.03	3.8	2	1.03	
329.8-02.1	BMP J1613-5406	16:13:02.0	-54:06:32	6.5	-11.06	-11.60±0.09	4.2	4	...	
341.0+09.4	SB 25	16:13:38.3	-37:59:58	1.5	-12.31	-12.50±0.12	1.8	3	...	4
329.4-02.7	Hen 2-149	16:14:24.3	-54:47:39	0.1	-11.86	-11.87±0.09	1.8	3	...	
329.3-02.8	Mz 2	16:14:32.4	-54:57:04	0.9	-10.79	-10.92±0.04	1.8	4	0.86	
336.1+04.1	PM 2-17	16:15:02.8	-45:11:54	0.4	-11.86	-11.92±0.06	1.8	3	...	6
333.4+01.1	Hen 2-152	16:15:20.0	-49:13:21	3.1	-10.66	-10.99±0.04	1.8	3	1.94	
326.0-06.5	Hen 2-151	16:15:42.3	-59:54:01	0.4	-11.12	-11.18±0.04	1.8	4	1	V
331.7-01.0	Mz 3	16:17:13.4	-51:59:10	1.6	-9.82	-10.02±0.04	1.8	2	1.91	1,C
330.6-02.1	Hen 2-153	16:17:14.4	-53:32:08	2.2	-11.07	-11.32±0.04	1.8	2	1.25	
338.8+05.6	IC 4599	16:19:23.1	-42:15:36	0.3	-10.82	-10.86±0.04	1.8	2	0.84	
013.3+32.7	Sn 1	16:21:04.4	00:16:11	0.0	-11.21	-11.21±0.04	1.8	3	0.19	
331.0-02.7	Hen 2-157	16:22:14.3	-53:40:54	1.0	-11.36	-11.50±0.05	1.8	3	1.2	
346.9+12.4	Abell 38	16:23:19.0	-31:44:59	11.0	-10.98	-11.67±0.06	2.6	2	...	C
327.8-06.1	Hen 2-158	16:23:30.6	-58:19:23	0.4	-11.42	-11.48±0.05	1.8	2	0.56	
336.2+01.9	Pe 1-6	16:23:54.3	-46:42:15	0.0	-11.98	-11.99±0.13	1.8	3	...	
331.8-02.3	MPA J1624-5250	16:24:02.9	-52:50:05	...	-11.96	...	1.8	3	...	
330.6-03.6	Hen 2-159	16:24:21.4	-54:36:03	0.0	-11.44	-11.44±0.05	1.8	4	0.87	
331.5-02.7	Hen 2-161	16:24:37.8	-53:22:34	0.2	-11.27	-11.30±0.05	1.8	3	1.06	
337.4+02.6	PHR J1625-4523	16:25:50.9	-45:22:39	1.0	-10.51	-10.65±0.05	6.9	2	...	1
331.4-03.5	Hen 2-162	16:27:50.9	-54:01:28	0.7	-11.14	-11.24±0.04	1.8	4	1.27	V

Table B2 – Continued

PNG	Name	RAJ2000	DEJ2000	$R_{[N\ II]}$	$\log F_{\text{red}}$	$\log F(\text{H}\alpha)$	r_{aper}	N_f	c_β	Note
327.8–07.2	Hen 2-163	16:29:31.3	–59:09:25	0.6	–11.38	–11.46±0.04	1.8	4	0.64	
332.0–03.3	Hen 2-164	16:29:53.3	–53:23:15	0.0	–11.29	–11.29±0.05	1.8	3	1.21	
331.5–03.9	Hen 2-165	16:30:00.1	–54:09:28	2.0	–10.93	–11.17±0.04	1.9	4	0.88	
337.4+01.6	Pe 1-7	16:30:25.9	–46:02:51	1.2	–11.09	–11.25±0.04	1.8	4	2.52	10,V
341.8+05.4	NGC 6153	16:31:30.8	–40:15:14	0.2	–9.93	–9.96±0.04	2.5	1	1.32	6
335.4–01.1	Hen 2-169	16:34:13.3	–49:21:13	3.9	–11.12	–11.51±0.07	1.8	5	4.41	
340.0+02.9	PM 1-112	16:34:43.1	–43:18:00	0.0	–11.70	–11.70±0.08	1.8	4	...	
332.3–04.2	Hen 2-170	16:35:21.2	–53:50:11	0.2	–11.26	–11.30±0.05	1.8	4	0.85	
337.4+00.3	PHR J1635-4654	16:35:51.9	–46:54:10	0.8	–11.45	–11.57±0.06	2.0	4	...	1
...	IRAS 16342-3814	16:37:39.9	–38:20:17	...	–12.12	...	1.8	2	...	2
331.1–05.7	PC 11	16:37:42.7	–55:42:26	0.1	–10.73	–10.74±0.05	2.6	2	0.88	1
335.4–01.9	PHR J1637-4957	16:37:44.9	–49:57:50	0.2	–11.95	–11.98±0.13	1.8	4	...	
339.1+00.9	PHR J1639-4516	16:39:22.3	–45:16:35	1.9	–11.45	–11.69±0.10	1.8	4	...	
345.6+06.7	Hen 2-175	16:39:28.1	–36:34:16	1.8	–11.54	–11.76±0.05	1.8	2	1.57	
333.4–04.0	HaTr 3	16:39:37.6	–52:49:13	0.7	–11.76	–11.86±0.08	1.8	3	...	
344.2+04.7	Vd 1-1	16:42:33.4	–38:54:32	0.3	–11.35	–11.39±0.09	1.8	3	...	
334.8–03.6	BMP J1643-5129	16:43:23.6	–51:29:29	...	–11.94	...	1.8	3	...	
000.1+17.2	PC 12	16:43:53.8	–18:57:12	0.5	–11.14	–11.21±0.04	1.8	4	0.75	
343.6+03.7	SuWt 3	16:44:24.1	–40:03:21	2.2	–11.11	–11.37±0.08	1.8	3	...	5
352.9+11.4	K 2-16	16:44:49.1	–28:04:05	1.1	–11.85	–12.00±0.08	1.8	3	...	10
335.2–03.6	HaTr 4	16:45:00.2	–51:12:20	0.1	–11.70	–11.71±0.06	1.8	3	...	
345.0+04.3	Vd 1-2	16:46:45.1	–38:36:58	0.5	–11.52	–11.58±0.11	1.8	2	...	
335.9–03.6	MeWe 1-7	16:47:57.1	–50:42:48	0.0	–12.21	–12.21±0.14	1.8	3	...	
359.1+15.1	Abell 40	16:48:34.5	–21:00:51	0.0	–12.25	–12.25±0.10	1.8	4	...	
335.6–04.0	MeWe 1-8	16:48:40.2	–51:09:20	...	–11.91	...	1.8	2	...	4
347.4+05.8	H 1-2	16:48:54.1	–35:47:09	0.2	–11.02	–11.05±0.04	1.8	4	...	
344.8+03.4	Vd 1-3	16:49:32.9	–39:21:09	0.7	–11.55	–11.65±0.11	1.8	4	...	4
351.9+09.0	PC 13	16:50:17.1	–30:19:56	0.0	–11.56	–11.57±0.05	1.8	5	...	
345.0+03.4	Vd 1-4	16:50:25.3	–39:08:19	0.3	–11.32	–11.36±0.11	1.8	4	...	4
...	PM 1-115	16:51:06.2	–32:23:01	3.3	–11.96	–12.31±0.08	1.8	3	...	
344.9+03.0	BMP J1651-3930	16:51:41.3	–39:30:27	...	–10.95	...	4.0	3	...	
350.9+07.8	PHR J1651-3148	16:51:46.7	–31:48:21	0.3	–11.84	–11.88±0.09	2.7	3	...	1,5,6
342.7+00.7	H 1-3	16:53:31.4	–42:39:23	1.4	–11.69	–11.88±0.14	1.8	3	...	
351.3+07.6	H 1-4	16:53:37.1	–31:40:33	0.1	–11.64	–11.65±0.07	1.8	3	...	
345.9+03.0	Vd 1-6	16:54:27.3	–38:44:11	1.1	–11.38	–11.53±0.08	1.8	5	...	
325.8–12.8	Hen 2-182	16:54:35.2	–64:14:28	0.3	–10.42	–10.47±0.04	1.8	3	0.01	
348.4+04.9	MPA J1655-3535	16:55:22.1	–35:35:24	...	–12.10	...	1.8	5	...	4,10
353.0+08.3	MyCn 26	16:55:47.3	–29:50:18	1.6	–11.11	–11.32±0.04	1.8	5	...	
340.1–02.2a	MPA J1657-4633	16:57:06.3	–46:33:60	...	–12.68	...	1.8	2	...	1,4
337.6–04.2	MeWe 1-9	16:57:28.9	–49:46:55	1.3	–11.70	–11.87±0.09	1.8	4	...	
334.6–06.7	MPA J1658-5341	16:58:17.0	–53:41:45	...	–12.25	...	1.8	4	...	4
336.3–05.6	Hen 2-186	16:59:36.1	–51:42:06	1.1	–11.32	–11.47±0.05	1.8	3	0.84	
349.8+04.4	M 2-4	17:01:06.2	–34:49:39	0.3	–11.03	–11.08±0.04	1.8	3	...	
321.3–16.7	Hen 2-185	17:01:17.3	–70:06:03	0.1	–11.04	–11.05±0.04	1.8	4	...	
343.3–00.6	HaTr 5	17:01:28.0	–43:05:55	...	–11.13	...	2.4	3	...	
000.3+12.2	IC 4634	17:01:33.6	–21:49:33	0.1	–10.25	–10.26±0.03	2.6	1	0.56	
337.5–05.1	Hen 2-187	17:01:37.0	–50:22:57	0.0	–11.59	–11.59±0.06	1.8	4	1.16	1
342.0–01.7	PHR J1702-4443	17:02:04.3	–44:43:20	5.8	–11.64	–12.14±0.08	2.1	4	...	
351.2+05.2	M 2-5	17:02:19.1	–33:10:05	1.4	–11.02	–11.21±0.04	1.8	2	...	V
...	K 5-21	17:02:35.0	–30:19:15	...	–12.03	...	1.8	3	...	1
338.1–04.8	PHR J1702-4943	17:02:42.0	–49:43:21	0.3	–12.17	–12.22±0.13	1.8	4	...	
352.0+05.7	PHR J1702-3219	17:02:43.1	–32:19:09	0.4	–12.06	–12.12±0.14	1.8	2	...	
334.8–07.4	Hen 3-1312	17:03:02.9	–53:55:54	0.4	–10.77	–10.83±0.04	1.8	4	0.7	V
351.1+04.8	M 1-19	17:03:46.8	–33:29:44	1.1	–11.12	–11.19±0.04	1.8	3	...	
353.3+06.3	M 2-6	17:04:18.3	–30:53:29	0.2	–11.37	–11.41±0.06	1.8	3	...	
350.9+04.4	H 2-1	17:04:36.3	–33:59:19	0.5	–10.60	–10.67±0.04	2.6	2	1.04	6,10,V
345.4+00.1	IC 4637	17:05:10.5	–40:53:08	0.1	–10.40	–10.41±0.04	1.8	4	1.13	
353.7+06.3	M 2-7	17:05:13.7	–30:32:18	0.6	–11.49	–11.57±0.05	1.8	2	...	
352.1+05.1	M 2-8	17:05:30.7	–32:32:08	0.8	–11.19	–11.31±0.05	1.8	2	...	10
010.8+18.0	M 2-9	17:05:38.0	–10:08:35	0.8	–10.38	–10.49±0.04	2.6	2	...	1,C
334.8–07.9	FP J1705-5415	17:05:38.9	–54:15:19	...	–10.75	...	8.6	1	...	1
358.0+09.3	Th 3-1	17:05:44.5	–25:25:02	0.0	–11.85	–11.85±0.08	1.8	3	...	

Table B2 – Continued

PNG	Name	RAJ2000	DEJ2000	$R_{[N\ II]}$	$\log F_{\text{red}}$	$\log F(\text{H}\alpha)$	r_{aper}	N_{f}	c_{β}	Note
349.6+03.1	PHR J1706-3544	17:06:01.9	-35:44:37	0.0	-12.5	-12.5±0.3	1.8	2	...	4
336.2-06.9	PC 14	17:06:14.8	-52:30:00	0.2	-10.89	-10.92±0.04	1.8	3	1.12	5,6,10
342.9-02.0	Pe 1-8	17:06:22.6	-44:13:10	0.1	-11.25	-11.26±0.05	1.8	4	...	
011.4+17.9	DHW 1-2	17:06:55.0	-09:46:59	0.1	-12.3	-12.3±0.3	1.8	3	...	1,5,6
344.2-01.2	H 1-6	17:06:58.9	-42:41:10	2.1	-11.23	-11.48±0.07	1.8	3	...	
...	Wray 15-1624	17:08:34.3	-35:48:06	...	-12.25	...	1.8	1	...	
332.9-09.9	Hen 3-1333	17:09:00.9	-56:54:48	2.8	-11.27	-11.58±0.04	1.8	4	...	10,V
...	K 5-25	17:09:25.7	-24:43:15	...	-12.53	...	1.8	3	...	
349.5+02.0	PHR J1709-3629	17:09:33.2	-36:29:31	2.5	-12.1	-12.3±0.2	2.3	1	...	4
336.8-07.2	K 2-17	17:09:35.9	-52:13:02	0.0	-11.94	-11.94±0.08	1.8	3	...	
345.2-01.2	H 1-7	17:10:27.4	-41:52:49	0.7	-10.67	-10.77±0.04	1.8	2	...	
357.2+07.4	M 4-3	17:10:41.8	-27:08:44	0.1	-11.59	-11.62±0.05	1.8	2	...	
340.9-04.6	Sa 1-5	17:11:27.4	-47:25:02	0.1	-12.01	-12.02±0.10	1.8	2	...	
...	PM 1-130	17:11:40.8	-30:28:49	...	-12.34	...	1.8	2	...	1,4
334.3-09.3	IC 4642	17:11:45.0	-55:24:01	0.0	-10.78	-10.78±0.04	1.8	4	0.17	
353.2+04.2	PHR J1711-3210	17:11:54.8	-32:10:29	0.1	-12.2	-12.3±0.2	1.8	2	...	4
355.9+06.1	PHR J1711-2851	17:11:59.4	-28:51:35	0.1	-12.08	-12.10±0.13	1.8	3	...	
354.0+04.7	PHR J1712-3114	17:12:10.1	-31:14:40	0.6	-11.69	-11.77±0.09	1.8	2	...	
358.0+07.5	Terz N 8	17:12:33.6	-26:25:24	3.8	-12.02	-12.40±0.09	1.8	1	...	
354.8+05.1	K 6-22	17:12:38.8	-30:21:36	0.0	-12.23	-12.23±0.12	1.8	3	...	
358.6+07.8	M 3-36	17:12:39.2	-25:43:37	0.1	-11.87	-11.89±0.07	1.8	3	...	
018.0+20.1	Na 1	17:12:51.9	-03:16:00	0.1	-11.31	-11.32±0.04	1.8	2	0.64	
349.5+01.0	NGC 6302	17:13:44.2	-37:06:16	2.8	-9.22	-9.53±0.03	6.9	1	1.70	
009.6+14.8	NGC 6309	17:14:04.3	-12:54:38	0.1	-10.53	-10.55±0.04	2.6	2	0.73	
354.2+04.3	M 2-10	17:14:07.0	-31:19:43	1.1	-11.29	-11.44±0.05	1.8	2	...	
352.6+03.0	H 1-8	17:14:42.9	-33:24:47	1.1	-11.96	-12.12±0.10	1.8	2	...	4
355.1+04.7	Terz N 140	17:15:03.1	-30:20:38	1.4	-12.16	-12.34±0.10	1.2	2	...	
001.2+08.6	BMP J1716-2313	17:16:20.9	-23:13:57	...	-12.27	...	2.9	2	...	1
331.3-12.1	Hen 3-1357	17:16:21.1	-59:29:23	0.3	-10.31	-10.36±0.04	1.8	4	...	6
356.5+05.1	Th 3-3	17:17:20.5	-28:59:30	0.8	-12.2	-12.3±0.2	1.8	3	...	
355.2+03.7	Terz N 137	17:19:03.3	-30:53:54	0.1	-12.2	-12.3±0.2	1.8	3	...	
359.8+06.9	M 3-37	17:19:13.4	-25:17:18	1.7	-11.91	-12.12±0.07	1.8	4	...	
354.9+03.5	Th 3-6	17:19:20.2	-31:12:41	1.0	-12.2	-12.4±0.2	1.8	1	...	
...	PM 1-139	17:19:26.2	-22:48:12	1.1	-12.07	-12.22±0.08	1.8	3	...	
342.9-04.9	Hen 2-207	17:19:33.0	-45:53:17	1.9	-11.03	-11.27±0.05	1.8	3	...	
348.3-01.3	PHR J1720-3927	17:20:14.4	-39:27:48	1.7	-11.23	-11.44±0.08	2.5	4	...	
356.9+04.5	M 2-11	17:20:33.3	-29:00:39	0.6	-11.48	-11.56±0.05	1.8	4	...	
338.1-08.3	NGC 6326	17:20:46.3	-51:45:15	0.3	-10.51	-10.56±0.04	1.8	2	0.21	
356.9+04.4	M 3-38	17:21:04.5	-29:02:59	0.7	-11.79	-11.88±0.07	1.8	4	...	
333.8-11.2	FP J1721-5654	17:21:09.0	-56:54:25	1.7	-10.83	-11.04±0.05	4.7	2	...	1
358.5+05.4	M 3-39	17:21:11.5	-27:11:38	0.3	-11.69	-11.74±0.05	1.8	3	2.44	
002.6+08.1	H 1-11	17:21:17.7	-22:18:35	0.1	-11.56	-11.57±0.04	1.8	2	...	
355.9+03.6	H 1-9	17:21:31.9	-30:20:48	0.3	-11.35	-11.39±0.04	1.8	4	...	10,V
357.1+04.4	Terz N 18	17:21:37.9	-28:55:14	0.0	-12.11	-12.11±0.09	1.8	4	...	
349.3-01.1	NGC 6337	17:22:15.7	-38:29:03	0.3	-10.41	-10.46±0.04	1.8	3	1.35	
358.7+05.2	M 3-40	17:22:28.3	-27:08:42	0.9	-12.16	-12.29±0.09	1.8	2	...	
337.4-09.1	Wray 16-266	17:22:37.0	-52:46:34	0.0	-11.86	-11.86±0.08	1.8	1	...	
000.2+06.1	Terz N 67	17:22:53.3	-25:25:01	2.1	-12.5	-12.8±0.2	1.8	3	...	4
357.3+04.0	H 2-7	17:23:24.9	-28:59:06	0.0	-11.97	-11.98±0.09	1.8	4	...	
359.8+05.6	M 2-12	17:24:01.5	-25:59:23	0.8	-11.34	-11.45±0.04	1.8	3	...	10
000.1+05.7	PHR J1724-2543	17:24:04.3	-25:43:14	0.3	-12.37	-12.42±0.15	1.8	1	...	
349.1-01.7	PHR J1724-3859	17:24:30.7	-38:59:44	10.0	-11.49	-12.17±0.12	2.7	4	...	
357.1+03.6	M 3-7	17:24:34.4	-29:24:19	0.2	-11.37	-11.41±0.05	1.8	3	1.33	
358.2+04.2	M 3-8	17:24:52.2	-28:05:55	0.7	-11.86	-11.95±0.07	1.8	2	...	
001.4+06.3	Bica 1	17:24:53.8	-24:19:21	4.2	-11.96	-12.38±0.09	1.9	3	...	
356.1+02.7	Th 3-13	17:25:19.3	-30:40:42	0.2	-12.20	-12.23±0.15	1.8	3	...	6,10
359.8+05.2	Terz N 19	17:25:23.7	-26:11:54	2.0	-12.1	-12.4±0.2	1.8	2	...	4
002.0+06.6	PHR J1725-2338	17:25:41.5	-23:38:29	0.9	-12.44	-12.57±0.14	1.8	2	...	4
359.9+05.1	M 3-9	17:25:43.4	-26:11:55	0.1	-11.79	-11.80±0.07	1.8	2	...	
357.3+03.3	M 3-41	17:25:59.8	-29:21:50	0.9	-11.43	-11.56±0.05	1.8	3	...	10,V
345.0-04.9	Cn 1-3	17:26:12.4	-44:11:25	0.3	-10.51	-10.55±0.04	1.8	4	...	
352.6+00.1	H 1-12	17:26:24.2	-35:01:41	0.2	-11.67	-11.70±0.09	1.8	3	...	

Table B2 – Continued

PNG	Name	RAJ2000	DEJ2000	$R_{[NII]}$	$\log F_{\text{red}}$	$\log F(\text{H}\alpha)$	r_{aper}	N_f	c_β	Note
007.9+10.1	MaC 1-4	17:26:38.1	-16:48:29	0.0	-12.06	-12.06±0.09	1.8	3	...	
357.5+03.2	M 3-42	17:26:59.8	-29:15:32	1.5	-11.96	-12.16±0.10	1.8	3	...	4
358.8+04.1	SaWe 2	17:27:00.2	-27:40:35	0.3	-11.85	-11.90±0.06	2.0	3	...	
358.8+04.0	Th 3-15	17:27:10.7	-27:43:59	0.3	-12.3	-12.4±0.2	1.8	3	...	4
358.2+03.6	M 3-10	17:27:20.2	-28:27:51	0.3	-11.39	-11.43±0.04	1.8	3	...	
358.2+03.5	H 2-10	17:27:32.9	-28:31:07	0.1	-12.09	-12.11±0.10	1.8	3	...	
002.9+06.5	PM 1-149	17:27:53.2	-22:57:22	0.0	-11.88	-11.88±0.06	1.8	1	...	
001.7+05.7	H 1-14	17:28:01.8	-24:25:23	0.0	-11.98	-11.98±0.07	1.8	4	...	
006.5+08.7	PHR J1728-1844	17:28:14.0	-18:44:31	0.4	-12.05	-12.11±0.09	1.8	3	...	
352.8-00.2	H 1-13	17:28:27.5	-35:07:32	0.4	-11.33	-11.38±0.05	1.8	3	...	
011.1+11.5	M 2-13	17:28:34.2	-13:26:21	0.7	-11.41	-11.51±0.08	3.4	1	1.06	
001.4+05.3	H 1-15	17:28:37.6	-24:51:07	0.3	-11.76	-11.80±0.06	1.8	4	...	
006.1+08.3	M 1-20	17:28:57.6	-19:15:54	0.2	-11.13	-11.15±0.04	1.8	5	1.01	
009.6+10.5	Abell 41	17:29:02.0	-15:13:05	0.3	-11.53	-11.57±0.05	1.8	3	0.66	
...	Sa 2-202	17:29:10.1	-42:32:46	...	-12.14	...	1.8	2	...	
002.4+05.8	NGC 6369	17:29:20.4	-23:45:34	0.3	-10.06	-10.10±0.03	5.0	2	2.38	6,10
000.1+04.3	H 1-16	17:29:23.4	-26:26:04	0.2	-11.79	-11.81±0.05	1.8	3	...	
000.7+04.7	H 2-11	17:29:26.0	-25:49:07	1.1	-12.18	-12.34±0.10	1.8	4	...	
358.3+03.0	H 1-17	17:29:40.6	-28:40:22	0.4	-11.70	-11.75±0.09	1.8	1	...	
357.6+02.6	H 1-18	17:29:42.8	-29:32:50	1.0	-11.64	-11.78±0.07	1.8	3	...	
000.4+04.4	K 5-1	17:29:52.4	-26:11:13	0.1	-12.34	-12.35±0.12	1.8	3	...	
358.9+03.4	H 1-19	17:30:02.6	-27:59:18	1.1	-11.79	-11.94±0.06	1.8	3	...	
359.3+03.6	Al 2-E	17:30:14.4	-27:30:19	0.4	-12.4	-12.5±0.2	1.8	3	...	4
002.6+05.5	K 5-3	17:30:41.2	-23:45:00	0.1	-12.09	-12.11±0.09	1.8	3	...	10
358.9+03.2	H 1-20	17:30:43.8	-28:04:07	0.9	-11.72	-11.84±0.06	1.8	3	...	
359.8+03.7	Th 3-25	17:30:46.7	-27:05:59	0.0	-12.01	-12.01±0.06	1.8	2	...	
358.8+03.0	Th 3-26	17:31:09.3	-28:14:50	0.7	-12.02	-12.13±0.10	1.8	3	...	
339.4-09.5	PHR J1721-5122	17:31:18.8	-51:22:03	...	-12.12	...	1.8	3	...	
016.0+13.5	Abell 42	17:31:29.1	-08:19:10	0.0	-11.67	-11.67±0.08	2.4	2	...	
358.5+02.6	HaWe 11	17:31:47.5	-28:42:03	0.3	-11.17	-11.21±0.07	2.6	2	...	
004.3+06.4	G4.4+6.4	17:31:52.7	-21:49:31	2.4	-10.97	-11.25±0.06	3.2	3	...	
...	IRAS 17292-1704	17:32:05.8	-17:06:52	...	-12.04	...	1.8	2	...	1
349.2-03.5	H 2-14	17:32:20.1	-39:51:26	0.0	-11.86	-11.86±0.10	1.8	3	...	
350.8-02.4	H 1-22	17:32:22.1	-37:57:24	0.4	-11.71	-11.77±0.08	1.8	2	...	
357.6+01.7	H 1-23	17:32:46.9	-30:00:15	0.4	-11.65	-11.71±0.08	1.8	4	...	
348.4-04.1	H 1-21	17:32:47.8	-40:58:29	0.8	-11.61	-11.73±0.07	1.8	3	...	
351.9-01.9	Wray 16-286	17:33:00.7	-36:43:53	0.3	-11.83	-11.87±0.10	1.8	2	...	
003.1+05.2	K 6-26	17:33:07.1	-23:28:01	0	-12.5	-12.5±0.2	1.8	1	...	
004.6+06.0	H 1-24	17:33:37.6	-21:46:25	0.3	-11.67	-11.72±0.05	1.8	3	...	
357.1+01.2	K 6-2	17:33:50.9	-30:42:37	...	-12.06	...	1.8	2	...	4
000.3+03.2	PHR J1733-2655	17:33:52.8	-26:55:26	0.0	-12.17	-12.17±0.10	1.8	3	...	
350.9-02.9	Wray 16-287	17:34:20.0	-38:09:06	6.8	-11.50	-12.05±0.06	2.1	3	...	
003.8+05.3	H 2-15	17:34:26.8	-22:53:20	2.8	-11.95	-12.27±0.08	1.8	3	...	
336.9-11.5	MeWe 1-10	17:34:28.2	-54:28:58	0.3	-11.96	-12.00±0.08	1.9	3	...	
358.6+02.0	JaSt 2-1	17:34:29.2	-29:02:04	1.0	-11.93	-12.07±0.09	1.9	4	...	1
000.7+03.2	Hen 2-250	17:34:54.7	-26:35:57	0.9	-11.97	-12.10±0.07	1.8	3	...	
341.4-09.0	Hen 3-1428	17:35:02.5	-49:26:26	0.0	-11.52	-11.52±0.05	1.8	4	...	1,3
007.5+07.4	M 1-22	17:35:10.2	-18:34:20	0.9	-11.36	-11.48±0.05	1.8	2	...	
358.6+01.8	M 4-6	17:35:14.0	-29:03:10	0.3	-12.19	-12.24±0.12	1.8	5	...	
005.5+06.1	M 3-11	17:35:21.2	-20:57:18	0.8	-11.45	-11.56±0.05	1.8	4	...	V
003.6+04.9	K 5-6	17:35:31.2	-23:11:48	0.0	-12.4	-12.4±0.2	1.8	3	...	
343.5-07.8	PC 17	17:35:41.7	-46:59:49	0.0	-11.14	-11.14±0.05	1.8	3	1.1	
349.3-04.2	Lo 16	17:35:41.8	-40:11:26	0.1	-10.75	-10.76±0.04	2.1	4	...	6
359.8+02.4	Th 3-33	17:35:48.1	-27:43:20	1.4	-12.4	-12.6±0.2	1.8	3	...	
002.6+04.2	Th 3-27	17:35:58.5	-24:25:29	1.9	-11.99	-12.22±0.07	1.8	4	...	
341.5-09.1	Hen 2-248	17:36:06.9	-49:25:45	0.0	-11.72	-11.72±0.08	1.8	3	...	
005.2+05.6	M 3-12	17:36:22.6	-21:31:12	0.2	-11.41	-11.44±0.05	1.8	2	...	
350.1-03.9	H 1-26	17:36:29.7	-39:21:57	0.1	-11.23	-11.24±0.04	1.8	2	...	10
334.3-13.4	PHR J1736-5736	17:36:33.2	-57:36:21	...	-12.60	...	1.9	1	...	
358.3+01.2	BI B	17:36:59.8	-29:40:09	1.3	-12.12	-12.30±0.12	1.8	3	...	
007.6+06.9	M 1-23	17:37:22.0	-18:46:42	0.2	-11.42	-11.45±0.05	1.8	3	...	
...	PM 1-165	17:38:07.4	-27:20:15	...	-12.27	...	1.8	3	...	1

Table B2 – Continued

PNG	Name	RAJ2000	DEJ2000	$R_{[N\ II]}$	$\log F_{\text{red}}$	$\log F(\text{H}\alpha)$	r_{aper}	N_f	c_β	Note
007.0+06.3	M 1-24	17:38:11.6	-19:37:38	0.2	-11.14	-11.17±0.04	1.8	3	...	
004.9+04.9	M 1-25	17:38:30.3	-22:08:39	1.0	-10.91	-11.05±0.04	1.8	2	...	10
008.2+06.8	Hen 2-260	17:38:57.4	-18:17:36	0.5	-11.19	-11.26±0.04	1.8	2	...	V
353.4-02.4	K 5-8	17:39:17.2	-35:46:59	...	-12.21	...	1.8	4	...	4
351.1-03.9	PHR J1739-3829	17:39:17.2	-38:29:44	1.6	-11.80	-12.01±0.08	1.8	3	...	4,5
346.3-06.8	Fg 2	17:39:19.9	-44:09:37	0.4	-11.08	-11.14±0.04	1.8	3	...	
005.8+05.1	H 2-16	17:39:55.6	-21:14:13	1.8	-11.77	-11.99±0.06	1.8	2	...	
347.9-06.0	SB 31	17:40:03.3	-42:24:06	0.0	-12.1	-12.1±0.2	1.8	1	...	4
003.1+03.4	H 2-17	17:40:07.4	-24:25:43	1.0	-11.71	-11.84±0.06	1.8	3	...	V
001.2+02.1	Hen 2-262	17:40:12.8	-26:44:21	0.2	-12.04	-12.07±0.08	1.8	2	...	
005.0+04.4	H 1-27	17:40:17.9	-22:19:18	0.6	-11.66	-11.75±0.05	1.8	2	...	
001.0+01.9	K 1-4	17:40:27.4	-27:01:03	4.1	-11.25	-11.65±0.04	1.8	2	...	
355.5-01.4	RPZM 30	17:40:30.5	-33:29:57	0.2	-12.09	-12.12±0.12	1.8	4	...	4
010.1+07.4	Sab 21	17:41:04.0	-16:24:47	0.0	-12.03	-12.03±0.12	1.8	2	...	
005.2+04.2	M 3-13	17:41:36.6	-22:13:02	0.1	-11.92	-11.95±0.08	1.8	2	...	
005.7+04.5	PTB 5	17:41:38.6	-21:44:32	0.0	-12.08	-12.09±0.09	1.8	1	...	
003.1+02.9	Hb 4	17:41:52.8	-24:42:08	0.4	-10.85	-10.91±0.05	2.6	2	1.81	10
003.6+03.1	M 2-14	17:41:57.3	-24:11:16	1.5	-11.20	-11.40±0.04	1.8	3	...	
010.7+07.4	Sa 2-230	17:42:02.0	-15:56:07	0.1	-11.90	-11.91±0.08	1.8	2	...	
017.0+11.1	GLMP 621	17:42:14.4	-08:43:19	0.0	-11.55	-11.55±0.04	1.8	4	...	
...	Sab 15	17:42:25.7	-20:26:39	...	-12.07	...	1.8	2	...	1
...	CBF 1	17:42:32.4	-18:09:44	...	-12.24	...	1.8	2	...	1,N
350.5-05.0	H 1-28	17:42:54.1	-39:36:24	2.0	-11.67	-11.91±0.07	1.8	5	...	
006.3+04.4	H 2-18	17:43:28.8	-21:09:51	0.0	-12.07	-12.08±0.10	1.8	2	...	
003.5+02.7	PTB 1	17:43:39.3	-24:31:53	0.0	-12.19	-12.19±0.10	1.8	3	...	4
002.6+02.1	Terz N 1580	17:43:39.4	-25:36:43	1.3	-11.97	-12.15±0.08	1.8	2	...	4
006.1+04.1	IRAS 17411-2128	17:44:10.6	-21:29:21	...	-11.92	...	1.8	2	...	1
355.2-02.5	H 1-29	17:44:13.8	-34:17:33	0.4	-11.9	-12.0±0.2	1.8	5	...	10
355.4-02.4	M 3-14	17:44:20.6	-34:06:41	1.2	-11.32	-11.48±0.05	1.8	5	...	
353.6-03.6	K 6-11	17:44:35.4	-36:14:02	...	-12.15	...	1.8	4	...	4
011.1+07.0	Sa 2-237	17:44:42.3	-15:45:11	0.0	-11.20	-11.20±0.04	1.8	3	...	
352.0-04.6	H 1-30	17:45:06.8	-38:08:49	2.6	-11.66	-11.96±0.06	1.8	4	...	
009.3+05.7	Hen 3-1475	17:45:14.2	-17:56:47	0.0	-11.57	-11.57±0.05	1.8	2	...	1,3
002.8+01.8	Terz N 1567	17:45:28.3	-25:38:10	1.9	-11.89	-12.12±0.08	1.8	2	...	
346.2-08.2	IC 4663	17:45:28.4	-44:54:16	0.1	-10.84	-10.85±0.04	1.8	4	0.41	10
006.8+04.1	M 3-15	17:45:31.7	-20:58:02	0.2	-11.41	-11.44±0.04	1.8	3	...	10
345.2-08.8	IC 1266	17:45:35.3	-46:05:24	0.5	-9.98	-10.06±0.03	3.8	1	0.43	6,V
005.0+03.0	Pe 1-9	17:45:36.9	-23:02:27	0.2	-11.89	-11.92±0.09	1.8	2	...	
002.8+01.7	H 2-20	17:45:39.8	-25:40:00	1.2	-12.01	-12.17±0.09	1.8	2	...	V
358.9-00.7	M 1-26	17:45:57.7	-30:12:01	0.6	-10.04	-10.12±0.03	2.6	2	1.79	V
358.2-01.1	Bl D	17:46:02.8	-31:03:39	1.7	-11.90	-12.11±0.08	1.8	4	...	
355.6-02.7	H 1-32	17:46:06.3	-34:03:46	0.2	-11.34	-11.37±0.05	1.8	5	...	
008.8+05.2	Th 4-2	17:46:09.8	-18:39:31	0.7	-11.75	-11.85±0.06	1.8	1	...	
355.5-02.8	MPA J1746-3412	17:46:18.5	-34:12:37	...	-11.76	...	1.8	5	...	
007.5+04.3	Th 4-1	17:46:20.8	-20:13:48	0.0	-12.06	-12.06±0.13	1.8	3	...	
356.5-02.3	M 1-27	17:46:45.5	-33:08:35	0.7	-10.98	-11.08±0.04	1.8	4	2.16	10?
011.0+06.2	M 2-15	17:46:54.5	-16:17:25	0.1	-11.42	-11.44±0.04	1.8	2	0.9	
007.9+04.3	PTB 12	17:47:15.5	-19:57:28	0.1	-12.23	-12.25±0.14	1.8	3	...	4
005.1+02.6	PHR J1747-2311	17:47:30.7	-23:11:49	0.1	-12.2	-12.2±0.2	1.8	1	...	
004.3+02.1	K 5-17	17:47:31.9	-24:13:07	0.1	-11.95	-11.97±0.10	1.8	3	...	
006.3+03.3	H 2-22	17:47:33.9	-21:47:23	1.3	-11.84	-12.01±0.08	1.8	2	...	
006.0+03.1	M 1-28	17:47:38.3	-22:06:20	5.5	-11.03	-11.52±0.07	2.6	2	...	
355.7-03.0	H 1-33	17:47:49.4	-34:08:05	0.4	-11.41	-11.48±0.07	1.8	5	...	
352.6-04.9	SB 37	17:47:52.7	-37:48:03	0.1	-12.3	-12.3±0.2	1.8	4	...	
359.3-00.9	Hb 5	17:47:56.2	-29:59:42	1.8	-10.23	-10.45±0.03	2.6	2	1.93	
005.5+02.7	H 1-34	17:48:07.6	-22:46:47	0.9	-12.2	-12.3±0.2	1.8	2	...	
354.5-03.9	Sab 41	17:48:16.3	-35:38:31	0.9	-11.28	-11.41±0.05	1.9	5	...	
011.0+05.8	NGC 6439	17:48:19.8	-16:28:44	0.5	-10.91	-10.99±0.04	1.8	2	0.73	
004.3+01.8	H 2-24	17:48:36.5	-24:16:34	0.5	-11.74	-11.81±0.07	1.8	3	...	
006.0+02.8	Th 4-3	17:48:37.4	-22:16:49	0.8	-11.79	-11.91±0.07	1.8	2	...	
351.9-05.6	PHR J1748-3844	17:48:45.1	-38:44:14	1.7	-11.86	-12.08±0.11	1.8	5	...	1
002.2+00.5	Terz N 2337	17:48:45.3	-26:43:29	20:	-12.20	-13.1±0.3	1.8	2	...	C

Table B2 – Continued

PNG	Name	RAJ2000	DEJ2000	$R_{[N\ II]}$	$\log F_{\text{red}}$	$\log F(\text{H}\alpha)$	r_{aper}	N_f	c_β	Note
355.7−03.4	H 2-23	17:48:58.0	−34:21:53	0.1	−11.64	−11.65±0.10	1.8	3	...	
004.8+02.0	H 2-25	17:49:00.5	−23:42:55	0.5	−12.08	−12.16±0.14	1.8	2	...	V
355.7−03.5	H 1-35	17:49:13.9	−34:22:53	0.2	−10.66	−10.69±0.04	1.8	4	...	
008.0+03.9	NGC 6445	17:49:15.3	−20:00:34	1.8	−10.01	−10.24±0.03	3.4	2	1.64	6
343.2−10.8	BMP J1749-4848	17:49:49.7	−48:48:32	...	−12.17	...	1.8	3	...	4
359.1−01.7	M 1-29	17:50:18.0	−30:34:55	1.4	−10.96	−11.14±0.04	1.8	3	...	
009.0+04.1	Th 4-5	17:50:28.4	−19:03:12	0.3	−11.93	−11.98±0.09	1.8	2	...	
351.6−06.2	H 1-37	17:50:44.6	−39:17:26	1.1	−11.24	−11.39±0.05	1.8	5	...	
353.2−05.2	H 1-38	17:50:45.2	−37:23:54	2.2	−11.74	−12.00±0.13	1.8	3	...	
009.9+04.5	PHR J1750-1803	17:50:47.6	−18:03:30	2.5	−12.4	−12.7±0.2	1.8	2	...	4
354.6−04.5	PPA J1750-3548	17:50:56.1	−35:48:49	0.1	−11.81	−11.82±0.12	1.8	3	...	4
009.3+04.1	Th 4-6	17:50:57.2	−18:46:48	0.1	−11.91	−11.92±0.09	1.8	3	...	
355.4−04.0	Hf 2-1	17:51:12.2	−34:55:24	0.4	−11.40	−11.47±0.06	1.8	4	...	10
359.3−01.8	M 3-44	17:51:18.9	−30:23:53	1.0	−11.70	−11.83±0.10	1.8	2	...	10
358.5−02.5	Al 2-O	17:51:44.7	−31:36:00	1.1	−12.11	−12.25±0.13	1.8	2	...	4
356.5−03.6	H 2-27	17:51:50.6	−33:47:36	0.8	−12.11	−12.22±0.14	1.8	4	...	4
...	JaSt 2-8	17:52:03.8	−29:16:42	...	−12.07	...	1.8	1	...	4
010.4+04.5	M 2-17	17:52:04.9	−17:36:05	0.2	−11.43	−11.47±0.05	1.8	3	...	
359.7−01.8	M 3-45	17:52:05.9	−30:05:14	0.1	−11.59	−11.61±0.12	1.8	3	...	4
016.1+07.7	PTB 20	17:52:15.0	−11:10:37	0.2	−12.09	−12.11±0.08	1.8	2	...	
009.4+03.9	PTB 14	17:52:17.9	−18:52:04	0.0	−12.3	−12.3±0.2	1.8	3	...	4
006.8+02.3	Th 4-7	17:52:22.6	−21:51:13	0.3	−11.79	−11.84±0.10	1.8	3	...	4
357.4−03.2	M 2-16	17:52:34.4	−32:45:51	0.9	−11.32	−11.44±0.05	1.8	2	...	
006.4+02.0	M 1-31	17:52:41.4	−22:21:57	0.7	−11.22	−11.31±0.05	1.8	3	...	
359.1−02.3	M 3-16	17:52:46.1	−30:49:34	0.2	−11.47	−11.51±0.07	1.8	3	...	
345.3−10.2	MeWe 1-11	17:52:47.1	−46:42:02	2.1	−11.82	−12.07±0.08	1.9	2	...	
355.9−04.2	M 1-30	17:52:59.0	−34:38:23	1.4	−10.83	−11.01±0.05	1.8	4	...	
357.6−03.3	H 2-29	17:53:16.8	−32:40:39	0.8	−11.96	−12.07±0.15	1.8	2	...	
356.5−03.9	H 1-39	17:53:21.0	−33:55:58	0.6	−11.31	−11.39±0.05	1.8	3	...	V
006.3+01.7	PHR J1753-2234	17:53:28.3	−22:34:23	3.0	−12.04	−12.37±0.13	2.0	3	...	
036.0+17.6	Abell 43	17:53:32.3	10:37:24	0.0	−11.56	−11.56±0.05	2.1	2	0.72	
357.4−03.5	M 2-18	17:53:37.8	−32:58:48	0.3	−11.53	−11.57±0.05	1.8	1	...	
000.2−01.9	M 2-19	17:53:45.6	−29:43:46	0.6	−11.34	−11.43±0.06	1.8	3	2.1	
332.5−16.9	HaTr 7	17:54:09.4	−60:49:58	0.0	−11.30	−11.30±0.07	2.9	4	...	
012.2+04.9	PM 1-188	17:54:21.1	−15:55:52	0.6	−12.10	−12.18±0.11	1.8	3	...	10,V
000.4−01.9	M 2-20	17:54:25.4	−29:36:08	0.5	−11.26	−11.33±0.05	1.8	3	...	10
014.9+06.4	K 2-5	17:54:26.2	−12:48:36	1.6	−11.84	−12.04±0.07	1.8	2	...	6
356.2−04.4	Cn 2-1	17:54:33.0	−34:22:21	0.2	−10.89	−10.91±0.05	1.8	3	0.81	
001.6−01.3	Bl Q	17:54:34.9	−28:12:43	0.5	−11.71	−11.79±0.09	1.8	2	...	
358.7−03.0	K 6-34	17:54:41.3	−31:31:43	...	−11.76	...	1.8	2	...	
359.1−02.9	M 3-46	17:55:05.8	−31:12:16	2.3	−11.93	−12.20±0.12	1.8	2	...	
007.2+01.8	IC 4670	17:55:07.0	−21:44:40	0.6	−10.83	−10.92±0.04	1.8	3	2.11	
000.1−02.3	Bl 3-10	17:55:20.5	−29:57:36	0.1	−12.1	−12.1±0.2	1.8	1	...	
001.0−01.9	K 6-35	17:55:43.1	−29:04:05	0.2	−11.74	−11.76±0.11	1.8	2	...	
013.1+05.0	Sa 3-96	17:55:46.4	−15:02:44	3.0	−11.82	−12.15±0.06	1.8	4	...	
...	K 6-36	17:55:52.8	−30:15:41	...	−11.99	...	1.8	2	...	
009.3+02.8	Th 4-9	17:56:00.6	−19:29:27	0.7	−11.80	−11.91±0.09	1.8	4	...	
001.7−01.6	H 2-31	17:56:02.4	−28:14:11	1.0	−12.1	−12.3±0.2	1.6	1	...	V
000.9−02.0	Bl 3-13	17:56:02.8	−29:11:16	0.0	−11.78	−11.79±0.11	1.8	3	...	
011.9+04.2	M 1-32	17:56:20.0	−16:29:04	2.3	−10.74	−11.01±0.04	1.8	3	...	10
016.8+07.0	PTB 22	17:56:21.4	−10:57:36	0.0	−12.4	−12.4±0.2	1.8	3	...	
359.3−03.1	M 3-17	17:56:25.6	−31:04:17	0.6	−11.64	−11.73±0.09	1.8	2	...	10?
348.8−09.0	Hen 2-306	17:56:33.7	−43:03:19	0.0	−11.19	−11.19±0.04	1.8	3	...	
356.6−04.7	PHR J1756-3414	17:56:48.2	−34:14:32	...	−11.97	...	1.8	3	...	4
011.5+03.7	PTB 15	17:57:06.0	−17:11:10	0.0	−12.3	−12.3±0.2	1.8	3	...	4,6
010.6+03.2	Th 4-10	17:57:06.6	−18:06:43	0.9	−11.82	−11.94±0.08	1.8	1	...	
012.5+04.3	Sab 10	17:57:10.5	−15:56:18	1.5	−11.97	−12.16±0.10	1.8	3	...	4
356.7−04.8	H 1-41	17:57:19.2	−34:09:49	0.0	−11.20	−11.20±0.05	1.8	3	...	
357.2−04.5	H 1-42	17:57:25.2	−33:35:43	0.1	−10.94	−10.96±0.04	1.8	2	...	
011.8+03.7	PHR J1757-1649	17:57:39.6	−16:49:19	0.0	−11.18	−11.18±0.07	2.7	3	...	5,C
000.7−02.7	M 2-21	17:58:09.6	−29:44:20	0.1	−11.35	−11.36±0.05	1.8	3	0.9	
358.9−03.7	H 1-44	17:58:10.6	−31:42:56	1.3	−11.86	−12.03±0.10	1.8	2	...	

Table B2 – Continued

PNG	Name	RAJ2000	DEJ2000	$R_{[N II]}$	$\log F_{\text{red}}$	$\log F(\text{H}\alpha)$	r_{aper}	N_f	c_β	Note
359.4–03.4	H 2-33	17:58:12.5	–31:08:06	0.1	–12.0	–12.0±0.2	1.8	2	...	4,6
357.1–04.7	H 1-43	17:58:14.4	–33:47:38	0.9	–11.45	–11.57±0.05	1.8	3	...	10
000.4–02.9	M 3-19	17:58:19.3	–30:00:39	0.1	–11.69	–11.71±0.12	1.8	3	...	
007.7+01.2	PHR J1758-2139	17:58:24.9	–21:39:46	0.4	–11.62	–11.68±0.09	2.7	3	...	
357.8–04.4	PHR J1758-3304	17:58:25.9	–33:04:59	2.5	–11.77	–12.06±0.09	1.8	2	...	1
014.0+04.8	PTB 19	17:58:25.9	–14:25:25	0.0	–12.24	–12.24±0.13	1.8	4	...	4,6
002.5–01.7	Pe 2-11	17:58:31.2	–27:37:05	2.7	–12.3	–12.6±0.2	1.8	2	...	4
357.4–04.6	M 2-22	17:58:32.6	–33:28:37	0.9	–11.53	–11.65±0.06	1.8	2	...	
013.1+04.1	M 1-33	17:58:58.8	–15:32:15	0.6	–10.98	–11.06±0.04	1.8	4	...	
358.5–04.2	H 1-46	17:59:02.5	–32:21:43	0.2	–11.18	–11.21±0.04	1.8	1	...	
000.5–03.1	KFL 1	17:59:15.6	–30:02:47	0.1	–11.9	–11.9±0.2	1.8	3	...	4
002.1–02.2	M 3-20	17:59:19.3	–28:13:48	0.1	–11.39	–11.40±0.08	1.8	2	1.69	
003.0–01.7	PHR J1759-2712	17:59:33.2	–27:12:50	1.2	–11.35	–11.51±0.06	2.0	2	...	
357.7–04.8	BMP J1759-3321	17:59:45.2	–33:21:13	...	–10.70	...	5.5	2	...	
358.0–04.6	Sa 3-107	17:59:55.0	–32:59:12	...	–11.98	...	1.8	2	...	4
359.0–04.1	M 3-48	17:59:56.8	–31:54:27	3.0	–11.94	–12.26±0.13	1.8	2	...	
011.3+02.8	Th 4-11	18:00:08.8	–17:40:43	0.1	–11.15	–11.17±0.04	1.8	3	...	
352.9–07.5	Fg 3	18:00:11.8	–38:49:53	0.4	–10.22	–10.28±0.04	1.8	3	...	
356.8–05.4	H 2-35	18:00:18.3	–34:27:39	0.8	–12.1	–12.2±0.2	1.8	2	...	
002.1–02.4	PPA J1800-2818	18:00:18.8	–28:18:35	1.5	–11.75	–11.94±0.10	1.8	2	...	
001.2–03.0	H 1-47	18:00:37.6	–29:21:50	1.1	–11.49	–11.63±0.06	1.8	3	...	10?
340.4–14.1	Sa 1-6	18:00:59.4	–52:44:20	0.1	–11.73	–11.75±0.05	1.8	3	...	
014.2+04.2	Sa 3-111	18:01:07.1	–14:30:19	0.9	–11.97	–12.09±0.09	1.8	4	...	
002.8–02.2	Pe 2-12	18:01:10.3	–27:38:20	1.3	–11.62	–11.79±0.10	1.8	2	...	V
357.9–05.1	M 1-34	18:01:22.2	–33:17:43	2.3	–11.23	–11.50±0.05	1.8	2	...	
002.7–02.4	PPA J1801-2746	18:01:32.4	–27:46:07	4.0	–11.53	–11.93±0.08	1.8	1	...	
002.2–02.7	M 2-23	18:01:42.6	–28:25:44	0.1	–10.76	–10.77±0.04	1.8	2	1.08	
358.0–05.1	Pe 1-11	18:01:42.8	–33:15:26	4.3	–11.25	–11.67±0.05	1.8	2	...	
356.9–05.8	M 2-24	18:02:02.9	–34:27:47	0.2	–11.17	–11.20±0.05	1.8	3	1.35	
000.7–03.7	M 3-22	18:02:19.2	–30:14:25	0.0	–11.72	–11.72±0.11	1.8	3	...	
356.3–06.2	M 3-49	18:02:32.1	–35:13:15	2.1	–11.79	–12.04±0.10	1.8	2	...	
355.1–06.9	M 3-21	18:02:32.3	–36:39:12	0.3	–10.71	–10.76±0.04	1.8	1	0.65	
359.0–04.8	M 2-25	18:02:46.7	–32:09:30	2.0	–11.24	–11.48±0.05	1.8	2	...	
003.0–02.6	KFL 4	18:02:51.6	–27:41:00	...	–12.00	...	1.8	3	...	4
354.7–07.2	SB 40	18:02:55.7	–37:08:14	0.0	–11.78	–11.78±0.09	1.8	2	...	
003.6–02.3	M 2-26	18:03:11.8	–26:58:30	0.9	–11.49	–11.62±0.09	1.8	2	...	6
003.5–02.4	IC 4673	18:03:18.4	–27:06:23	0.1	–11.05	–11.08±0.05	1.8	3	0.96	
003.9–02.3	M 1-35	18:03:39.3	–26:43:33	0.8	–11.20	–11.31±0.05	1.8	3	1.81	
359.9–04.5	M 2-27	18:03:52.6	–31:17:47	0.7	–11.14	–11.24±0.04	1.8	3	1.59	
358.7–05.2	H 1-50	18:03:53.5	–32:41:42	0.3	–11.03	–11.08±0.04	1.8	3	...	
001.7–03.6	MPA J1804-2918	18:04:05.0	–29:18:47	...	–10.90	...	1.8	4	...	1
357.1–06.1	M 3-50	18:04:05.2	–34:28:37	2.3	–11.98	–12.25±0.14	1.8	4	...	
002.4–03.2	Wray 17-107	18:04:05.4	–28:27:51	1.9	–11.64	–11.87±0.09	1.8	3	...	
002.3–03.4	H 2-37	18:04:28.9	–28:37:35	0.5	–11.87	–11.95±0.13	1.8	3	...	
356.7–06.4	H 1-51	18:04:29.3	–34:58:01	1.0	–11.85	–11.98±0.14	1.8	4	...	
353.3–08.3	SB 39	18:04:31.6	–38:47:40	0.3	–12.0	–12.0±0.2	2.2	3	...	
347.4–11.4	FP J1804-4528	18:04:32.1	–45:28:28	1.0	–11.20	–11.34±0.06	4.9	3	...	1,6
358.6–05.5	M 3-51	18:04:56.2	–32:54:01	1.2	–11.76	–11.92±0.11	1.8	2	...	
354.4–07.8	H 1-52	18:04:57.6	–37:38:08	0.8	–11.78	–11.89±0.11	1.8	2	...	
000.3–04.6	M 2-28	18:05:02.7	–30:58:17	2.2	–11.43	–11.69±0.05	1.8	3	1.41	
001.7–03.8	ShWi 2-7	18:05:05.6	–29:20:12	0.8	–11.58	–11.69±0.08	1.8	4	1.44	
010.1+00.7	NGC 6537	18:05:13.1	–19:50:35	1.7	–10.25	–10.47±0.04	3.4	3	1.48	
356.4–06.8	SB 48	18:05:14.4	–35:28:08	0.0	–11.70	–11.70±0.13	1.8	3	...	
002.6–03.4	M 1-37	18:05:25.8	–28:22:04	0.9	–11.08	–11.20±0.05	1.8	3	1.29	10?,V
355.3–07.5	SB 42	18:05:52.6	–36:45:37	0.1	–11.91	–11.92±0.14	1.8	2	...	6
004.3–02.6	H 1-53	18:05:57.4	–26:29:42	1.2	–11.65	–11.80±0.07	1.8	3	...	
028.0+10.2	WeSb 3	18:06:00.8	00:22:39	0.0	–12.2	–12.2±0.2	1.8	5	...	
002.4–03.7	M 1-38	18:06:05.8	–28:40:29	0.7	–11.06	–11.16±0.04	1.8	3	1.15	10,V
004.0–03.0	M 2-29	18:06:40.9	–26:54:56	0.1	–11.45	–11.46±0.06	1.8	3	...	
357.6–06.5	PHR J1806-3416	18:06:46.3	–34:16:04	1.0	–11.89	–12.03±0.13	1.8	4	...	4
356.0–07.4B	SB 45	18:06:52.5	–36:06:43	0.0	–11.72	–11.72±0.10	1.8	2	...	4
010.2+00.3	PHR J1806-1956	18:06:55.3	–19:56:18	1.9	–12.2	–12.4±0.2	1.9	2	...	4

Table B2 – Continued

PNG	Name	RAJ2000	DEJ2000	$R_{[N\ II]}$	$\log F_{\text{red}}$	$\log F(\text{H}\alpha)$	r_{aper}	N_f	c_β	Note
019.8+05.6	CTS 1	18:06:59.8	-08:55:33	0.3	-11.84	-11.88±0.06	1.8	4	...	
000.9-04.8	M 3-23	18:07:06.2	-30:34:17	0.1	-11.40	-11.41±0.08	2.6	2	...	
002.1-04.2	H 1-54	18:07:07.2	-29:13:06	0.3	-11.01	-11.05±0.04	1.8	4	1.18	
001.7-04.4	H 1-55	18:07:14.5	-29:41:25	1.2	-11.51	-11.67±0.07	1.8	4	1.52	10,V
003.8-03.2	PHR J1807-2715	18:07:15.0	-27:15:51	0.8	-11.9	-12.1±0.2	1.8	3	...	4
342.5-14.3	Sp 3	18:07:15.8	-51:01:10	0.3	-10.33	-10.38±0.04	1.8	3	...	
359.9-05.4	KFL 9	18:07:19.4	-31:42:57	0.0	-12.1	-12.1±0.2	1.8	2	...	4
015.9+03.3	M 1-39	18:07:30.7	-13:28:48	1.7	-11.29	-11.50±0.04	1.8	3	...	
005.5-02.5	M 3-24	18:07:53.9	-25:24:03	0.4	-11.32	-11.38±0.06	1.8	3	...	
359.7-05.7	PHR J1808-3201	18:08:11.8	-32:01:28	3.3	-11.9	-12.2±0.2	2.9	2	...	1,4
008.3-01.1	M 1-40	18:08:26.0	-22:16:53	1.6	-11.12	-11.32±0.11	1.8	2	...	
000.1-05.6	H 2-40	18:08:30.6	-31:36:35	1.7	-11.74	-11.96±0.08	1.8	3	...	
000.5-05.3	SB 2	18:08:35.0	-31:06:51	0.4	-11.85	-11.90±0.11	1.8	3	...	
015.5+02.8	BMP J1808-1406	18:08:35.1	-14:06:43	4.8	-11.21	-11.66±0.08	5.3	3	...	
351.0-10.4	HaTr 9	18:08:58.9	-41:48:38	0.0	-11.20	-11.20±0.07	2.7	3	...	
005.9-02.6	MaC 1-10	18:09:12.9	-25:04:33	2.5	-11.41	-11.69±0.08	1.8	3	...	10
005.1-03.0	H 1-58	18:09:13.8	-26:02:29	0.4	-11.55	-11.62±0.07	1.8	2	...	
006.7-02.2	M 1-41	18:09:29.9	-24:12:23	4.9	-11.2	-11.6±0.2	2.3	1	...	
356.6-07.8	H 1-57	18:09:49.2	-35:44:13	1.0	-11.71	-11.85±0.12	1.8	3	...	
013.3+01.1	Sh 2-42	18:10:13.6	-16:47:49	...	-10.72	...	2.8	1	...	
018.9+04.1	M 3-52	18:10:26.4	-10:29:05	2.2	-12.7	-13.0±0.3	1.8	2	...	4
002.7-04.8	M 1-42	18:11:05.0	-28:58:59	0.8	-10.76	-10.88±0.05	2.6	2	0.9	
003.8-04.3	H 1-59	18:11:29.3	-27:46:16	0.3	-11.82	-11.86±0.09	1.8	2	...	
003.3-04.6	Ap 1-12	18:11:35.1	-28:22:37	0.8	-11.20	-11.31±0.05	1.8	3	...	10,V
009.8-01.1	PHR J1811-2100	18:11:39.0	-21:00:44	2.0	-11.55	-11.79±0.12	1.8	2	...	4
358.3-07.3	SB 52	18:11:39.9	-34:00:22	0.0	-11.79	-11.79±0.09	1.8	3	...	4
011.7+00.0	M 1-43	18:11:48.9	-18:46:22	0.1	-11.21	-11.23±0.07	1.8	3	...	
003.5-04.6	NGC 6565	18:11:52.5	-28:10:42	1.7	-10.44	-10.65±0.04	1.8	3	0.34	
358.5-07.3	NGC 6563	18:12:02.8	-33:52:07	3.2	-10.14	-10.48±0.03	2.8	2	0.34	
034.6+11.8	NGC 6572	18:12:06.4	06:51:12	0.3	-9.19	-9.23±0.04	7.9	1	0.41	10
018.9+03.6	M 4-8	18:12:09.6	-10:42:58	0.5	-11.91	-11.98±0.08	1.8	2	...	
000.7-06.1	SB 3	18:12:14.4	-31:19:59	0.2	-11.60	-11.63±0.07	1.9	2	...	
003.8-04.5	H 2-41	18:12:23.8	-27:52:14	0.2	-11.65	-11.68±0.10	1.8	3	...	
004.2-04.3	H 1-60	18:12:25.2	-27:29:13	0.0	-11.74	-11.74±0.10	1.8	3	...	
006.5-03.1	H 1-61	18:12:34.0	-24:50:00	1.1	-11.61	-11.76±0.12	1.8	4	...	
003.7-04.6	M 2-30	18:12:34.4	-27:58:12	0.1	-11.35	-11.36±0.07	1.8	3	0.41	
005.7-03.6	KFL 13	18:12:45.0	-25:44:24	0.5	-11.56	-11.63±0.07	1.8	3	...	
003.4-04.8	H 2-43	18:12:48.0	-28:19:60	0.5	-11.9	-12.0±0.2	1.8	3	...	1,4,6
351.7-10.9	Wray 16-385	18:12:52.9	-41:30:27	...	-12.02	...	1.8	3	...	4
001.6-05.9	SB 6	18:13:15.8	-30:25:58	2.5	-12.2	-12.5±0.2	1.8	3	...	4
006.0-03.6	M 2-31	18:13:16.0	-25:30:05	0.3	-11.17	-11.22±0.04	1.8	4	1.35	10
000.0-06.8	H 1-62	18:13:18.0	-32:19:43	1.0	-11.02	-11.16±0.04	1.8	2	...	V
006.4-03.4	PHR J1813-2505	18:13:27.0	-25:05:52	0.0	-12.03	-12.03±0.10	1.8	3	...	6
005.5-04.0	H 2-44	18:13:40.6	-26:08:39	0.0	-12.1	-12.1±0.2	1.8	3	...	4
011.7-00.6	NGC 6567	18:13:45.1	-19:04:34	0.1	-10.32	-10.33±0.04	1.8	4	0.45	
358.8-07.6	PHR J1814-3340	18:14:02.2	-33:40:48	1.0	-12.4	-12.6±0.3	1.8	2	...	4,5
001.1-06.4	SB 4	18:14:14.2	-31:11:09	0.6	-12.04	-12.12±0.14	1.8	1	...	4
024.2+05.9	M 4-9	18:14:18.4	-04:59:21	1.8	-11.09	-11.31±0.04	1.8	3	...	
006.2-03.7	KFL 15	18:14:19.3	-25:20:51	0.0	-11.91	-11.92±0.13	1.8	3	...	4
006.8-03.4	H 2-45	18:14:28.8	-24:43:38	0.0	-12.00	-12.00±0.15	1.6	1	...	
359.8-07.2	M 2-32	18:14:50.6	-32:36:55	0.0	-11.41	-11.41±0.05	1.8	2	...	
002.0-06.2	M 2-33	18:15:06.5	-30:15:33	0.0	-11.27	-11.28±0.05	1.8	4	...	
022.5+04.8	MA 2	18:15:13.4	-06:57:12	0.0	-12.27	-12.27±0.11	1.8	2	...	
019.7+03.2	M 3-25	18:15:17.0	-10:10:09	0.5	-11.52	-11.60±0.05	1.8	3	...	
006.5-03.9	PHR J1815-2513	18:15:23.8	-25:13:48	...	-12.05	...	1.8	2	...	
004.2-05.2	SB 8	18:15:50.4	-27:48:57	3.2	-11.83	-12.17±0.14	1.8	3	...	
004.8-05.0	M 3-26	18:16:11.4	-27:14:57	0.1	-11.49	-11.50±0.07	1.8	3	...	
001.5-06.7	SwSt 1	18:16:12.2	-30:52:09	0.4	-9.88	-9.93±0.03	2.6	2	...	10,V
010.8-01.8	NGC 6578	18:16:16.5	-20:27:03	0.1	-10.63	-10.65±0.05	1.8	4	1.40	
004.9-04.9	M 1-44	18:16:17.4	-27:04:32	1.0	-11.16	-11.30±0.04	1.8	3	0.77	V
002.2-06.3	H 1-63	18:16:19.3	-30:07:36	0.2	-11.00	-11.02±0.04	1.8	4	...	
007.8-03.7	M 2-34	18:17:15.9	-23:58:55	1.1	-11.58	-11.72±0.07	1.8	2	...	10

Table B2 – Continued

PNG	Name	RAJ2000	DEJ2000	$R_{[NII]}$	$\log F_{\text{red}}$	$\log F(\text{H}\alpha)$	r_{aper}	N_f	c_β	Note
038.2+12.0	Cn 3-1	18:17:34.1	10:09:04	0.9	-10.22	-10.34±0.03	3.8	2	0.44	6,V
000.7-07.4	M 2-35	18:17:37.2	-31:56:47	2.2	-11.49	-11.75±0.05	1.8	2	...	5,6
003.2-06.2	M 2-36	18:17:41.4	-29:08:20	0.5	-10.78	-10.86±0.04	1.8	4	...	
...	Sa 3-128	18:17:47.5	-24:02:39	...	-11.77	...	1.8	4	...	
006.3-04.6	PPA J1818-2541	18:18:01.5	-25:41:02	0.5	-12.1	-12.2±0.2	1.8	3	...	
...	Hen 2-375	18:18:09.0	-57:11:13	0.0	-10.12	-10.12±0.03	4.6	1	...	1,2
008.4-03.6	H 1-64	18:18:23.9	-23:24:57	0.9	-11.51	-11.64±0.11	1.8	3	...	1,V
348.0-13.8	IC 4699	18:18:32.0	-45:59:02	0.0	-11.19	-11.19±0.04	1.8	2	0.14	
000.8-07.6	H 2-46	18:18:37.4	-31:54:45	1.1	-12.00	-12.15±0.11	1.8	2	...	
004.2-05.9	M 2-37	18:18:38.4	-28:08:01	0.5	-11.65	-11.72±0.07	1.8	3	...	
006.6-04.7	PHR J1818-2531	18:18:50.7	-25:31:36	0.1	-11.83	-11.85±0.13	1.8	4	...	
009.1-03.4	PHR J1818-2239	18:18:58.8	-22:39:39	0.7	-10.91	-11.01±0.06	3.0	2	...	1
015.5-00.0	PHR J1818-1526	18:18:59.2	-15:26:21	6.5	-12.4	-12.8±0.2	1.3	1	...	1
005.7-05.3	M 2-38	18:19:25.2	-26:35:20	0.3	-11.61	-11.65±0.06	1.8	3	...	
359.4-08.5	SB 55	18:19:26.3	-33:37:05	0	-11.94	-11.94±0.11	1.8	3	...	
007.8-04.4	H 1-65	18:20:08.9	-24:15:05	0.9	-11.25	-11.37±0.05	1.8	4	...	10,V
011.0-02.9	CGMW 3-2111	18:20:53.8	-20:48:12	0.1	-12.05	-12.06±0.11	1.8	3	...	4
008.7-04.2	PHR J1821-2324	18:21:08.9	-23:24:08	0.3	-11.90	-11.95±0.10	1.8	1	...	4
...	MWC 922	18:21:15.9	-13:01:27	0.1	-11.45	-11.46±0.09	1.8	3	...	3
021.9+02.7	MaC 1-12	18:21:21.1	-08:31:42	0.1	-11.68	-11.70±0.05	1.8	3	...	
024.1+03.8	M 2-40	18:21:23.9	-06:01:56	0.7	-11.37	-11.47±0.04	1.8	4	...	
020.6+01.9	PHR J1821-1001	18:21:40.6	-10:01:44	1.5	-11.23	-11.43±0.07	2.9	4	...	1
008.1-04.7	M 2-39	18:22:01.2	-24:10:40	0.2	-11.33	-11.36±0.05	1.8	3	...	
008.2-04.8	M 2-42	18:22:32.0	-24:09:28	0.2	-11.36	-11.39±0.05	1.8	3	...	
002.3-07.8	M 2-41	18:22:34.4	-30:43:30	2.0	-11.29	-11.53±0.04	1.8	4	...	
005.8-06.1	NGC 6620	18:22:54.2	-26:49:17	1.2	-10.94	-11.10±0.04	1.8	2	0.53	
012.6-02.7	M 1-45	18:23:08.0	-19:17:05	1.0	-11.50	-11.64±0.07	1.8	3	...	
032.9+07.8	K 3-1	18:23:21.7	03:36:28	0.0	-11.86	-11.86±0.07	1.8	3	...	
026.9+04.4	FP J1824-0319	18:24:40.9	-03:19:59	0.9	-10.27	-10.42±0.05	14.7	1	...	
032.1+07.0	PC 19	18:24:44.5	02:29:28	0.0	-11.36	-11.36±0.04	1.8	3	...	
007.0-06.0	H 1-66	18:24:57.5	-25:41:56	0.6	-11.42	-11.46±0.05	1.8	2	...	
030.6+06.2	Sh 2-68	18:24:58.5	00:51:37	1.7	-10.15	-10.36±0.04	10.3	4	...	1,8
028.5+05.1	K 3-2	18:25:00.6	-01:30:53	1.0	-11.85	-11.99±0.05	1.8	3	...	
009.8-04.6	H 1-67	18:25:05.0	-22:34:53	0.4	-11.39	-11.46±0.07	1.8	2	...	10?
009.4-05.5	NGC 6629	18:25:42.5	-23:12:11	0.1	-10.16	-10.17±0.03	2.6	1	0.88	6,10?
013.8-02.8	SaWe 3	18:26:04.3	-18:12:32	6.2	-10.81	-11.33±0.04	2.3	2	...	
027.6+04.2	M 2-43	18:26:40.1	-02:42:58	0.3	-11.27	-11.31±0.04	1.8	3	...	10
353.7-12.8	Wray 16-411	18:26:41.8	-40:29:53	0.0	-11.91	-11.91±0.06	1.8	4	...	
031.2+05.9	K 3-3	18:27:09.3	01:14:27	0.1	-12.03	-12.04±0.08	1.8	4	...	
017.6-01.1	VSP 2-18	18:27:13.5	-14:08:33	0.3	-11.80	-11.84±0.12	1.8	4	...	
024.6+02.5	BMP J1827-0611	18:27:16.4	-06:11:51	...	-12.17	...	2.6	4	...	1,4
043.3+11.6	M 3-27	18:27:48.3	14:29:06	0.1	-10.81	-10.82±0.04	1.8	1	1.74	1,N
356.8-11.7	Lo 17	18:27:49.9	-37:15:52	0.4	-11.44	-11.50±0.05	2.3	3	...	
016.4-01.9	M 1-46	18:27:56.3	-15:32:54	0.6	-10.59	-10.69±0.04	1.8	3	...	V
007.0-06.8	Vy 2-1	18:27:59.6	-26:06:48	0.5	-10.85	-10.92±0.04	1.8	2	...	
022.5+01.0	MaC 1-13	18:28:35.2	-08:43:23	3.3	-11.74	-12.09±0.05	1.8	3	...	
011.0-05.1	M 1-47	18:29:11.2	-21:46:53	0.0	-11.24	-11.24±0.05	1.8	2	...	
014.9-03.1	SaSt 3-166	18:29:11.3	-17:27:13	1.0	-11.45	-11.59±0.06	1.8	2	...	
002.2-09.4	Cn 1-5	18:29:11.7	-31:29:59	1.8	-10.45	-10.68±0.04	1.8	2	0.23	10
013.4-03.9	M 1-48	18:29:30.0	-19:05:45	2.6	-11.35	-11.64±0.08	1.8	3	...	
013.0-04.3	Pe 2-14	18:29:59.6	-19:40:38	0.2	-11.50	-11.52±0.07	1.8	3	...	
011.8-05.0	PM 1-239	18:30:07.7	-21:05:03	0.0	-11.86	-11.86±0.11	1.8	2	...	4
015.6-03.0	Abell 44	18:30:11.2	-16:45:26	1.9	-11.26	-11.49±0.06	1.8	2	...	
020.2-00.6	Abell 45	18:30:15.4	-11:36:57	5.1	-10.80	-11.26±0.10	4.8	2	...	
...	V-V 3-4	18:30:34.1	-19:14:46	...	-11.68	...	1.8	3	...	
032.7+05.6	K 3-4	18:31:00.2	02:25:27	0.8	-11.75	-11.86±0.05	1.8	1	...	6
009.3-06.5	SB 15	18:31:14.6	-23:58:05	0.0	-12.02	-12.03±0.11	1.8	3	...	4
034.3+06.2	K 3-5	18:31:45.8	04:05:09	0.0	-12.06	-12.06±0.08	1.8	3	...	
018.0-02.2	PTB 23	18:31:50.6	-14:15:29	0.0	-11.8	-11.8±0.2	1.9	3	...	
008.6-07.0	Hen 2-406	18:31:52.8	-24:46:17	2.4	-11.82	-12.10±0.11	1.8	3	...	
018.8-01.9	PTB 25	18:32:04.5	-13:26:08	0.0	-11.75	-11.76±0.09	1.8	3	...	
005.1-08.9	Hf 2-2	18:32:30.9	-28:43:20	0.1	-11.28	-11.30±0.04	1.8	3	...	

Table B2 – Continued

PNG	Name	RAJ2000	DEJ2000	$R_{[N\ II]}$	$\log F_{\text{red}}$	$\log F(\text{H}\alpha)$	r_{aper}	N_f	c_β	Note
027.8+02.7	PHR J1832-0317	18:32:31.3	-03:17:45	2.7	-12.30	-12.60±0.10	1.8	2	...	4
008.3-07.3	NGC 6644	18:32:34.6	-25:07:44	0.2	-10.43	-10.45±0.04	3.0	2	0.25	
021.8-00.4	M 3-28	18:32:41.3	-10:05:50	3.9	-11.53	-11.92±0.05	1.8	3	...	
021.7-00.6	M 3-55	18:33:14.8	-10:15:19	3.4	-12.26	-12.61±0.10	1.8	3	...	
031.0+04.1	K 3-6	18:33:17.5	00:11:47	0.2	-12.29	-12.31±0.11	1.8	2	...	
014.6-04.3	M 1-50	18:33:20.9	-18:16:37	0.1	-11.23	-11.24±0.07	2.6	1	...	
020.9-01.1	M 1-51	18:33:29.0	-11:07:26	1.8	-11.35	-11.58±0.05	1.8	2	...	10
002.9-10.2	PHR J1833-3115	18:33:42.8	-31:15:43	0.1	-12.05	-12.07±0.13	1.8	1	...	4
010.7-06.4	IC 4732	18:33:54.6	-22:38:41	0.1	-10.94	-10.95±0.04	1.8	2	0.43	
017.7-02.9	M 1-52	18:33:58.5	-14:52:25	0.1	-11.68	-11.70±0.11	1.8	3	...	
025.6+01.1	PHR J1833-0556	18:33:59.7	-05:56:07	1.0	-12.36	-12.50±0.14	1.8	2	...	1,4
044.3+10.4	We 3-1	18:34:02.3	14:49:10	0.0	-11.39	-11.39±0.07	2.5	1	...	
028.7+02.7	K 3-7	18:34:13.6	-02:27:36	0.0	-12.06	-12.06±0.08	1.2	1	...	
010.7-06.7	Pe 1-13	18:34:51.7	-22:43:17	0.0	-11.94	-11.94±0.08	1.8	3	...	
006.8-08.6	Al 1	18:34:55.3	-27:06:18	0.0	-12.07	-12.07±0.12	1.8	2	...	
027.0+01.5	PHR J1835-0429	18:35:11.6	-04:29:06	0.0	-11.50	-11.50±0.05	1.8	3	...	
030.8+03.4	Abell 47	18:35:22.6	00:13:50	0.6	-12.5	-12.6±0.2	1.8	3	...	4
006.2-09.1	CGMW 4-1723	18:35:44.6	-27:51:21	0.0	-12.09	-12.09±0.12	1.8	2	...	
015.4-04.5	M 1-53	18:35:48.3	-17:36:09	0.0	-11.23	-11.23±0.05	1.8	3	...	
016.0-04.3	M 1-54	18:36:08.4	-16:59:57	2.8	-10.62	-10.93±0.04	2.6	2	...	
014.0-05.5	Sa 1-7	18:36:32.3	-19:19:28	0.1	-11.37	-11.38±0.05	1.8	4	...	
011.7-06.6	M 1-55	18:36:33.8	-21:49:03	0.9	-11.07	-11.20±0.04	1.8	3	0.71	5,V
014.3-05.5	V-V 3-6	18:37:11.1	-19:02:22	0.2	-11.58	-11.61±0.06	1.8	4	...	
028.5+01.6	M 2-44	18:37:36.9	-03:05:56	0.7	-11.42	-11.52±0.06	1.8	3	...	
016.1-04.7	M 1-56	18:37:46.3	-17:05:47	0.5	-11.35	-11.42±0.06	1.8	4	...	
005.9-09.8	CGMW 4-2031	18:37:54.6	-28:27:31	1.2	-12.09	-12.25±0.10	1.8	1	...	4
027.7+00.7	M 2-45	18:39:21.8	-04:19:51	0.4	-11.90	-11.97±0.09	1.8	4	...	
004.0-11.1	M 3-29	18:39:25.8	-30:40:37	0.3	-11.17	-11.22±0.04	1.8	2	...	
014.4-06.1	SB 19	18:39:40.1	-19:14:12	0.0	-12.3	-12.3±0.2	1.8	5	...	
011.1-07.9	SB 17	18:40:19.9	-22:54:29	1.2	-12.26	-12.43±0.15	1.8	2	...	3,(10),C
022.1-02.4	M 1-57	18:40:20.3	-10:39:47	1.8	-11.16	-11.38±0.04	1.8	5	...	
...	PM 1-248	18:40:22.0	-31:56:49	0.1	-11.80	-11.82±0.07	1.8	2	...	3
...	PM 2-37	18:40:48.6	-17:04:38	...	-12.30	...	1.8	4	...	3
005.2-10.8	PPA J1840-2931	18:40:50.6	-29:31:23	0.1	-11.73	-11.75±0.06	1.8	2	...	
023.8-01.7	K 3-11	18:41:07.3	-08:55:59	0.8	-12.3	-12.4±0.2	1.8	4	...	4
017.9-04.8	M 3-30	18:41:14.9	-15:33:44	0.2	-11.47	-11.50±0.06	1.8	4	1.03	10
019.2-04.4	PM 1-251	18:42:24.8	-14:15:12	0.0	-12.07	-12.07±0.11	1.8	4	...	
029.0+00.4	Abell 48	18:42:46.9	-03:13:17	0.3	-11.47	-11.52±0.06	1.8	3	...	10
022.0-03.1	M 1-58	18:42:57.0	-11:06:53	0.1	-11.24	-11.26±0.04	1.8	4	...	
031.7+01.7	PC 20	18:43:03.5	00:16:37	1.1	-12.11	-12.26±0.09	1.8	5	...	
023.9-02.3	M 1-59	18:43:20.2	-09:04:49	1.1	-10.78	-10.93±0.04	1.8	3	...	
019.7-04.5	M 1-60	18:43:38.1	-13:44:49	0.8	-11.10	-11.21±0.04	1.8	4	...	10
029.8+00.5	PHR J1843-0232	18:43:56.9	-02:32:08	4.0	-11.79	-12.18±0.07	1.9	3	...	
026.8-01.0	MPA J1843-0556	18:43:57.9	-05:56:20	...	-11.65	...	1.8	4	...	
014.2-07.3	M 3-31	18:44:01.8	-19:54:53	0.1	-11.46	-11.48±0.05	1.8	2	...	5,6
004.7-11.8	Hen 2-418	18:44:14.6	-30:19:37	0.0	-11.80	-11.80±0.08	1.8	3	...	
009.4-09.8	M 3-32	18:44:43.1	-25:21:34	0.1	-11.62	-11.64±0.05	1.8	3	...	5,6
027.6-00.8	PHR J1844-0503	18:44:45.7	-05:03:54	2.3	-11.72	-11.99±0.08	1.8	2	...	
027.4-00.9	PHR J1844-0517	18:44:54.0	-05:17:36	5.0	-11.95	-12.41±0.12	1.8	3	...	1,4
011.3-09.1	PTB 32	18:45:10.8	-23:21:50	1.1	-11.67	-11.82±0.09	2.4	3	...	6
013.8-07.9	PC 21	18:45:35.2	-20:34:58	0.0	-11.44	-11.44±0.05	1.8	4	...	
026.6-01.5	K 4-5	18:45:36.7	-06:18:40	3.9	-11.37	-11.76±0.07	1.8	3	...	
002.0-13.4	IC 4776	18:45:51.1	-33:20:40	0.2	-10.24	-10.26±0.04	3.5	1	0.03	
019.4-05.3	M 1-61	18:45:55.1	-14:27:38	0.4	-10.58	-10.64±0.04	1.8	4	...	
024.8-02.7	M 2-46	18:46:34.6	-08:28:02	1.3	-11.55	-11.72±0.07	1.8	2	...	V
011.3-09.4	My 121	18:46:35.2	-23:26:48	0.6	-10.48	-10.56±0.04	1.8	3	...	V
022.0-04.3	AS 321	18:47:04.0	-11:41:12	1.0	-11.37	-11.51±0.04	1.8	3	...	3
026.3-02.2	Pe 1-16	18:47:32.3	-06:54:04	0.4	-11.43	-11.49±0.05	1.8	3	...	5,6
030.5-00.2	PHR J1847-0215	18:47:47.4	-02:15:30	4.0	-12.6	-13.0±0.2	1.8	2	...	
024.3-03.3	Pe 1-17	18:47:48.8	-09:09:07	1.5	-11.88	-12.07±0.08	1.8	4	...	
...	IPHASX J1848+0254	18:48:00.7	02:54:17	...	-12.00	...	1.9	2	...	1
016.0-07.6	SB 21	18:48:11.3	-18:29:43	0.0	-12.3	-12.3±0.2	1.8	2	...	4

Table B2 – Continued

PNG	Name	RAJ2000	DEJ2000	$R_{[NII]}$	$\log F_{\text{red}}$	$\log F(\text{H}\alpha)$	r_{aper}	N_f	c_β	Note
009.6–10.6	M 3-33	18:48:12.1	–25:28:52	0.0	–11.41	–11.41±0.04	1.8	3	...	
024.4–03.5	PHR J1848-0912	18:48:32.7	–09:12:02	1.8	–12.25	–12.48±0.12	1.8	4	...	
042.0+05.4	K 3-14	18:48:32.8	10:35:51	0.8	–11.57	–11.68±0.05	1.8	2	...	
028.5–01.4	PHR J1848-0435	18:48:40.7	–04:35:58	4.0	–12.10	–12.50±0.09	1.8	2	...	4
027.3–02.1	Pe 1-18	18:48:46.5	–05:56:08	0.5	–12.0	–12.0±0.2	1.8	3	...	4
014.8–08.4	PHR J1849-1952	18:49:24.2	–19:52:14	0.0	–12.10	–12.10±0.10	1.8	4	...	
026.5–03.0	Pe 1-19	18:49:44.6	–07:01:35	0.1	–11.55	–11.56±0.08	1.8	2	...	
031.3–00.5	HaTr 10	18:50:24.8	–01:40:20	6.5	–11.86	–12.39±0.07	1.8	2	...	
012.5–09.8	M 1-62	18:50:26.0	–22:34:23	0.0	–11.36	–11.36±0.05	1.8	3	...	
031.9–00.3	WeSb 4	18:50:40.3	–01:03:11	8.0	–11.70	–12.31±0.07	1.8	3	...	
020.7–05.9	Sa 1-8	18:50:44.3	–13:31:02	0.0	–11.42	–11.42±0.05	1.8	3	...	
044.1+05.8	CTSS 2	18:50:46.8	12:37:30	0.0	–12.5	–12.5±0.2	1.8	1	...	4
021.1–05.9	M 1-63	18:51:30.9	–13:10:37	1.8	–11.30	–11.53±0.04	1.8	2	...	
026.2–03.4	PHR J1851-0732	18:51:31.3	–07:32:29	0.4	–11.38	–11.44±0.06	1.8	2	...	
032.5–00.3	Te 7	18:51:47.5	00:28:29	2.7	–12.31	–12.61±0.13	1.8	1	...	4
044.0+05.2	K 3-16	18:53:01.6	12:15:59	0.2	–12.6	–12.6±0.2	1.8	1	...	
027.3–03.4	Abell 49	18:53:28.3	–06:28:47	1.3	–11.55	–11.72±0.06	1.8	1	...	
027.4–03.5	Vy 1-4	18:54:01.9	–06:26:20	0.0	–11.23	–11.23±0.04	1.8	2	...	
020.4–07.0	MPA J1854-1420	18:54:14.7	–14:20:19	...	–11.74	...	2.6	3	...	1
024.2–05.2	M 4-11	18:54:17.7	–10:05:14	0.1	–11.21	–11.23±0.04	1.8	3	...	
025.3–04.6	K 4-8	18:54:20.0	–08:47:33	0.1	–11.68	–11.70±0.07	1.8	3	...	
025.4–04.7	IC 1295	18:54:37.2	–08:49:39	0.1	–10.63	–10.65±0.04	2.1	3	...	
031.6–01.5	PHR J1854-0151	18:54:41.2	–01:51:15	1.6	–11.97	–12.17±0.10	1.8	1	...	
...	LSE 67	18:54:45.7	–29:21:12	...	–12.25	...	1.8	3	...	1
038.7+01.9	YM 16	18:54:57.3	06:02:31	5.2	–11.03	–11.50±0.06	3.9	3	...	
012.1–11.2	CGMW 4-3783	18:55:04.9	–23:28:12	0.1	–11.83	–11.84±0.07	1.8	3	...	
013.7–10.6	Y-C 2-32	18:55:30.7	–21:49:39	0.0	–11.51	–11.51±0.05	1.8	3	...	
003.9–14.9	Hb 7	18:55:38.0	–32:15:47	0.0	–10.77	–10.77±0.04	1.8	2	...	
032.0–01.7	CBSS 2	18:56:15.7	–01:34:00	0.2	–11.88	–11.92±0.09	1.8	2	...	4
039.8+02.1	K 3-17	18:56:18.2	07:07:26	1.0	–12.06	–12.19±0.09	1.8	2	...	
...	Fr 2-27	18:56:27.8	–31:11:19	...	–10.10	...	tba	2	...	1,N
043.1+03.8	M 1-65	18:56:33.6	10:52:10	0.5	–11.26	–11.34±0.04	1.8	2	1.1	V
023.8–06.2	BMP J1857-1054	18:57:09.8	–10:54:51	...	–11.91	–	3.0	3	...	1
028.7–03.9	Pe 1-21	18:57:49.6	–05:27:40	0.0	–12.12	–12.12±0.11	1.8	2	...	4
020.7–08.0	MPA J1858-1430	18:58:19.3	–14:30:26	...	–12.18	–	3.1	3	...	4
032.7–02.0	M 1-66	18:58:26.3	–01:03:46	0.3	–11.17	–11.22±0.04	1.8	2	...	5,6
033.2–01.9	Sa 3-151	18:58:51.7	00:32:55	...	–11.88	...	1.8	2	...	5,6
033.7–02.0	CBSS 1	19:00:16.1	00:14:33	0.0	–12.12	–12.12±0.13	1.8	4	...	
032.0–03.0	K 3-18	19:00:34.8	–02:11:58	0.5	–11.98	–12.05±0.08	1.8	3	...	V
017.6–10.2	Abell 51	19:01:01.1	–18:12:15	0.0	–11.56	–11.56±0.05	1.9	2	0.0	5,6
023.3–07.6	MaC 1-16	19:01:21.8	–11:58:20	1.9	–11.78	–12.00±0.05	1.8	3	...	
032.9–02.8	K 3-19	19:01:36.6	–01:19:08	0.5	–11.84	–11.91±0.07	1.8	3	...	
035.9–01.1	Sh 2-71	19:01:59.3	02:09:18	5.1	–10.38	–10.89±0.09	5.1	1	...	
032.5–03.2	K 3-20	19:02:10.2	–01:48:45	0.9	–11.65	–11.77±0.05	1.8	2	...	V
014.7–11.8	SaWe 4	19:02:16.1	–21:26:51	...	–11.82	...	2.1	3	...	
043.3+02.2	PM 1-276	19:02:17.9	10:17:34	0.0	–11.93	–11.93±0.08	1.8	2	...	
033.8–02.6	NGC 6741	19:02:37.1	00:26:57	1.3	–10.45	–10.63±0.04	1.8	4	0.73	
036.9–01.1	HaTr 11	19:02:59.4	03:02:21	1.7	–11.97	–12.19±0.09	1.8	3	...	4
046.8+03.8	Sh 2-78	19:03:10.1	14:06:59	4.0	–10.33	–10.72±0.04	7.0	2	...	
...	IRAS 19021+0209	19:04:38.4	02:14:23	...	–11.85	...	1.8	3	...	1
013.1–13.2	GLMP 869	19:04:43.6	–23:26:09	...	–12.35	...	1.8	1	...	1,3,4
...	IPHASX J1905+1613	19:05:12.4	16:13:47	...	–12.88	...	1.9	1	...	1
003.8–17.1	Hb 8	19:05:36.4	–33:11:39	0.1	–11.37	–11.39±0.04	1.8	2	...	
029.2–05.9	NGC 6751	19:05:55.6	–05:59:33	1.0	–10.50	–10.64±0.04	2.6	2	0.5	10
033.2–04.0	PHR J1906-0133	19:06:16.3	–01:33:10	1.6	–11.73	–11.93±0.10	2.7	3	...	1
044.1+01.5	PM 1-281	19:06:32.2	10:43:24	...	–12.25	...	1.8	3	...	4
019.7–10.7	MPA J1906-1634	19:06:32.8	–16:34:00	...	–11.57	...	3.4	2	...	
040.3–00.4	Abell 53	19:06:45.9	06:23:52	1.4	–11.42	–11.61±0.04	1.8	4	1.71	
341.2–24.6	Lo 18	19:09:47.8	–55:35:11	3.0	–11.79	–12.12±0.05	1.8	4	...	
033.0–05.3	Abell 55	19:10:25.8	–02:20:23	1.0	–11.22	–11.35±0.04	1.9	2	...	
020.9–11.3	PHR J1911-1546	19:11:04.4	–15:46:07	0.5	–11.29	–11.37±0.07	2.7	2	...	
025.4–09.2	PHR J1911-1049	19:11:06.7	–10:49:18	0.5	–12.26	–12.33±0.11	1.8	2	...	4

Table B2 – Continued

PNG	Name	RAJ2000	DEJ2000	$R_{[N\ II]}$	$\log F_{\text{red}}$	$\log F(\text{H}\alpha)$	r_{aper}	N_f	c_β	Note
035.6–04.2	MPA J1911+0027	19:11:24.8	00:27:45	...	-12.00	...	1.8	3	...	
047.2+01.7	PM 1-286	19:11:35.8	13:31:12	0.3	-12.05	-12.10±0.08	1.8	1	...	
044.7+00.2	AGP 1	19:12:16.1	10:36:33	2.6	-12.26	-12.56±0.11	1.8	2	...	
...	FP J1912-0331	19:12:31.4	-03:31:32	...	-10.36	...	11.3	2	...	1,4,N
049.4+02.4	Hen 2-428	19:13:05.2	15:46:40	0.6	-11.37	-11.45±0.04	1.8	1	...	
037.9–03.4	Abell 56	19:13:06.1	02:52:48	...	-11.02	...	3.3	1	...	
038.4–03.3	K 4-19	19:13:22.6	03:25:00	0.6	-12.27	-12.36±0.14	1.8	1	...	4
039.5–02.7	M 2-47	19:13:34.6	04:38:04	0.1	-11.44	-11.46±0.05	1.8	3	...	
044.9+00.0	AGP 2	19:13:37.2	10:39:31	5.4	-12.21	-12.68±0.11	1.8	2	...	
048.7+01.9	Hen 2-429	19:13:38.4	14:59:19	0.9	-11.26	-11.39±0.04	1.8	1	...	10
038.7–03.3	M 1-69	19:13:54.0	03:37:42	0.3	-11.30	-11.34±0.05	1.8	2	...	
029.8–07.8	LSA 1	19:13:55.7	-06:18:52	0.1	-12.17	-12.19±0.13	1.8	2	...	
013.7–15.3	We 4-5	19:14:11.5	-23:41:28	0.0	-11.99	-11.99±0.08	1.8	3	...	
005.2–18.6	StWr 2-21	19:14:23.3	-32:34:17	0.0	-12.06	-12.07±0.10	1.8	3	...	10,C
033.1–06.3	NGC 6772	19:14:36.4	-02:42:25	0.7	-10.54	-10.64±0.04	2.1	2	1.81	
035.7–05.0	K 3-26	19:14:39.2	00:13:36	0.1	-11.79	-11.81±0.06	1.8	3	...	6
048.1+01.1	K 3-29	19:15:30.6	14:03:50	0.7	-12.19	-12.28±0.10	1.8	1	...	4
040.4–03.1	K 3-30	19:16:27.7	05:13:19	0.1	-11.77	-11.78±0.07	1.8	3	...	
027.6–09.6	IC 4846	19:16:28.2	-09:02:37	0.1	-10.74	-10.75±0.04	1.8	3	0.42	
019.4–13.6	DeHt 3	19:17:04.2	-18:01:37	1.5	-11.48	-11.68±0.05	1.8	3	...	
358.3–21.6	IC 1297	19:17:23.5	-39:36:46	0.2	-10.47	-10.50±0.04	1.8	2	0.00	10
043.2–02.0	PM 2-40	19:17:50.6	08:15:08	...	-11.89	...	1.8	2	...	
025.9–10.9	Na 2	19:18:19.5	-11:06:15	1.6	-11.58	-11.79±0.05	1.8	3	...	
037.5–05.1	Abell 58	19:18:20.5	01:46:60	1.5	-12.17	-12.37±0.11	1.8	1	...	4,10,C
034.5–06.7	NGC 6778	19:18:24.9	-01:35:47	1.1	-10.42	-10.57±0.04	1.8	3	0.42	
041.8–02.9	NGC 6781	19:18:28.1	06:32:19	2.7	-9.80	-10.10±0.03	6.0	2	2.03	
025.0–11.6	Abell 60	19:19:17.8	-12:14:37	1.5	-11.75	-11.94±0.05	2.0	3	...	
043.0–03.0	M 4-14	19:21:00.7	07:36:52	2.4	-11.55	-11.82±0.05	1.8	3	...	
037.7–06.0	MPA J1921+0132	19:21:44.5	01:32:41	...	-12.30	...	1.8	2	...	4,10
006.8–19.8	Wray 16-423	19:22:10.6	-31:30:39	0.1	-11.56	-11.58±0.05	1.8	2	...	10,C
037.8–06.3	NGC 6790	19:22:57.0	01:30:46	0.1	-10.23	-10.25±0.03	3.0	2	0.6	
045.4–02.7	Vy 2-2	19:24:22.2	09:53:57	0.1	-10.59	-10.61±0.04	1.8	3	1.54	
048.7–01.5	DeHt 4	19:26:26.7	13:19:35	2.0	-12.18	-12.43±0.10	1.8	1	...	4
031.0–10.8	M 3-34	19:27:01.9	-06:35:05	0.0	-11.05	-11.05±0.04	1.8	3	...	
046.3–03.1	PB 9	19:27:44.8	10:24:21	0.0	-11.81	-11.81±0.05	1.8	2	...	5,6
048.0–02.3	PB 10	19:28:14.4	12:19:36	0.2	-11.45	-11.48±0.05	1.8	1	...	6
034.1–10.5	HaWe 13	19:31:07.2	-03:42:32	...	-11.89	...	1.8	3	...	
046.4–04.1	NGC 6803	19:31:16.5	10:03:22	0.4	-10.47	-10.54±0.04	1.8	2	0.58	
045.7–04.5	NGC 6804	19:31:35.2	09:13:32	0.0	-10.61	-10.61±0.04	1.9	2	0.73	
004.8–22.7	Hen 2-436	19:32:06.7	-34:12:57	0.1	-11.77	-11.79±0.09	2.6	2	...	10,C
044.3–05.6	K 3-36	19:32:39.6	07:27:52	0.0	-11.71	-11.71±0.07	1.8	2	...	
...	GLMP 923	19:32:55.1	14:13:37	...	-12.33	...	1.8	1	...	2
047.1–04.2	Abell 62	19:33:17.7	10:37:04	2.0	-10.85	-11.09±0.05	2.7	2	1.44	
320.3–28.8	Hen 2-434	19:33:49.4	-74:32:59	0.0	-10.92	-10.92±0.06	2.6	2	0.16	
042.9–06.9	NGC 6807	19:34:33.5	05:41:03	0.1	-10.84	-10.85±0.04	1.8	2	0.55	
034.5–11.7	PM 1-308	19:36:17.5	-03:53:25	0.6	-11.30	-11.39±0.04	1.8	3	...	3
052.5–02.9	Me 1-1	19:39:09.8	15:56:48	1.0	-10.74	-10.88±0.04	1.8	2	0.17	
019.4–19.6	K 2-7	19:40:29.1	-20:27:06	...	-11.87	...	2.6	4	...	
051.9–03.8	M 1-73	19:41:09.3	14:56:59	0.5	-10.76	-10.83±0.04	1.8	2	...	
051.0–04.5	PC 22	19:42:03.5	13:50:37	0.3	-11.51	-11.55±0.05	1.8	2	...	
052.2–04.0	M 1-74	19:42:18.9	15:09:08	0.2	-11.00	-11.03±0.04	1.8	2	0.82	
025.8–17.9	NGC 6818	19:43:57.9	-14:09:12	0.2	-9.92	-9.95±0.03	6.6	2	0.22	6
017.3–21.9	Abell 65	19:46:34.2	-23:08:13	0.2	-10.91	-10.95±0.06	3.1	2	0.71	6
019.8–23.7	Abell 66	19:57:31.5	-21:36:45	0.2	-10.77	-10.80±0.05	3.6	2	...	
...	Pa 11	19:57:59.3	04:47:31	2.5	-11.87	-12.16±0.06	2.2	3	...	6
014.8–25.6	HaWe 14	19:58:13.1	-26:28:16	...	-12.13	...	1.8	2	...	
043.5–13.4	Abell 67	19:58:27.0	03:02:52	0.6	-11.81	-11.89±0.07	1.9	3	...	
042.5–14.5	NGC 6852	20:00:39.2	01:43:40	0.1	-11.48	-11.50±0.05	1.8	4	...	
029.1–21.2	LS IV -12 111	20:01:49.8	-12:41:18	...	-11.49	...	1.8	3	...	3
...	PM 1-322	20:14:50.9	12:03:50	...	-11.95	...	1.8	1	...	1
054.1–12.1	NGC 6891	20:15:08.8	12:42:16	0.0	-10.14	-10.15±0.03	4.2	1	0.14	
359.2–33.5	CRBB 1	20:19:28.7	-41:31:27	0.3	-11.14	-11.20±0.04	1.8	3	...	V

Table B2 – Continued

PNG	Name	RAJ2000	DEJ2000	$R_{[N\ II]}$	$\log F_{\text{red}}$	$\log F(\text{H}\alpha)$	r_{aper}	N_f	c_β	Note
...	Fr 2-15	20:27:19.4	11:47:44	1.0	-10.53	-10.67±0.04	11.3	1	...	1,6
038.1–25.4	Abell 70	20:31:33.2	-07:05:18	1.7	-11.86	-12.07±0.05	1.8	2	...	
059.7–18.7	Abell 72	20:50:02.1	13:33:30	0.1	-11.69	-11.70±0.05	2.4	1	...	5,6
037.7–34.5	NGC 7009	21:04:10.9	-11:21:48	0.1	-9.28	-9.29±0.04	6.7	1	0.1	
...	Fr 2-16	21:18:30.0	12:01:36	...	-11.05	...	15.5	1	...	1
066.7–28.2	NGC 7094	21:36:53.0	12:47:19	0.0	-11.23	-11.23±0.04	2.2	1	0.26	
002.7–52.4	IC 5148/50	21:59:35.2	-39:23:08	0.5	-10.45	-10.52±0.04	2.5	3	...	
036.1–57.1	NGC 7293	22:29:38.5	-20:50:14	1.8	-8.64	-8.86±0.04	11.0	2	0.20	8,C

Notes: (1) Possible PN; (2) pre-PN; (3) transition object; (4) uncertain counts; (5) confused with nearby object; (6) bad pixels in aperture; (7) object near field edge; (8) flux excludes halo; (9) flux corrected for CSPN; (10) Wolf-Rayet CSPN; (N) previously unpublished object; (V) very low excitation PN; (C) specific comment given: BoBn 1 — possibly related to Sgr dSph tidal stream; Te 11 — possible CV bowshock nebula; Abell 12 is confused with a bright star; K 2-2 — flux is for bright inner region only; KLSS 1-8 — $R_{[N\ II]}$ is uncertain; HFG 2 — flux includes superimposed H II region; Hen 2-25 — probable symbiotic outflow; Abell 33 — nebula is confused with nearby star; Lo 4 — variable emission-line central star; Abell 35 — unlikely PN (Frew 2008); Mu 1 — discovered by A. Murrell; Cn 1-1 — yellow symbiotic star; Mz 3 — probable symbiotic outflow; Abell 38 — $R_{[N\ II]}$ is uncertain; M 2-9 — probable symbiotic outflow; Terz N 2337 — $R_{[N\ II]}$ is very uncertain; PHR J1757-1649 — flux includes superimposed H II region; SB 17 — central star is V348 Sgr, a hot R CrB star; StWr 2-21, Wray 16-423 and Hen 2-436 are Sgr dSph members; Abell 58 — born-again object; NGC 7293 — total flux including outer halo is $\log F(\text{H}\alpha) = -8.84$.

Table B3: (Table 4): H α fluxes for 178 true and possible PNe measured from VTSS

PNG	Name	RAJ2000	DEJ2000	logF(H α)	r_{aper}	N_f	c_β	Note
118.0−08.6	Vy 1-1	00:18:42.2	53:52:20	−10.95±0.09	4.8	1	0.38	6,10?
119.3+00.3	BV 5-1	00:20:00.5	62:59:03	−11.62±0.18	5.0	1	...	4,5
119.6−06.1	Hu 1-1	00:28:15.6	55:57:55	−11.00±0.08	3.2	1	0.44	
121.6+00.0	BV 5-2	00:40:21.6	62:51:34	−11.60±0.14	3.2	1	...	1,4
122.1−04.9	Abell 2	00:45:34.7	57:57:35	−11.61±0.10	3.2	2	...	6
124.3−07.7	WeSb 1	01:00:53.3	55:03:48	−12.1±0.2	9.3	1	...	
126.3+02.9	K 3-90	01:24:58.6	65:38:36	−11.90±0.12	3.2	1	...	5,6
130.3−11.7	M 1-1	01:37:19.4	50:28:12	−11.33±0.10	3.2	1	...	
130.9−10.5	NGC 650/1	01:42:20.0	51:34:31	−10.19±0.05	3.2	1	0.10	
138.8+02.8	IC 289	03:10:19.3	61:19:01	−10.82±0.07	3.2	1	1.29	
...	Fr 2-23	03:14:46.0	48:12:06	−10.15±0.12	31.5	1	...	1,N
149.4−09.2	HaWe 4	03:27:15.4	45:24:20	−11.45±0.11	3.2	1	...	5
147.4−02.3	M 1-4	03:41:43.4	52:17:00	−11.28±0.09	3.2	1	...	
149.7−03.3	IsWe 1	03:49:05.9	50:00:15	−10.88±0.10	12.5	1	...	
171.3−25.8	Ba 1	03:53:36.6	19:29:39	−11.69±0.12	3.2	2	...	6
147.8+04.1	M 2-2	04:13:15.0	56:56:58	−11.14±0.09	3.2	1	...	
151.4+00.5	K 3-64	04:13:27.3	51:51:01	−12.3±0.2	3.2	2	...	4,6
167.4−09.1	K 3-66	04:36:37.2	33:39:30	−11.42±0.10	3.2	1	...	
174.2−14.6	H 3-29	04:37:23.5	25:02:41	−11.63±0.11	3.2	1	...	
165.5−06.5	K 3-67	04:39:47.9	36:45:43	−11.14±0.09	3.2	2	...	
166.4−06.5	CRL 618	04:42:53.7	36:06:53	−11.98±0.14	3.2	2	...	2,4
205.8−26.7	MaC 2-1	05:03:41.9	−06:10:03	−12.1±0.2	3.2	2	...	4
190.3−17.7	J 320	05:05:34.3	10:42:23	−10.79±0.07	4.0	1	0.45	5
167.0−00.9	Abell 8	05:06:38.4	39:08:11	−12.00±0.14	3.2	1	...	4
173.7−05.8	K 2-1	05:07:09.1	30:49:28	−11.03±0.05	3.2	1	1.01	5,6
...	IPHASX J0511+3028	05:11:51.3	30:28:14	−11.78±0.13	5.8	1	...	1,N
215.2−24.2	IC 418	05:27:28.2	−12:41:50	−9.02±0.04	8.0	1	0.32	
178.3−02.5	K 3-68	05:31:35.9	28:58:42	−11.80±0.13	3.2	1	...	4
197.2−14.2	Abell 10	05:31:45.5	06:56:02	−11.40±0.14	3.2	1	...	
193.6−09.5	H 3-75	05:40:45.0	12:21:23	−11.47±0.11	3.2	1	1.0:	
170.7+04.6	K 3-69	05:41:22.2	39:15:08	−12.3±0.2	3.2	1	...	4
196.6−10.9	NGC 2022	05:42:06.2	09:05:11	−10.54±0.05	4.0	2	0.41	
184.0−02.1	M 1-5	05:46:50.0	24:22:02	−11.19±0.09	3.2	1	...	
181.5+00.9	Pu 1	05:52:48.4	28:05:59	−12.4±0.2	3.2	1	...	4
193.0−04.5	KLSS 1-5	05:57:08.0	15:25:31	−12.1±0.2	3.2	1	...	4
197.4−06.4	WDHS 1	05:59:24.8	10:41:41	−10.40±0.14	19.2	1	...	
204.0−08.5	Abell 13	06:04:47.9	03:56:36	−11.45±0.11	4	1	...	
201.9−04.6	We 1-4	06:14:33.7	07:34:30	−12.2±0.2	3.2	1	...	4
221.3−12.3	IC 2165	06:21:42.8	−12:59:14	−10.25±0.08	4.8	1	0.60	
218.9−10.7	HDW 5	06:23:37.1	−10:13:24	−11.10±0.15	5.6	1	...	1,6,V
204.8−03.5	K 3-72	06:23:54.9	05:30:13	−11.67±0.13	3.2	1	...	
194.2+02.5	J 900	06:25:57.3	17:47:27	−10.50±0.05	4	1	1.13	
170.3+15.8	NGC 2242	06:34:07.4	44:46:38	−11.58±0.11	3.2	1	...	
189.8+07.7	M 1-7	06:37:21.0	24:00:35	−11.09±0.08	3.2	1	1.57	
153.7+22.8	Abell 16	06:43:55.5	61:47:25	−11.68±0.11	4.8	1	...	
224.3−05.5	PHR J0652-1240	06:52:20.3	−12:40:34	−11.62±0.12	3.2	1	...	1
204.1+04.7	K 2-2	06:52:23.2	09:57:56	−10.07±0.08	10.4	1	...	1,C
210.3+01.9	M 1-8	06:53:33.8	03:08:27	−11.73±0.13	3.2	1	...	
221.0−01.4	PHR J0701-0749	07:01:09.3	−07:49:21	−11.79±0.13	3.2	1	...	4
226.4−03.7	PB 1	07:02:46.8	−13:42:35	−11.9±0.3	3.2	1	...	4
212.0+04.3	M 1-9	07:05:19.2	02:46:59	−10.92±0.09	4.8	1	...	
217.4+02.0	St 3-1	07:06:50.9	−03:05:10	−11.61±0.13	3.2	1	...	
215.6+03.6	NGC 2346	07:09:22.6	00:48:23	−10.55±0.10	4	1	0.57	9
224.9+01.0	We 1-6	07:17:26.0	−10:10:38	−11.38±0.15	3.2	1	...	
227.1+00.5	PHR J0719-1222	07:19:46.7	−12:22:47	−11.54±0.13	3.2	1	...	5
222.1+03.9	PFP 1	07:22:17.7	−06:21:46	−10.74±0.14	11.0	1	...	
214.9+07.8	Abell 20	07:22:57.7	01:45:33	−11.65±0.12	3.2	1	...	
221.7+05.3	M 3-3	07:26:34.2	−05:21:52	−11.81±0.12	3.2	1	...	
226.7+05.6	M 1-16	07:37:19.0	−09:38:50	−11.24±0.09	3.2	1	...	
228.8+05.3	M 1-17	07:40:22.2	−11:32:30	−11.28±0.10	3.2	1	...	

Table B3 – Continued

PNG	Name	RAJ2000	DEJ2000	logF(H α)	r_{aper}	N_f	c_β	Note
231.8+04.1	NGC 2438	07:41:50.5	-14:44:08	-10.32 \pm 0.05	3.2	1	0.80	
231.4+04.3	M 1-18	07:42:04.2	-14:21:13	-11.45 \pm 0.11	3.2	1	...	5
...	Fr 2-25	08:04:04.4	-06:30:57	-11.10 \pm 0.10	8.4	1	...	1,4,N
219.1+31.2	Abell 31	08:54:13.2	08:53:53	-10.16 \pm 0.08	12.0	1	...	7
016.1+07.7	PTB 20	17:52:15.0	-11:10:37	-12.2 \pm 0.2	3.2	1	...	
053.3+24.0	Vy 1-2	17:54:23.0	27:59:58	-11.07 \pm 0.08	3.2	1	0.01	
014.0+04.8	PTB 19	17:58:25.9	-14:25:25	-12.4 \pm 0.3	3.2	1	...	4
096.4+29.9	NGC 6543	17:58:33.4	66:37:59	-9.10 \pm 0.04	6.5	1	...	
014.2+03.8	PM 1-205	18:02:38.2	-14:42:05	-12.1 \pm 0.2	3.2	1	...	4
019.8+05.6	CTS 1	18:06:59.8	-08:55:33	-11.84 \pm 0.13	3.2	1	...	
015.5+02.8	BMP J1808-1406	18:08:35.1	-14:06:43	-11.70 \pm 0.14	3.2	1	...	
022.5+04.8	MA 2	18:15:13.4	-06:57:12	-12.03 \pm 0.15	3.2	1	...	4
023.0+04.3	MA 3	18:17:49.4	-06:48:22	-12.05 \pm 0.14	3.2	1	...	4
021.9+02.7	MaC 1-12	18:21:21.1	-08:31:42	-11.65 \pm 0.12	3.2	1	...	
020.6+01.9	PHR J1821-1001	18:21:40.6	-10:01:44	-11.38 \pm 0.10	3.2	1	...	1
094.0+27.4	K 1-16	18:21:52.2	64:21:54	-11.68 \pm 0.12	3.2	1	...	
044.3+10.4	We 3-1	18:34:02.3	14:49:10	-11.47 \pm 0.10	3.2	1	...	
042.0+05.4	K 3-14	18:48:32.8	10:35:51	-11.42 \pm 0.10	3.2	1	...	5
051.4+09.6	Hu 2-1	18:49:47.6	20:50:39	-10.15 \pm 0.08	4.8	1	0.60	
041.8+04.4	K 3-15	18:51:41.5	09:54:53	-11.57 \pm 0.12	3.2	1	...	V
044.0+05.2	K 3-16	18:53:01.6	12:15:59	-11.91 \pm 0.14	3.2	1	...	4
063.1+13.9	NGC 6720	18:53:35.1	33:01:45	-9.56 \pm 0.07	4.8	1	0.19	
038.7+01.9	YM 16	18:54:57.3	06:02:31	-11.30 \pm 0.10	6.4	1	...	
039.8+02.1	K 3-17	18:56:18.2	07:07:26	-11.80 \pm 0.14	3.2	1	...	4
043.1+03.8	M 1-65	18:56:33.6	10:52:10	-11.31 \pm 0.10	3.2	1	...	
068.7+14.8	Sp 4-1	19:00:26.5	38:21:07	-11.37 \pm 0.10	3.2	1	...	
035.9-01.1	Sh 2-71	19:01:59.3	02:09:18	-10.82 \pm 0.05	7.2	1	1.01	
046.8+03.8	Sh 2-78	19:03:10.1	14:06:59	-10.61 \pm 0.09	6.4	1	...	
051.5+06.1	K 1-17	19:03:37.4	19:21:23	-11.82 \pm 0.13	3.2	1	...	
050.4+05.2	Abell 52	19:04:32.3	17:57:07	-11.93 \pm 0.14	3.2	1	...	
048.5+04.2	K 4-16	19:04:51.5	15:47:38	-12.0 \pm 0.2	3.2	1	...	4,5,6
...	IPHASX J1905+1613	19:05:12.4	16:13:47	-12.2 \pm 0.2	3.2	1	...	1
044.1+01.5	PM 1-281	19:06:32.2	10:43:24	-11.96 \pm 0.14	3.2	1	...	
040.3-00.4	Abell 53	19:06:45.9	06:23:52	-11.66 \pm 0.12	3.2	1	...	
055.3+06.6	Abell 54	19:08:39.6	22:58:58	-12.1 \pm 0.2	3.2	1	...	4
062.4+09.5	NGC 6765	19:11:06.5	30:32:43	-11.30 \pm 0.07	8.0	1	0.40	
035.6-04.2	MPA J1911+0027	19:11:24.8	00:27:45	-11.79 \pm 0.13	3.2	1	...	
049.4+02.4	Hen 2-428	19:13:05.2	15:46:40	-11.39 \pm 0.10	3.2	1	...	
037.9-03.4	Abell 56	19:13:06.1	02:52:48	-11.56 \pm 0.14	5.1	1	...	
039.5-02.7	M 2-47	19:13:34.6	04:38:04	-11.36 \pm 0.11	3.2	1	...	
048.7+01.9	Hen 2-429	19:13:38.4	14:59:19	-11.25 \pm 0.09	3.2	1	...	10
038.7-03.3	M 1-69	19:13:54.0	03:37:42	-11.24 \pm 0.10	4.0	1	...	
051.0+03.0	Hen 2-430	19:14:04.2	17:31:33	-11.41 \pm 0.10	3.2	1	...	
051.0+02.8	WhMe 1	19:14:59.8	17:22:46	-12.11 \pm 0.13	3.2	1	...	1,4,5
040.4-03.1	K 3-30	19:16:27.7	05:13:19	-11.56 \pm 0.12	3.2	1	...	
058.6+06.1	Abell 57	19:17:05.7	25:37:33	-11.86 \pm 0.13	3.2	1	...	
041.8-02.9	NGC 6781	19:18:28.1	06:32:19	-10.01 \pm 0.08	5.6	1	1.11	
052.9+02.7	K 3-31	19:19:02.7	19:02:21	-12.04 \pm 0.14	4.0	1	...	6
077.6+14.7	Abell 61	19:19:10.2	46:14:52	-11.38 \pm 0.05	7.7	1	...	
051.3+01.8	PM 1-295	19:19:18.8	17:11:48	-12.01 \pm 0.14	3.2	1	...	4
076.3+14.1	Pa 5	19:19:30.5	44:45:43	-11.56 \pm 0.12	3.7	1	...	
043.0-03.0	M 4-14	19:21:00.7	07:36:52	-11.73 \pm 0.13	3.2	1	...	
055.3+02.7	He 1-1	19:23:46.9	21:06:39	-12.1 \pm 0.2	3.2	3	...	6
056.0+02.0	K 3-35	19:27:44.0	21:30:04	-12.4 \pm 0.2	3.2	1	...	3,4
061.3+03.6	M 1-91	19:32:57.7	26:52:43	-11.74 \pm 0.12	3.2	1	...	1
059.4+02.3	K 3-37	19:33:46.8	24:32:27	-12.1 \pm 0.2	3.2	1	...	4
064.7+05.0	BD +30 3639	19:34:45.2	30:30:59	-9.41 \pm 0.06	4.8	1	0.51	10,V
059.9+02.0	K 3-39	19:35:54.5	24:54:48	-12.3 \pm 0.2	3.2	1	...	4
055.5-00.5	M 1-71	19:36:26.9	19:42:24	-10.96 \pm 0.08	4.0	1	2.44	
060.5+01.8	Hen 2-440	19:38:08.4	25:15:41	-11.73 \pm 0.12	3.2	1	...	
052.5-02.9	Me 1-1	19:39:09.8	15:56:48	-10.81 \pm 0.07	4.0	1	0.38	
061.8+02.1	Hen 2-442	19:39:43.4	26:29:33	-11.57 \pm 0.12	3.2	1	...	

Table B3 – Continued

PNG	Name	RAJ2000	DEJ2000	logF(H α)	r_{aper}	N_f	c_β	Note
051.9–03.8	M 1-73	19:41:09.3	14:56:59	-10.84±0.07	3.2	1	...	
054.4–02.5	M 1-72	19:41:34.0	17:45:18	-11.20±0.09	3.2	1	...	
053.8–03.0	Abell 63	19:42:10.4	17:05:15	-11.47±0.11	3.2	1	...	
052.2–04.0	M 1-74	19:42:18.9	15:09:08	-10.98±0.08	4.0	1	0.98	6
054.2–03.4	IPHASX J1943-1709	19:43:59.5	17:09:01	-11.88±0.14	3.2	1	...	4
059.1–00.7	Kn 9	19:44:59.0	22:45:48	-11.10±0.11	4.5	2	...	1
057.9–01.5	Hen 2-447	19:45:22.2	21:20:04	-11.61±0.12	3.2	1	...	
043.5–13.4	Abell 67	19:58:27.0	03:02:52	-11.90±0.14	3.2	1	...	4
060.0–04.3	Abell 68	20:00:10.6	21:42:55	-11.61±0.12	3.2	1	...	
058.6–05.5	WeSb 5	20:01:42.0	19:54:41	-11.32±0.10	3.2	2	...	5
107.0+21.3	K 1-6	20:04:13.4	74:26:28	-11.37±0.10	4.0	2	...	
082.1+07.0	NGC 6884	20:10:23.7	46:27:40	-10.57±0.06	3.2	1	0.26	
057.2–08.9	NGC 6879	20:10:26.7	16:55:21	-11.03±0.08	3.2	1	0.29	
060.3–07.3	Hen 1-5	20:11:56.1	20:20:04	-11.42±0.10	3.2	1	...	
060.1–07.7	NGC 6886	20:12:42.8	19:59:23	-10.63±0.09	4.8	1	...	
066.9–05.2	PC 24	20:19:38.1	27:00:11	-11.37±0.10	3.2	1	...	
058.3–10.9	IC 4997	20:20:08.7	16:43:54	-9.92±0.08	7.2	1	...	6
061.4–09.5	NGC 6905	20:22:22.9	20:06:17	-10.48±0.05	4.0	1	0.00	10
...	PM 1-329	20:50:13.6	59:45:51	-12.2±0.2	3.2	1	...	1,4
101.6+13.0	Kn 49	20:55:48.0	65:34:00	-11.67±0.12	3.2	2	...	1,C
089.0+00.3	NGC 7026	21:06:18.2	47:51:05	-10.16±0.08	4.8	1	0.88	10
084.9–03.4	NGC 7027	21:07:01.7	42:14:10	-9.29±0.06	6.4	2	1.20	
084.2–04.2	K 3-80	21:07:39.7	40:57:52	-11.80±0.13	3.2	1	...	1,4
082.1–07.8	Kn 24	21:13:37.7	37:15:37	-11.29±0.11	4.0	1	...	
089.8–00.6	Sh 1-89	21:14:07.6	47:46:22	-11.38±0.11	3.2	1	...	
088.7–01.6	NGC 7048	21:14:15.2	46:17:18	-10.85±0.06	7.6	1	...	
072.7–17.1	Abell 74	21:16:52.3	24:08:52	-10.76±0.09	7.2	2	...	
080.3–10.4	MWP 1	21:17:08.3	34:12:27	-10.74±0.10	4.8	1	...	7
089.3–02.2	M 1-77	21:19:07.4	46:18:47	-11.21±0.09	3.2	1	...	V
093.9–00.1	IRAS 21282+5050	21:29:58.1	51:04:00	-11.71±0.16	3.2	1	...	3,4,10
096.3+02.3	K 3-61	21:30:00.7	54:27:27	-11.87±0.14	3.2	1	...	4,10
093.3–00.9	K 3-82	21:30:51.6	50:00:07	-11.7±0.2	3.2	2	...	
089.8–05.1	IC 5117	21:32:31.0	44:35:49	-10.55±0.05	4.0	1	1.16	
086.5–08.8	Hu 1-2	21:33:08.4	39:38:10	-10.57±0.09	4.8	1	0.57	
094.5–00.8A	LeDu 1	21:36:05.5	50:54:10	-12.2±0.3	5.0	1	...	4
066.7–28.2	NGC 7094	21:36:53.0	12:47:19	-11.24±0.09	3.2	1	...	
093.3–02.4	M 1-79	21:37:01.5	48:56:03	-10.95±0.08	3.2	2	1.01	
095.0–05.5	GLMP 1047	21:56:32.9	47:36:13	-11.82±0.14	3.2	1	...	3
103.2+00.6	M 2-51	22:16:03.9	57:28:34	-11.14±0.09	3.2	1	...	
104.1+01.0	Bl 2-1	22:20:16.6	58:14:17	-11.55±0.14	3.2	1	...	4
103.7+00.4	M 2-52	22:20:30.8	57:36:22	-11.69±0.14	3.2	1	...	4
100.6–05.4	IC 5217	22:23:55.7	50:58:00	-10.64±0.06	4.0	2	0.01	
102.9–02.3	Abell 79	22:26:17.3	54:49:38	-11.20±0.12	3.2	1	...	9
099.7–08.8	HaWe 15	22:30:33.4	47:31:24	-11.29±0.10	4.0	1	...	1
100.0–08.7	Me 2-2	22:31:43.7	47:48:04	-10.68±0.06	4.0	1	...	
104.4–01.6	M 2-53	22:32:17.7	56:10:26	-11.45±0.11	3.2	1	...	6
102.8–05.0	Abell 80	22:34:45.6	52:26:06	-11.45±0.11	3.2	2	...	
107.8+02.3	NGC 7354	22:40:19.9	61:17:08	-10.49±0.05	3.2	1	1.98	
104.8–06.7	M 2-54	22:51:38.9	51:50:43	-11.20±0.09	3.2	2	...	1,3
107.7–02.2	M 1-80	22:56:19.8	57:09:21	-11.50±0.13	3.2	1	...	
104.2–29.6	Jones 1	23:35:53.3	30:28:06	-10.82±0.09	4.8	1	...	7
110.6–12.9	K 1-20	23:39:10.8	48:12:29	-12.2±0.2	3.2	1	...	
114.0–04.6	Abell 82	23:45:47.8	57:03:59	-11.37±0.10	3.2	2	...	
112.9–10.2	Abell 84	23:47:44.3	51:23:56	-11.13±0.09	3.2	1	...	
116.2+08.5	M 2-55	23:31:52.7	70:22:10	-11.21±0.09	3.2	1	...	

Notes: (1) Possible PN; (2) pre-PN; (3) transition object; (4) uncertain counts; (5) confused with nearby object; (6) bad pixels in aperture; (7) object near field edge; (8) flux excludes halo; (9) flux corrected for CSPN; (10) Wolf-Rayet CSPN; (N) previously unpublished object; (V) very low excitation PN; (C) specific comment given: K 2-2 — flux is for bright inner region only; Kn 49 — possibly an isolated SNR filament.